UNIVERSITÀ DEGLI STUDI DI MILANO

SCUOLA DI DOTTORATO
FISICA, ASTROFISICA E FISICA APPLICATA

DIPARTIMENTO
FISICA

CORSO DI DOTTORATO DI RICERCA IN
FISICA, ASTROFISICA E FISICA APPLICATA
CICLO XXIII

Open Quantum Systems Dynamics within and beyond the Jaynes-Cummings Model

Settore Scientifico Disciplinare FIS/03

Supervisore:
Prof. Federico CASAGRANDE
Coordinatore:
Prof. Marco BERSANELLI

Tesi di Dottorato di:
Matteo BINA

Anno Accademico 2009 - 2010

...to my great small nephew Edoardo

In Hinduism, Shiva the Cosmic Dancer, is perhaps the most perfect personification of the dynamic universe. Through his dance, Shiva sustains the manifold phenomena in the world, unifying all things by immersing them in his rhythm and making them participate in the dance - a magnificent image of the dynamic unity of the Universe.

- Fritjof Capra, The Tao of Physics -

Abstract

The object of this PhD Thesis is light and matter quantum interaction including studies on cavity and circuit quantum electrodynamics (CQED and cQED), quantum information theory and entanglement dynamics in open systems. In recent years both theoretical and experimental efforts have been devoted to study problems regarding the transfer of quantum correlations, quantum memories, entanglement protection against decoherence and new regimes accessible in cQED. One of the fundamental model underlying these topics is the well known Jaynes-Cummings (JC) one for light-matter interaction, introduced in quantum optics already in 1963. This paradigmatic model describes the coherent exchange of a single excitation between a qubit (a two-level system) and a mode of a quantized harmonic oscillator. The JC model describes a lot of purely quantum effects such as Rabi oscillations and generation of entangled quantum states, which were confirmed by several sophisticated experiments in CQED. This model has been then applied in many other frameworks. Analytical results can be derived only under the so-called rotating wave approximation (RWA), which allows to neglect the energy contributions coming from the counter-rotating terms, which describe the simultaneous excitation (or de-excitation) of the qubit and the field mode. In this Thesis a first interesting investigation, based on the JC model, is related to the realization of quantum memories. The main aspect is the transfer of generic quantum entangled states of a propagating radiation to some qubits, such as two-level atoms placed in separated optical cavities. Generalizing previous results for bipartite entangled systems, I investigated the more complex case of tripartite systems, where the very quantification of entanglement is still an open problem. This issue is broadened to open systems in contact with a common environment which induces decoherence effects unavoidable in realistic implementations. The main result of this analysis is that it is possible to map in an optimal way a quantum state from radiation to qubits in the unitary dynamics, and even in the presence of a dissipative environment a significative amount of entanglement can be transferred. This study has been carried on with either theoretical calculations or numerical simulations performed adopting the powerful Monte Carlo wave function method.
A second important problem for quantum memories faced in this PhD Thesis, regards the

protection of qubits entanglement for long enough times in order to implement quantum information tasks. A possible way to obtain this goal is to add an external coherent field driving two or more two-level atoms interacting with a common mode of a cavity electromagnetic field. In fact it is possible to demonstrate that, under certain conditions, an effective Hamiltonian of the whole system involves, together with the familiar JC terms, also the counter-rotating ones. The main feature that comes out from this analysis is the possibility to freeze, during system dynamics, peculiar quantum entangled states of the atomic qubits in so called decoherence-free subspaces. This important property allows to store the entanglement in matter qubits, isolating the quantum state from environment induced decoherence. Though the system includes dissipation, analytical results have been obtained for multipartite entanglement and decoherence by solving the master equation through a projection on a suitable basis and using the method of characteristics. In particular it is possible to monitor the rate of decoherence via measurements of joint atomic probabilities, shading light on the fascinating border between the quantum and the classical world.
A last topic investigated in this Thesis concerns the recently developed and quite promising implementation of the JC model well outside CQED, that is cQED. Here superconductive circuits, which play the role of artificial atoms, interact on-chip with transmission line resonators, instead of the usual electromagnetic cavities. These systems have the advantage of being quite easily engineered exploiting the most advanced available technologies. Moreover they allow a great flexibility in handling the relevant parameters, since the inter-system coupling is here of capacitive or inductive nature, instead of the usual electric dipole interaction in CQED. In this way a strong and ultrastrong coupling regime have become available, giving a direct access to the physics beyond the JC model and its possible applications. I first performed a detailed characterization of system dynamics in order to test the main approximations usually introduced to describe superconductive circuits as qubits. Then I described, both analytically and numerically, the dissipative dynamics of a superconductive qubit coupled to a resonator mode in the deep ultrastrong regime.

CONTENTS

Introduction

The system composed by a two-level atom and a quantized mode of a harmonic oscillator is at the heart of our description of radiation-matter interaction. An almost ideal framework is provided by Cavity quantum electrodynamics (CQED), where this interaction occurs within optical cavities or microwave resonators, allowing the observation of quantum coherence effects. Similar dynamics was later observed e.g. in trapped-ion systems and in solid-state semiconductor or superconductor devices. The nature of the coupling can be different and may span several regimes for the matter-light interaction. The most paradigmatic example is the Jaynes-Cummings (JC) model [1], firstly analyzed in the field of Quantum Optics, where the main assumption is that the dipole interaction strength is much smaller than the two-level system transition frequency and a rotating wave approximation (RWA) can be performed. The JC model is fully solvable and it has been widely studied, extended and applied in several experiments of large conceptual and practical extent [2].

The dynamics of a qubit-oscillator system described by the JC model, is nowadays well understood in terms of either Rabi oscillations, collapses and revivals for the populations of the energy qubit levels, and bare and dressed states of the whole system. Basically only a finite portion of the Hilbert space is involved in the JC dynamics, and this renders the model simple and physically intuitive, to the extent that it is the most important benchmark for matter-light interaction. To achieve these and other results in the lab, the strong coupling (SC) regime is required, that is, the qubit-oscillator coupling has to be comparable or larger than all decoherence rates. In CQED this kind of interaction can be investigated experimentally under carefully controlled conditions. Under the SC condition it was possible the implementation of the micromaser [3] and the microlaser [4]. Other fundamental results were obtained in important experiments both in the microwave [5, 6] and optical [7] regime of CQED, in solid-state superconducting [8] and in trapped ions [9] systems.

Extensions of the JC model to more atoms and more modes have been developed and, presently, we enjoy a vast number of theoretical and experimental studies. A particularly interesting case is provided by adding an external classical driving field acting on the cavity mode or directly on the two-level system.

Circuit QED (cQED) is a novel subject of interest in the field of solid-state quantum computation. It appears from the association of quantum-optical cavity QED with macroscopic quantum mechanics. This approach offers the prospect of reaching an upper limit for the coupling of a quantum-mechanical two-level system to a single mode of the electromagnetic field. Actually the interaction between superconducting circuits (also called artificial atoms) and modes of a coplanar transmission line resonator can be raised until very high values, comparable or greater than the qubit transition frequency. This happens since, for these kind of systems, the qubit-oscillator coupling is of inductive or capacitive nature and provides high values of the interaction strength before unachievable in CQED. In this regime, the RWA breaks down and the model becomes analytically unsolvable, except for some limits [10], allowing the advent of the ultrastrong coupling (USC) regime. Moreover, due to the impressive fast development of current technology, higher values should be achieved in the near future, bringing the coupled system to what is called deep SC (DSC) regime, a completely new arena open to innovative concepts.

The advent of quantum information [11] has been a fresh input in the field of CQED [2], reshaping concepts and using it for fundamental tests and initial steps in the demanding field of quantum information processing. Entanglement is the key resource for quantum information (QI) processing, where it allowed a number of achievements such as teleportation [12], cryptography [13] and enhanced measurements [14]. The deep meaning of multipartite entanglement, its quantification and detection [15] and the possible applications are the object of massive investigation. As a matter of fact, optical systems have been a privileged framework for encoding and manipulating quantum information, since bipartite and multipartite entanglement may be effectively generated either in the discrete or continuous variable (CV) regime. On the other hand, the development of QI also requires localized registers, e.g. for the storage of entanglement in quantum memories. Here, coherence and the generation of entanglement play an important role, and in particular the manner in which they are affected by the presence of a dissipative environment [16]. Understanding how decoherence induced by dissipation acts on the dynamics of an interacting system has a two-fold value. Firstly it allows to predict the behaviour of the observables of open systems in order to provide a realistic description taking into account different noisy channels. It is also possible to find conditions to avoid decoherence effect, preserving the quantum properties of the systems in such a way they can be implemented for QI protocols. Secondly the analysis of decoherence provides a better knowledge on the subtle border between quantum and classical worlds.

Outline

This PhD thesis is organized as follows.
The first chapter is devoted to some preliminary concepts and tools useful for a better understanding and a more flowing reading. In particular we will resume the JC model, the

entanglement quantification for bipartite and multipartite systems and, finally, the Monte Carlo wave function (MCWF) method for numerical simulations.
The second chapter concerns the problem of the transfer of quantum entangled correlations from radiation to matter qubits. We treat a tripartite case and we will face the issue of multipartite entanglement, entanglement sudden death and birth (ESD and ESB) and open system dynamics. The underlying structure is the JC model applied to a system composed by three radiation modes interacting with three cavity modes, coupled in turn to three two-level atoms, all in contact with a common dissipative environment.
In the third chapter we deal with an extension of the JC model, which takes into account the interaction between N qubits, inside an optical cavity supporting one radiation mode and an external classical driving field. Under proper assumptions and unitary transformations, we obtain an effective interaction that includes simultaneously resonant and anti-resonant JC terms, providing interesting effects on the dynamics of the system. In particular, by a theoretical analysis, we show how multipartite entanglement can be protected against decoherence and we analyze several examples.
In the last chapter we face another extension of the JC model, which arises naturally in the new promising and appealing research field of superconducting qubits and cQED. In this framework the anti-resonant terms of the qubit-oscillator interaction come spontaneously by the increasing of the coupling constant between a qubit and a resonator electromagnetic field mode, as they cannot be neglected. We enter into the details of the new regime of USC and DSC, introducing new physical intuitions and key concepts to describe in a direct way the dynamics of the system, which is also in contact with a dissipative environment.

CHAPTER 1

Preliminary concepts and tools

In this chapter we introduce the main key concepts and tools of Quantum Optics and Quantum Information useful for a better understanding of the present thesis. We describe in Sec. 1.1 the JC model in its natural framework of CQED, which is a milestone of the matter-radiation interaction at the quantum level. Then we introduce in Sec. 1.2 some elements of open system dynamics and the method of quantum trajectories (or the Monte Carlo wavefunction method) to solve numerically a master equation in a more efficient way. In Secs.1.3 and 1.4 we provide a short overview on the bipartite and multipartite entanglement both for pure and mixed states, illustrating some separability criteria and entanglement measures.

1.1 The JC model

A single atom in free space can interact with a continuous of electromagnetic field modes and the dynamics is characterized by the spontaneous emission phenomenon. On the other hand, when the atom is placed in an electromagnetic resonator supporting only discrete field modes, because of boundaries conditions, the situation dramatically changes. When the field mode inside a cavity is treated as a quantum harmonic oscillator, by the annihilation $\hat{a}$ and creation $\hat{a}^\dagger$ operators, satisfying the commutation relation $[\hat{a}, \hat{a}^\dagger] = \hat{\mathbb{1}}$, and the atom as a two-level system, excited $|e\rangle$ and ground $|g\rangle$ energy levels, the dynamics of this fully quantum interacting system is described by the well known Jaynes-Cummings (JC) model, introduced in 1963 [1]. The most interesting properties of the dynamics of such a system are best appreciated under a quasi-resonance condition, between the cavity field frequency ω and the atomic transition frequency ω_0 between the two energy levels.

1.1.1 The interaction Hamiltonian

The Hamiltonian of the bare energies for the atomic and the cavity mode subsytems is

$$\hat{\mathcal{H}}_0 = \hbar\frac{\omega_0}{2}\hat{\sigma}_z + \hbar\omega\hat{a}^\dagger\hat{a} \tag{1.1}$$

where $\hat{\sigma}_z = |e\rangle\langle e| - |g\rangle\langle g|$ and the two field operators $\hat{a}^\dagger$ and $\hat{a}$ are given by electromagnetic field quantization

$$\hat{\vec{E}}(\vec{x}) = \mathrm{i}\sqrt{\frac{\hbar\omega}{2\varepsilon_0 V}}\hat{\varepsilon}(\hat{a}\mathrm{e}^{\mathrm{i}\vec{k}\cdot\vec{x}} - \hat{a}^\dagger\mathrm{e}^{-\mathrm{i}\vec{k}\cdot\vec{x}}) \tag{1.2}$$

with ε_0 is the vacuum dielectric constant, $\hat{\varepsilon}$ is the reference frame unit vector, $\vec{k}$ and $\vec{x}$ are the momentum and position vectors.
The interaction between the atom and the quantized field is given by the electric dipole coupling and it is described by the Hamiltonian

$$\hat{\mathcal{H}}_1 = -\hat{\vec{d}}\cdot\hat{\vec{E}}(0) = \hbar g(\hat{\sigma} + \hat{\sigma}^\dagger)(\hat{a} + \hat{a}^\dagger) \tag{1.3}$$

where the electric dipole operator $\hat{\vec{d}} = \vec{d}(\hat{\sigma} + \hat{\sigma}^\dagger)$, $\vec{d}$ real for simplicity, $\hat{\sigma} = |g\rangle\langle e|$ and $\hat{\sigma}^\dagger = |e\rangle\langle g|$ the lowering and the raising atomic operators, which define the Pauli operator $\hat{\sigma}_x \equiv \hat{\sigma} + \hat{\sigma}^\dagger$. The coupling constant $g = \sqrt{\frac{\omega}{2\varepsilon_0\hbar V}}\hat{\varepsilon}\cdot\hat{\vec{d}}$ and a change of global phase for the field operators has been applied to obtain the second equality in Eq. (1.3). The total Hamiltonian of the system is then $\hat{\mathcal{H}} = \hat{\mathcal{H}}_0 + \hat{\mathcal{H}}_1$.
By analyzing the four terms in the interaction Hamiltonian (1.3) we notice that they are related to processes of absorption and emission of a photon, in fact

$$\hat{\sigma}^\dagger\hat{\mathbf{a}} \quad\longleftrightarrow\quad \text{Transition } |g\rangle \to |e\rangle \text{ and } \textit{absorption} \text{ of a photon} \tag{1.4a}$$

$$\hat{\sigma}\hat{\mathbf{a}}^\dagger \quad\longleftrightarrow\quad \text{Transition } |e\rangle \to |g\rangle \text{ and } \textit{emission} \text{ of a photon} \tag{1.4b}$$

$$\hat{\sigma}\hat{\mathbf{a}} \quad\longleftrightarrow\quad \text{Transition } |e\rangle \to |g\rangle \text{ and } \textit{absorption} \text{ of a photon} \tag{1.4c}$$

$$\hat{\sigma}^\dagger\hat{\mathbf{a}}^\dagger \quad\longleftrightarrow\quad \text{Transition } |g\rangle \to |e\rangle \text{ and } \textit{emission} \text{ of a photon.} \tag{1.4d}$$

The first two terms are commonly referred as "energy conserving" terms, while the second ones are "non-conserving energy" terms. This can be better illustrated by going into the interaction picture with respect to $\hat{\mathcal{H}}_0$, through the unitary operator $\hat{U}_0 = \mathrm{e}^{\mathrm{i}/\hbar\hat{\mathcal{H}}_0 t}$, obtaining

$$\hat{\mathcal{H}}_I(t) = \hat{U}_0\hat{\mathcal{H}}_1\hat{U}_0^\dagger = \hbar g(\hat{\sigma}^\dagger\hat{a}^\dagger\mathrm{e}^{\mathrm{i}(\omega+\omega_0)t} + \hat{\sigma}\hat{a}\mathrm{e}^{-\mathrm{i}(\omega+\omega_0)t} + \hat{\sigma}^\dagger\hat{a}\mathrm{e}^{-\mathrm{i}(\omega-\omega_0)t} + \hat{\sigma}\hat{a}^\dagger\mathrm{e}^{\mathrm{i}(\omega-\omega_0)t}). \tag{1.5}$$

We assume now a quasi-resonant condition between the atomic transition frequency ω_0 and the cavity mode frequency ω, that corresponds to have a small detuning parameter $\Delta \equiv \omega - \omega_0$. Tipically in CQED the highest values of the ratio between the coupling constant and the resonator mode frequency are of the order $\frac{g}{\omega} \simeq 10^{-6} - 10^{-7}$, to which usually it is referred as the strong coupling (SC) regime, since $g \gg \{\kappa, \gamma\}$ where κ and γ are, respectively, the cavity decay rate and the atomic spontaneous emission rate. Now we

consider the Dyson series of the system evolution operator $\hat{U}(t) = \mathrm{e}^{-\mathrm{i}/\hbar\hat{\mathcal{H}}_I(t)t}$

$$\hat{U}(t) = \hat{\mathbb{1}} - \frac{\mathrm{i}}{\hbar}\int_0^t dt_1\hat{\mathcal{H}}_I(t_1) - \left(\frac{\mathrm{i}}{\hbar}\right)^2\int_0^t dt_1\int_0^{t_1} dt_2\hat{\mathcal{H}}_I(t_1)\hat{\mathcal{H}}_I(t_2) + \cdots \tag{1.6}$$

Integrating term by term Eq. (1.6) it is straightforward to see that the non-conserving energy terms in (1.4) are related to powers of the ratio $\frac{g}{\omega+\omega_0}$ that are very small when the resonance condition $\delta \simeq 0$ is considered, whereas the resonant terms are the relevant ones as they are related to the ratio $\frac{g}{\omega-\omega_0}$. Equivalently the exponentials in the interaction Hamiltonian $\hat{\mathcal{H}}_I$ are rapidly oscillating and during the time evolution they average to zero. This means that considering the resonant dynamics of such an interacting system in CQED, we are allowed to neglect the contributions due to the anti-resonant terms $\hat{\sigma}^\dagger\hat{a}^\dagger$ and $\hat{\sigma}\hat{a}$, and we can consider the effective Hamiltonian in the Schrödinger picture

$$\hat{\mathcal{H}} = \hbar\frac{\omega_0}{2}\hat{\sigma}_z + \hbar\omega\hat{a}^\dagger\hat{a} + \hbar g(\hat{\sigma}^\dagger\hat{a} + \hat{\sigma}\hat{a}^\dagger). \tag{1.7}$$

Eq. (1.7) is commonly referred as the Hamiltonian of the JC model and the procedure used to obtain it is known as rotating wave approximation RWA.

1.1.2 Dynamics of the system: Rabi oscillations

Before solving the dynamics of the system, we notice that the total number of excitations $\hat{N}_e \equiv |e\rangle\langle e| + \hat{a}^\dagger\hat{a}$ is a constant of motion $[\hat{N}_e, \hat{\mathcal{H}}] = 0$. This fact reduces the whole Hilbert space of the system for the dynamics to the subspace spanned by the states $\{|e,n\rangle, |g,n+1\rangle\}$ for each initial number of photons n. The ground state of the system is the state $|g,0\rangle$, which does not evolve in time. According to this feature, the Hamiltonian (1.7) may rewritten in matrix form on this basis, fixing the number of photons n, as

$$(\hat{\mathcal{H}})_n = \frac{\hbar}{2}\begin{pmatrix} (2n+1)\omega + \Delta & \Omega_n \\ \Omega_n & (2n+1)\omega - \Delta \end{pmatrix} \tag{1.8}$$

where $\Delta = \omega - \omega_0$ is the detuning parameter and $\Omega_n \equiv 2g\sqrt{n+1}$ is the so-called Rabi frequency, which depends on the coupling constant g and the number of photons.
Setting a resonance condition $\Delta = 0$, the resulting dynamics is quite simple and it is described by the state $|\Psi\rangle(t) = c_{e,n}(t)|e,n\rangle + c_{g,n+1}(t)|g,n+1\rangle$ where the coefficients are

$$\begin{pmatrix} c_{e,n}(t) \\ c_{g,n+1}(t) \end{pmatrix} = \begin{pmatrix} \cos(\frac{\Omega_n}{2}t) & -\mathrm{i}\sin(\frac{\Omega_n}{2}t) \\ -\mathrm{i}\sin(\frac{\Omega_n}{2}t) & \cos(\frac{\Omega_n}{2}t) \end{pmatrix}\begin{pmatrix} c_{e,n}(0) \\ c_{g,n+1}(0) \end{pmatrix} \tag{1.9}$$

where the normalization condition $|c_{e,n}(t)|^2 + |c_{g,n+1}(t)|^2 = 1$ holds $\forall t$ and $\forall n$.
If the system is prepared initially in the state $|e,n\rangle$, the evolved coefficients are

$$c_{e,n}(t) = \cos\left(\frac{\Omega_n}{2}t\right) \tag{1.10a}$$

$$c_{g,n+1}(t) = -\mathrm{i}\sin\left(\frac{\Omega_n}{2}t\right) \tag{1.10b}$$

and the time evolution of the corresponding probabilities

$$P_{e,n}(t) = |c_{e,n}(t)|^2 = \frac{1}{2}\left[1 + \cos(\Omega_n t)\right] \tag{1.11a}$$

$$P_{g,n+1}(t) = |c_{g,n+1}(t)|^2 = \frac{1}{2}\left[1 - \cos(\Omega_n t)\right]. \tag{1.11b}$$

We remark that the evolved state oscillates between the maximally entangled states $|\Psi\rangle(t) = \frac{1}{\sqrt{2}}\left(|e,n\rangle \mp \mathrm{i}|g,n+1\rangle\right)$, at times $\Omega_n t = \frac{(2k+1)\pi}{2}$ (the sign - corresponds to k even and + to k odd) and the basis states $|e,n\rangle$ at $\Omega_n t = 2k\pi$ or $|g,n+1\rangle$ at $\Omega_n t = (2k+1)\pi$, with k integer. The periodic behavior of the probabilities (1.11) are usually called *Rabi oscillations*, particularly interesting when the cavity field is initially in the vacuum state. In this case it is remarkable the fact that the two-level atom can emit a photon only to the single accessible cavity mode and, after some time, absorbing it again according to the so-called phenomenon of reversible spontaneous emission.

1.2 Elements of open system dynamics

In this section we provide some basic elements of the theory describing the dynamics of a quantum system interacting with a dissipative environment. In particular we describe how to derive a master equation (ME) in the Lindblad form through a deductive approach coming from quantum information principles. Finally we illustrate a very efficient numerical protocol to solve such a ME, called Monte Carlo wavefunction (MCWF) method [17].

1.2.1 Kraus representation of operators

Let us consider a system A whose state is given in terms of a density operator $\hat{\rho}_A$ with an associated Hilbert space $\mathbb{H}_A$. We define a linear quantum map

$$\hat{\rho}_A \longrightarrow \hat{\mathcal{L}}(\hat{\rho}_A) \tag{1.12}$$

with the following properties:

1. $\hat{\mathcal{L}}$ is linear: $\hat{\mathcal{L}}(p\hat{\rho}_A + q\hat{\rho}'_A) = p\hat{\mathcal{L}}(\hat{\rho}_A) + q\hat{\mathcal{L}}(\hat{\rho}'_A)$
2. $\hat{\mathcal{L}}$ is hermitean: $[\hat{\mathcal{L}}(\hat{\rho}_A)]^\dagger = \hat{\mathcal{L}}(\hat{\rho}_A)$
3. $\hat{\mathcal{L}}$ is trace-preserving: $Tr[\hat{\mathcal{L}}(\hat{\rho}_A)] = \mathbb{1}$
4. $\hat{\mathcal{L}}$ is positive: ${}_A\langle\phi|\hat{\mathcal{L}}(\hat{\rho}_A)|\phi\rangle_A \geq 0 \quad \forall|\phi\rangle_A \in \mathbb{H}_A$
5. $\hat{\mathcal{L}}$ is complete-positive (CP): suppose A is entangled with another system B and the global system described by $\hat{\rho}_{AB}$. The whole dynamics is given by the operator $\hat{\mathcal{L}}(\hat{\rho}_A)\otimes \mathbb{1}_B$ and the complete positivity reads ${}_A\langle\phi|\hat{\mathcal{L}}(\hat{\rho}_A)\otimes\mathbb{1}_B|\phi\rangle_A \geq 0 \quad \forall|\phi\rangle_{AB} \in \mathbb{H}_{AB}$.

Suppose that the system A is coupled to an environment B, then the evolution of the system A only is described in terms of the quantum map given by the partial trace over the degrees of freedom of B:

$$\hat{\mathcal{L}}(\hat{\rho}_A) = Tr_B[\hat{U}(\hat{\rho}_A \otimes |\phi_0\rangle_B\langle\phi_0|)\hat{U}^\dagger] \tag{1.13}$$

where $|\phi_0\rangle_B$ is a reference state of B, chosen among an orthonormal basis $\{|\phi_\mu\rangle_B\}$ of $\mathbb{H}_B$, and $\hat{U}$ is the unitary evolution of A and B. Eq. (1.13) may be rewritten as

$$\hat{\mathcal{L}}(\hat{\rho}_A) = \sum_\mu {}_B\langle\phi_\mu|\hat{U}|\phi_0\rangle_B \hat{\rho}_A {}_B\langle\phi_0|\hat{U}^\dagger|\phi_\mu\rangle_B = \sum_\mu \hat{M}_\mu \hat{\rho}_A \hat{M}_\mu^\dagger \tag{1.14}$$

and it is known as *operator-sum representation* or *Kraus representation*, where the Kraus operators are $\hat{M}_\mu \equiv {}_B\langle\phi_\mu|\hat{U}|\phi_0\rangle_B$. Since the quantum map must fulfill the trace-preserving property $Tr[\hat{\mathcal{L}}(\hat{\rho}_A)] = \mathbb{1}$, the Kraus operators must satisfy the completeness relation

$$\sum_\mu \hat{M}_\mu^\dagger \hat{M}_\mu = \mathbb{1} \tag{1.15}$$

that must be true[1] for all $\hat{\rho}_A$. There is a nice interpretation that can be given to the Kraus representation. Imagine that a measurement of the environment is performed in the basis $|\phi\rangle_\mu$ after the unitary trasnformation $\hat{U}$ has been applied, then the state of the system given that outcome μ occurs, is

$$\hat{\rho}_{A,\mu} = \frac{\hat{M}_\mu \hat{\rho}_A \hat{M}_\mu^\dagger}{Tr[\hat{M}_\mu \hat{\rho}_A \hat{M}_\mu^\dagger]}. \tag{1.16}$$

The probability of outcome μ is given by

$$p(\mu) = Tr[\hat{M}_\mu \hat{\rho}_A \hat{M}_\mu^\dagger] \tag{1.17}$$

thus

$$\hat{\mathcal{L}}(\hat{\rho}_A) = \sum_\mu p(\mu)\hat{\rho}_{A,\mu} = \sum_\mu \hat{M}_\mu \hat{\rho}_A \hat{M}_\mu^\dagger. \tag{1.18}$$

The action of the quantum map is equivalent to taking the state $\hat{\rho}_A$ and randomly replacing it by $\hat{\rho}_{A,\mu}$ with probability $p(\mu)$. It is very similar to the concept of noisy communication channels used in classical information theory [11].

1.2.2 Master equation in the Lindblad form

Here we use a deductive approach [2] from Quantum Information principles to derive a ME in the standard Lindblad form, without any specific model for the environment. We want to obtain a first-order differential ME for a system A in contact with an environment E and we begin with writing

$$\hat{\rho}_A(t+\tau) - \hat{\rho}_A(t) = \tau \frac{d\hat{\rho}_A}{dt} \tag{1.19}$$

[1] There exist, actually, quantum operations for which $\sum_\mu \hat{M}_\mu^\dagger \hat{M}_\mu \leq \mathbb{1}$, but they describe processes in which an extra information about what occurred in the process is obtained by measurements.

assuming that the environment E is a "large" system, with many degrees of freedom, whose evolution is not appreciably affected by its interaction with A, such as $\tau \ll T_r$, where T_r is the characteristic time of A's evolution. Then $\hat{\rho}_A$ is computed at successive time steps τ. Suppose that a time t the global system A+E state is expressed as a tensor product

$$\hat{\rho}_{AE}(t) = \hat{\rho}_A(t) \otimes \hat{\rho}_{E,0} \tag{1.20}$$

with $\hat{\rho}_{E,0}$ the steady state of E. This assumption comes from the Markov approximation and it means that when the conditions of a large environment are met, all happens for the incremental evolution of $\hat{\rho}_A$ over a finite time interval τ as if the A+E system was initially described by Eq. (1.20). We apply the Kraus representation formalism at the infinitesimal steps τ

$$\hat{\rho}_A(t+\tau) = \hat{\mathcal{L}}_\tau(\hat{\rho}_A(t)) = \sum_{\mu=0}^{N_\mu - 1} \hat{M}_\mu(\tau)\hat{\rho}_A(t)\hat{M}_\mu^\dagger(\tau) \tag{1.21}$$

where the $\hat{M}_\mu(\tau)$ are $N_\mu \leq N_A^2$, the dimension of $\mathbb{H}_A$. Since $\hat{\mathcal{L}}_\tau(\hat{\rho}_A(t)) = \hat{\rho}_A(t) + O(\tau)$ where $O(\tau)$ is a first-order contribution in τ, one of the operators $\hat{M}_\mu$ should be of the order of unity. We write it, without loss of generality, as

$$\hat{M}_0(\tau) = \mathbb{1} - \mathrm{i}\hat{K}\tau + O(\tau^2) \tag{1.22}$$

where $\hat{K}$ is independent of τ. We build now the hermitian and anti-hermitian parts in $\hat{K}$, defining two hermitian operators

$$\hat{H} = \hbar\frac{\hat{K} + \hat{K}^\dagger}{2} \tag{1.23a}$$

$$\hat{J} = \mathrm{i}\frac{\hat{K} - \hat{K}^\dagger}{2} \tag{1.23b}$$

from which we obtain

$$\hat{K} = \frac{\hat{H}}{\hbar} - \mathrm{i}\hat{J}. \tag{1.24}$$

Up to the first order in τ we have

$$\hat{M}_0(\tau)\hat{\rho}_A(t)\hat{M}_0^\dagger(\tau) = \hat{\rho}_A(t) - \frac{\mathrm{i}\tau}{\hbar}[\hat{H}, \hat{\rho}_A(t)] - \tau(\hat{J}\hat{\rho}_A(t) + \hat{\rho}_A(t)\hat{J}) \tag{1.25}$$

where we recognize a commutator describing a unitary evolution induced by the Hamiltonian-like term $\hat{H}$. This term can be easily substituted by $\hat{H} \to \hat{\mathcal{H}}_A$, the Hamiltonian of the system A, including a renormalization of the energy levels of A, due to small shifts induced by the interaction with the environment E. All other terms, for $\mu \neq 0$ in the Kraus sum are of order τ and we can write

$$\hat{M}_\mu(\tau) = \sqrt{\tau}\hat{L}_\mu \tag{1.26}$$

which must satisfy the normalization condition for Kraus operators

$$\sum_{\mu=0}^{N_k - 1} \hat{M}_\mu^\dagger(\tau)\hat{M}_\mu(\tau) = \mathbb{1} \Longrightarrow \mathbb{1} - 2\tau\hat{J} + \tau\sum_{\mu\neq 0}\hat{L}_\mu^\dagger\hat{L}_\mu = \mathbb{1}$$

leading to the relation

$$\hat{J} = \frac{1}{2}\sum_{\mu\neq 0}\hat{L}_\mu^\dagger \hat{L}_\mu. \tag{1.27}$$

Finally, from Eq. (1.19), we obtain the first-order ME

$$\frac{d\hat{\rho}_A(t)}{dt} = -\frac{\mathrm{i}}{\hbar}[\hat{\mathcal{H}}_A, \hat{\rho}_A(t)] + \sum_{\mu\neq 0}\left(\hat{L}_\mu\hat{\rho}_A(t)\hat{L}_\mu^\dagger - \frac{1}{2}\hat{L}_\mu^\dagger\hat{L}_\mu\hat{\rho}_A(t) - \frac{1}{2}\hat{\rho}_A(t)\hat{L}_\mu^\dagger\hat{L}_\mu\right) \tag{1.28}$$

This derivation of the ME is based on very general arguments, stemming from the Kraus sum formulation and the Markov approximation.

Let us now consider the evolution of $\hat{\rho}_A(t)$ from the point of view of measurement, when A is in contact with a system B smaller than E (a so-called "environment simulator"), in a Hilbert space with a dimension of the same number of Kraus operators. Moreover we consider a complete orthonormal basis $|\phi_\mu\rangle_B$ whose elements are associated to each Kraus operator $\hat{M}_\mu(\tau)$. We suppose that, at time t, the global system is in the product state $|\phi\rangle_A \otimes |\phi_0\rangle_B$, where, for simplicity, we consider a pure state[2] for the system A. This state evolves according to a unitary operator $\hat{U}$:

$$\begin{aligned}\hat{U}(|\phi\rangle_A \otimes |\phi_0\rangle_B) &= (\hat{M}_0|\phi\rangle_A)\otimes|\phi_0\rangle_B + \sum_{\mu\neq 0}(\hat{M}_\mu|\phi\rangle_A)\otimes|\phi_\mu\rangle_B = \\ &= \left[\mathbb{1} - \frac{\mathrm{i}}{\hbar}\hat{\mathcal{H}}_A\tau - \hat{J}\tau\right]|\phi\rangle_A\otimes|\phi_0\rangle_B + \sqrt{\tau}\sum_{\mu\neq 0}(\hat{L}_\mu|\phi\rangle_A)\otimes|\phi_\mu\rangle_B\end{aligned} \tag{1.29}$$

An unread measurement of B for an observable whose eigenvectors are $|\phi_\mu\rangle_B$, provides the evolution of A according to the quantum map $\hat{\mathcal{L}}_\tau(|\phi\rangle_A\langle\phi|)$, as in Eq. (1.13). On the other hand, if a measurement is performed on system B, we have already shown that the same result of an unread measurement is recovered as in Eq. (1.18). Applied to the ME (1.28), where the Kraus operators have an explicit form, we obtain two cases:

1. if the result of a measurement on B is $|\phi_0\rangle_B$, the projected state of A is

$$|\phi\rangle_{0,A} = \frac{\hat{M}_0}{\sqrt{p_0}}|\phi\rangle_A = \frac{\mathbb{1} - \frac{\mathrm{i}}{\hbar}\hat{\mathcal{H}}_A\tau - \hat{J}\tau}{\sqrt{p_0}}|\phi\rangle_A \tag{1.30}$$

with a probability

$$p_0 = {}_A\langle\phi|\hat{M}_0^\dagger\hat{M}_0|\phi\rangle_A = \mathbb{1} - \tau\sum_{\mu\neq 0}{}_A\langle\phi|\hat{L}_\mu^\dagger\hat{L}_\mu|\phi\rangle_A. \tag{1.31}$$

When this event occurs, with a probability p_0 close to unity, A undergoes an infinitesimal change, which can be viewed as an elementary time step in a continuous, non-unitary evolution described by an effective non-hermitian Hamiltonian

$$\hat{\mathcal{H}}_e = \hat{\mathcal{H}}_A - \mathrm{i}\hbar\hat{J} = \hat{\mathcal{H}}_A - \frac{\mathrm{i}\hbar}{2}\sum_\mu \hat{L}_\mu^\dagger\hat{L}_\mu \tag{1.32}$$

[2]The general case is recovered simply by the property of linearity of the quantum map $\hat{\mathcal{L}}$, when a density matrix of A is decomposed as $\hat{\rho}_A = \sum_i q_i|\phi^{(i)}\rangle_A\langle\phi^{(i)}|$, where $|\phi^(i)\rangle_A$ is a pure state.

2. if the result of a measurement on B is $|\phi_0\rangle_\mu$, with $\mu \neq 0$, the projected state of A is

$$|\phi\rangle_{\mu,A} = \sqrt{\frac{\tau}{p_\mu}}\hat{L}_\mu|\phi\rangle_A \tag{1.33}$$

with a small probability

$$p_\mu = \tau_A\langle\phi|\hat{L}_\mu^\dagger\hat{L}_\mu|\phi\rangle_A \tag{1.34}$$

When such an event occurs, with a small probability of order τ, the state of A undergoes a drastic change. It jumps from $|\phi\rangle_A$ to the completely different state $\hat{L}_\mu|\phi\rangle_A$ (within a normalization). The evolution of A is thus mostly a slow non-unitary evolution, where $\hat{L}_\mu$ are usually called *jump operators*[3] (or *collapse operators*).

By combining this two cases and the fact that the measurement process is fictitious, in the sense that it is equivalent to an evolution obtained by unread measurements, the ME in the Lindblad form (1.28) can be written as

$$\frac{d\hat{\rho}_A(t)}{dt} = -\frac{\mathrm{i}}{\hbar}\left(\hat{\mathcal{H}}_e\hat{\rho}_A(t) - \hat{\rho}_A(t)\hat{\mathcal{H}}_e^\dagger\right) + \sum_{\mu\neq 0}\hat{L}_\mu\hat{\rho}_A(t)\hat{L}_\mu^\dagger. \tag{1.35}$$

1.2.3 The MCWF method

Most often, the Lindblad master equation which describes the relaxation process in a complete way cannot be solved analytically. One has then to resort to numerical solutions, which are difficult to obtain when A is large. The number of elements of the density matrix, $\hat{\rho}_A$, is the square of the Hilbert space dimension, N_A^2. The calculations rapidly become too cumbersome to be performed, even with supercomputers. In comparison, it is much simpler to follow the Hamiltonian evolution of a wave function, since it involves only N_A complex variables.

We have seen above that the environment simulator description allows us to understand the systems relaxation from t to $t+\tau$ as an elementary unitary evolution entangling A to an external system B having as many states as the number of Lindblad operators plus one. The infinitesimal evolution of the density matrix is recovered by tracing the quantum state at $t+\tau$ over all results of measurements virtually performed on B. Computing the quantum state resulting from the elementary unitary A+B interaction is as simple as following an ordinary Hamiltonian evolution. By extending this procedure to the whole time interval, we now introduce the notion of random evolutions of the systems state vectors, quantum Monte Carlo trajectories, whose average over many realizations allow us to recover the full density matrix [17]. This is a very efficient scheme for numerical simulations.

The evolution is divided in small time steps, each with a duration τ. At the end of the first step, a measurement is performed on system B (the environment simulator for E) indicating

[3] We point out that we will consider as Kraus operators only a small finite number of jump operators, corresponding to the dissipative processes of photon cavity loss and atomic spontaneous emission.

whic jump occurred, if any. Instead of tracing over all possible measurement results, we assume that it is kept a record of the obtained value. This measurment thus project A onto a new state vector which is taken as the initial condition for the next step. The system B is then re-prepared in its neutral state $|\phi_\mu\rangle_B$, which reflects the fact that the short-memory real environment E is not modified during the relaxation process (Markov approximation) and that its entanglement with A, at the beginning of each time interval, can be neglected to compute the system's state at the end of this interval.
In a numerical simulation the measurement performed on B are conditioned to classical dice tosings, reproducing the probabilities of outcomes of the various jumps undergone by the system. The recursive algorithm to simulate the evolution of A is as follows:

- from the initial state of A at time t, $|\phi(t)\rangle_A$, compute the no-jump probability p_0 in Eq. (1.31) and the $N_k - 1$ jump probabilities p_μ in Eq. (1.34) associated to the jump operators $\hat{L}_\mu$;
- choose whether a jump occurs or not and if it occurs, choose randomly the corresponding jump operator $\hat{L}_\nu$. These choices are performing by drawing a single random value $0 \leq r \leq 1$. No jump occurs if $r < p_0$. If a jump takes place, its index ν is the smallest integer such that $\sum_{\mu=0}^{\nu} p_\mu > r$;
- in the no-jump case, compute the elementary evolution of $|\phi(t)\rangle_A$ under the effective non-hermitian Hamiltonian (1.32). Renormalize the final result using the value of p_0 in Eq. (1.30);
- in the event of a jump, compute the new state and renormalize it with p_ν in Eq. (1.33);
- repeat the sequence of steps with the resulting state $|\phi(t+\tau)\rangle_A$ as a new initial state.

A large number $N_{\rm tr}$ of individual quantum trajectories $|\phi_j(t)\rangle_A$, all starting from the same initial state $|\phi(0)\rangle_A$, are constructed in this way. From the definition of the procedure, the time-dependent density matrix $\overline{\Pi}(t) = \frac{1}{N_{\rm tr}} \sum_j^{\rm tr} |\phi_j(t)\rangle_A \langle\phi_j(t)|$ is the average over the $N_{\rm tr}$ trajectories. After a time interval τ, $\overline{\Pi}(t+\tau)$ is both a mixture of the no-jump and the jump wavefunctions, with weights p_0 and $1-p_0$, and the average of $\hat{\rho}_{A,j}(t+\tau)$:

$$\begin{aligned}\overline{\Pi}(t+\tau) &= \frac{1}{N_{\rm tr}} \sum_{j=1}^{N_{\rm tr}} \left[p_0 \frac{\hat{M}_0 |\phi_j(t)\rangle_A}{\sqrt{p_0}} \frac{{}_A\langle\phi_j(t)|\hat{M}_0^\dagger}{\sqrt{p_0}} + \sum_\mu p_\mu \frac{\hat{L}_\mu |\phi_j(t)\rangle_A}{\sqrt{p_\mu/\tau}} \frac{{}_A\langle\phi_j(t)|\hat{L}_\mu^\dagger}{\sqrt{p_\mu/\tau}} \right] \\ &= \overline{\Pi}(t) - \frac{\mathrm{i}}{\hbar}\tau[\hat{\mathcal{H}}_A, \overline{\Pi}(t)] + \tau \sum_{\mu\neq 0} \hat{L}_\mu \overline{\Pi}(t) \hat{L}_\mu^\dagger \end{aligned} \tag{1.36}$$

that combined with the first derivative $d\overline{\Pi}/dt = (\overline{\Pi}(t+\tau) - \overline{\Pi}(t))/\tau$ we obtain the ME in the Lindblad form

$$\frac{d\overline{\Pi}(t)}{dt} = -\frac{\mathrm{i}}{\hbar}(\hat{\mathcal{H}}_e \overline{\Pi}(t) - \overline{\Pi}(t)\hat{\mathcal{H}}_e) + \sum_{\mu\neq 0} \hat{L}_\mu \overline{\Pi}(t) \hat{L}_\mu^\dagger. \tag{1.37}$$

Since $\overline{\Pi}(0)$ coincides, by construction, with the initial density matrix, then $\hat{\rho}_A(t)$ and $\overline{\Pi}(t)$ coincide at all times, showing that Lindblad ME and Monte Carlo approaches are fully equivalent.

1.3 Bipartite entanglement quantification

We focus here on the case of bipartite entanglement, which has been widely studied and for which by now it exists a solid theory. We analyze the two main categories of quantum states, pure and mixed, and then we show some ways to establish whether a state is separable or inseparable.

1.3.1 Pure states

Suppose we are given two quantum discrete systems each one described by states in Hilbert spaces $\mathcal{H}_A$ and $\mathcal{H}_B$. The composite system is in a quantum state that belongs to a greater Hilbert state, tensor prouct of the previous two $\mathcal{H} = \mathcal{H}_A \otimes \mathcal{H}_B$. Any state is a vector $|\Psi\rangle \in \mathcal{H}$ written in the form:

$$|\Psi\rangle = \sum_{i,j}^{d_A,d_B} c_{ij}|a_i\rangle \otimes b_j \tag{1.38}$$

where d_A and d_B are the dimensions of $\mathcal{H}_A$ and $\mathcal{H}_B$ and c_{ij} are complex coefficients.
A pure state $|\Psi\rangle \in \mathcal{H}$ is called *separable* if we can find states $|\phi\rangle_A \in \mathcal{H}_A$ and $|\phi\rangle_B \in \mathcal{H}_B$ such that

$$|\Psi\rangle = |\phi\rangle_A \otimes |\phi\rangle_B$$

otherwise the state $|\Psi\rangle$ is called *entangled*. Separable states (or product states) can be locally prepared and measured without any mutual influence on each subsystem A or B.
A very useful tool is the so-called *Schmidt decomposition*, for which every pure bipartite state can be written as a sum of bi-orthogonal terms. There exists at least one orthonormal basis $\{|u_k\rangle \otimes |v_k\rangle\}$ in $\mathcal{H}$ such that

$$|\Psi\rangle = \sum_{k}^{R} \lambda_k |u_k\rangle \otimes |v_k\rangle$$

where λ_k are non-negative real numbers, square roots of the eigenvalues of the matrix $CC^\dagger$ (with $C = (c_{ij})$), satisfying $\sum_k \lambda_k^2 = 1$, known as *Schmidt coefficients*. The number $R \leq \min\{d_A, d_B\}$ is also called the *Schmidt number* (or *Schmidt rank*) of $|\Psi\rangle$ and it coincides with the number of non-zero amplitudes λ_k. This is the powerful consequence of the Schmidt decomposition: the Schmidt number of a state is greater than 1 *if and only if* it is entangled. On the contrary when it is equal to one, it means that the bipartite pure state is factorizable, that is separable.
Now we give two examples of two-dimensional bipartite states (qubits) in Schmidt form that

are very useful in quantum computation and quantum information theory. The first is the *bell basis* formed of these four pure states

$$|\Psi^{\pm}\rangle = \frac{1}{\sqrt{2}}\left(|01\rangle \pm |10\rangle\right)$$
$$|\Phi^{\pm}\rangle = \frac{1}{\sqrt{2}}\left(|00\rangle \pm |11\rangle\right)$$

in the computational basis, which are symmetrical and antisymmetrical under qubit exchange. Another basis of two qubits that turns out to be natural for concurrence-based entanglement studies (see ahead), is the so called *magic basis*

$$|m_1\rangle = \frac{1}{2}\left(|00\rangle + |11\rangle\right)$$
$$|m_2\rangle = \frac{\mathrm{i}}{2}\left(|00\rangle - |11\rangle\right)$$
$$|m_3\rangle = \frac{\mathrm{i}}{2}\left(|01\rangle + |10\rangle\right)$$
$$|m_4\rangle = \frac{1}{2}\left(|01\rangle - |10\rangle\right)$$

which is similar to the Bell basis except for phases and norm. In both these cases the Schmidt number is equal to 2 and it means that these states are all inseparable, in particular they are maximally entangled states.

1.3.2 Mixed states

The definition of entanglement can be extended to include mixed states, in particular those states which cannot be written as convex combination of products

$$\rho = \sum_k p_k \rho_k^A \otimes \rho_k^B \tag{1.39}$$

where $p_k \in [0,1]$ and $\sum_k p_k = 1$, ρ^A and ρ^B being statistical operators on subsystem Hilbert space $\mathcal{H}_A$ and $\mathcal{H}_B$. Quantum states in the form of Eq. 1.39 are by definition mixtures of product states and so can only be created by local oprations and classical communication (LOCC) from pure product states.

1.3.3 Separability criteria and entanglement measures

Given the definition of entanglement and separability it is quite natural to ask whether a given density matrix is separable or not. This constitutes the so-called *separability problem*, to which several criteria and entanglement measures are addressed. The criteria help in the detection of entanglement while the entanglement measures (or entanglement monotones) quantify the amount of entanglement of a quantum state. As explained in detail in the literature [11], it is desirable that a generic entanglement quantifier $E(\rho)$ fulfills the following requirements:

(i) $E(\rho)$ is zero if ρ is separable;

(ii) an entanglement measure is invariant under local unitary transformations $E(\rho) = E(U_A \otimes U_B \rho U_A^\dagger \otimes U_B^\dagger)$;

(iii) as entanglement cannot be created by LOCC, it is reasonable that $E(\rho)$ does not increase under a LOCC positive map Λ^{LOCC}, that is $E[\Lambda^{\mathrm{LOCC}}(\rho)] \leq E(\rho)$;

(iv) entanglement has to decrease under mixing of two or more states $E(\sum_k p_k \rho_k) \leq \sum_k p_k E(\rho_k)$. This the convexity property that express the fact that if one starts from an ensamble ρ_k of states and looses information about the single ρ_k, then the entanglement decreases.

PPT criterion and negativity

Let us start with the criterion called *positive partial transposition* (PPT). We note that a generic density matrix of a compiste quantum system, can be always expanded in a chosen product basis as

$$\rho = \sum_{i,j}^{N} \sum_{k,l}^{M} \rho_{ij,kl} |i\rangle\langle j| \otimes |k\rangle\langle l|.$$

The operation of partial transposition of ρ is obtained by transposing only one of the two subsystems. Thus, for instance, the partial transposition with respect to the subsystem A is

$$\rho^{T_A} = \sum_{i,j}^{N} \sum_{k,l}^{M} \rho_{ij,kl} |j\rangle\langle i| \otimes |k\rangle\langle l|$$

and similarly ρ^{T_B} can be obtained by exchanging only k and l. The PPT criterion (also called Peres-Horodecki criterion), originally introduced in [18], affirms that if ρ is a bipartite separable state then ρ is PPT, that is it is positive semidefinite matrix, with no negative eigenvalues:

$$\rho^{T_A} \geq 0 \Leftrightarrow \rho^{T_B} \geq 0.$$

This powerful theorem allows to easily detect entanglement by calculating the spectrum of the partial transpose of a density matrix. If there is at least one negative eigenvalue, the state is entangled. But PPT is only a necessary condition for separability and it is not sufficient to ensure a state to be separable. It was shown that the PPT criterion is actually necessary and sufficient for bipartite systems of dimension 2×2 or 2×3. This statement goes under the name of Horodecki theorem [19] and formally affirms that if ρ is a state in a 2×2 or 2×3 system, then $\rho^{T_A} \geq 0$ implies that ρ is separable.
The amount of violation of the PPT condition can be used to quantify entanglement. In [20] the authors introduced an entanglement measure called *negativity*, which takes the mathematical form:

$$N(\rho) = \frac{\|\rho^{T_B}\|_1 - 1}{2} \tag{1.40}$$

where $\|\ldots\|_1$ denotes the trace norm, i.e. the sum of all singular values, of the partially transpose density matrix. The negativity is quite easy to compute and it is a convex measure, but, by construction, it fails to recognize entanglement in PPT states.

Entanglement of formation

The entanglement of formation is defined as the convex roof of the von Neumann entropy

$$E_F(\hat{\rho}) = \inf_{p_k, |\phi_k\rangle} \sum_k p_k S[(\hat{\rho}_A)_k] \tag{1.41}$$

where the infimum is taken over all possible decompositions of $\hat{\rho}$, i.e., over all p_k and $|\phi_k\rangle$ with $\hat{\rho} = \sum_k p_k |\phi_k\rangle\langle\phi_k|$. Physically, the entanglement of formation may be interpreted as a minimal number of singlets that is required to build a single copy of the state.

Concurrence

A practical measure of bipartite entanglement that has a geometrical meaning and can often be easily calculated is the *concurrence*, firstly introduced by Hill and Wootters [22] in 1997 for pure states according to the definition

$$C(|\Psi\rangle) = \sqrt{2(1 - Tr[\hat{\rho}_A^2])} \tag{1.42}$$

where $\hat{\rho}_A$ denotes the reduced state of a bipartite pure state $|\Psi\rangle$ made of two parties A and B. Another way of representing C for two qubits is

$$C(|\Psi\rangle) = \langle\Psi|\theta|\Psi\rangle \tag{1.43a}$$

$$\theta\Psi = \sigma_y \otimes \sigma_y \Psi^* \tag{1.43b}$$

with Ψ^* the complex conjugate of Ψ on the standard basis and σ_y is a Pauli matrix. It turns out that this last definition is extended to mixed states via the convex roof construction. Namely one has

$$C(\hat{\rho}) = \max\{0, \lambda_1 - \lambda_2 - \lambda_3 - \lambda_4\} \tag{1.44}$$

where the λ_i are the decreasingly ordered eigenvalues of the matrix

$$X = \sqrt{\sqrt{\hat{\rho}}(\sigma_y \otimes \sigma_y)\hat{\rho}^*(\sigma_y \otimes \sigma_y)\sqrt{\hat{\rho}}}.$$

The importance of the concurrence measure stems from the fact that it allows to compute entanglement of formation for two qubits according to

$$E_F(\hat{\rho}) = H\left(\frac{1 + \sqrt{1 - C^2(\hat{\rho})}}{2}\right) \tag{1.45}$$

where H is the binary entropy $H(x) = -x\log_2 x - (1-x)\log_2(1-x)$. For other dimensions, however, such a relation does not hold and the physical interpretation of the concurrence is not so clear. Moreover, the concurrence is not additive.

1.4 Multipartite entanglement quantification

In this section we discuss the structure of entanglement when more than two parties are involved. It turns out that this structure is much richer than the structure of entanglement in the bipartite case, especially, that several inequivalent classes of entanglement exist. We will not present the complete set of results on the multipartite entanglement case, but we limit ourselves in describing the main achievements and the still open problems related to it.

1.4.1 Entanglement of three qubits

Let us first consider pure three-qubit states. There are two different types of separability: the "fully separable" states that can be written as

$$|\phi\rangle_{A|B|C} = |\alpha\rangle_A \otimes |\beta\rangle_B \otimes |\gamma\rangle_C \tag{1.46}$$

and the "biseparable" states that can be written as a product state in the bipartite system. A biseparable state can be created, if two of the three qubits are grouped together to one party. There are three possibilities of grouping two qubits together, hence there are three classes of biseparable states:

$$|\phi\rangle_{A|BC} = |\alpha\rangle_A \otimes |\delta\rangle_{BC} \tag{1.47a}$$

$$|\phi\rangle_{B|AC} = |\alpha\rangle_B \otimes |\delta\rangle_{AC} \tag{1.47b}$$

$$|\phi\rangle_{C|AB} = |\alpha\rangle_C \otimes |\delta\rangle_{AB} \tag{1.47c}$$

here $|\delta\rangle$ denotes a two-party state that might be entangled. Finally, a pure state is called "genuine tripartite entangled" if it is neither fully separable nor biseparable. Examples of such states are the Greenberger-Horne-Zeilinger (GHZ) state [23]

$$|GHZ\rangle = \frac{1}{\sqrt{2}}(|000\rangle + |111\rangle), \tag{1.48}$$

and the so-called W state

$$|W\rangle = \frac{1}{\sqrt{3}}(|100\rangle + |010\rangle + |001\rangle). \tag{1.49}$$

It was proved in [24] that there are two different equivalence classes of genuine tripartite entangled states, which cannot be transformed into another by SLOCC. One class, the class of GHZ states is represented by the GHZ state (1.48). The other class, the class of W states can be transformed via SLOCC into (1.49). In this sense there are two different classes of tripartite entanglement. There are many more pure GHZ class states than W class states: by local unitary operations one can transform any pure three-qubit state into

$$|\Psi\rangle = \lambda_0|000\rangle + \lambda_1 e^{i\theta}|100\rangle + \lambda_2|101\rangle + \lambda_3|110\rangle + \lambda_4|111\rangle \tag{1.50}$$

where $\lambda_i \geq 0$, $\sum_i \lambda_i^2 = 1$ and $\theta \in [0; \pi]$ (see [25]). Thus, six real parameters are necessary to characterize the nonlocal properties of a pure state. For the W class states, however, $\theta = \lambda_4 = 0$ holds, which shows that they are a set of measure zero in the set of all pure states.

Physically, there are also differences between the two classes: on one hand, the GHZ state is maximally entangled and a generalization of the Bell states of two qubits. For instance, for the most known Bell inequalities the violation is maximal for GHZ states. On the other hand, the entanglement of the W state is more robust against particle losses: if one particle is lost in the GHZ state, the state $\hat{\rho}_{AB} = Tr_C[|GHZ\rangle\langle GHZ|]$ is separable, for the W state the resulting reduced density matrix $\hat{\rho}_{AB} = Tr_C[|W\rangle\langle W|]$ is entangled. Indeed, it can be shown that the W state is the state with the maximal possible bipartite entanglement in the reduced two-qubit states.

1.4.2 Tangle measure

The three-tangle τ (or residual tangle), introduced in [26], is an entanglement measure for three-qubit states. An arbitrarily pure three-qubit state fulfills the monogamy relation

$$C^2_{A|BC}(|\Psi\rangle) = C^2_{AB}(\hat{\rho}_{AB}) + C^2_{AC}(\hat{\rho}_{AC}) + \tau(|\Psi\rangle) \tag{1.51}$$

where $C^2_{A|BC}(|\Psi\rangle) = 2\sqrt{\det(\hat{\rho}_A)}$ is the concurrence between A and the other two qubits, and $C^2_{AB}(\hat{\rho}_{AB})$ is the concurrence between A and B. It can be proved [24], exploiting the fact that it is invariant under local unitaries, that the 3-tangle is an entanglement monotone, i.e. it decreases on average under LOCC in all the three parties. The three-tangle may be zero for pure states that are three-entangled, i.e., that are not a product with respect to any cut. An example is the W state and a large number of pure states that are called W-like states, although none of their qubits is separable (the three reduced states are all of them non-pure). The tangle vanishes on any states that are separable under any cut, and is non-zero, for example, on the GHZ state. Therefore, the three-tangle is not a good measure of full tripartite entanglement even for pure states, as pointed out in [27].

There was an attempt by Wong and Christensen [28] to generalize the tangle measure to the case of N qubits, to what was called the N-tangle measure. We recall that the pure-state concurrence for two qubits was also defined as in (1.43) in order to get a more general form for the case of N qubits

$$C_N = |\langle\Psi|\tilde{\Psi}\rangle|^2 \tag{1.52a}$$

$$|\tilde{\Psi}\rangle = \sigma_y^{\otimes N}|\Psi^*\rangle \tag{1.52b}$$

where $|\tilde{\Psi}\rangle$ stands for an N-qubit state. As proved in [28] the N-tangle measure $\tau_N = C_N^2$ in the case of N even. The N-tangle is a good measure of entanglement since it possess the property to be a monotone under LOCC, as proved for the 3-tangle. Let us have a look at

the generalized form $|W_N\rangle$ of the state $|W\rangle$ (1.49). We define the state

$$|W_N\rangle = \frac{1}{\sqrt{N}}|N-1,1\rangle \tag{1.53}$$

where $|N-1,1\rangle$ denotes the totally symmetric state including $N-1$ zeros and 1 ones. For example, we obtain for $N-4$,

$$|W_4\rangle = \frac{1}{\sqrt{4}}(|0001\rangle + |0010\rangle + |0100\rangle + |1000\rangle).$$

One immediately observes that the entanglement of this state is ery robust against particle losses, i.e. the state remains entangled even if any $N-2$ parties lose the information about their particle. This means that any two out of N parties possess an entangled state, independently of whether the remaining $(N-2)$ parties decide to cooperate with them or not. This can be seen by computing the reduced density operator $\hat{\rho}_{AB}$ of $|W_N\rangle$, by tracing out all but the first and the second systems. By symmetry of the state (1.53), we have that all reduced density operators $\hat{\rho}_{\kappa\mu}$ are identical and we obtain

$$\hat{\rho}_{\kappa\mu} = \frac{1}{N}\left(2|\Psi^+\rangle\langle\Psi^+| + (N-2)|00\rangle\langle 00|\right). \tag{1.54}$$

The concurrence can easily be determined, according to (1.44), to be $C_{\kappa\mu}(|W_N\rangle) = \frac{2}{N}$, which shows that $\hat{\rho}_{\kappa\mu}$ is entangled. A conjecture in [24] affirms that the average value of the squared concurrence for (1.53)

$$\frac{2}{N(N-1)}\sum_{\kappa}\sum_{\mu\neq\kappa} C^2_{\kappa\mu}(|W_N\rangle) = \overline{C^2} = \frac{4}{N^2} \tag{1.55}$$

is again the maximal value achievable for any state of N qubits.

1.4.3 Tripartite negativity

An ideal measure of the full tripartite entanglement of three qubits should have at least the following characteristics:

i) to be zero for any fully separable or biseparable state and non-zero for any fully entangled state;

ii) to be invariant under LU;

iii) to be non increasing under LOCC, that is, to be an entanglement monotone.

Von Neumann's entropy of reduced states is an unambiguous measure of entanglement only for pure states, and the concurrence, although well defined for non-pure states of two qubits, has been extended in a practical way to higher dimensions only for pure states. Therefore, in order to have a measure of tripartite entanglement valid also for non-pure states we will use the negativity. In [27] it is defined the following "tripartite negativity" of a state $\hat{\rho}$ as

$$N_{ABC}(\hat{\rho}) = (N_{A-BC}N_{B-AC}N_{C-AB})^{1/3} \tag{1.56}$$

where the bipartite negativities are defined as in (1.40) or, equivalently, as

$$N_{I-JK} = -2\sum_i \sigma_i(\hat{\rho}^{TI}) \tag{1.57}$$

with $I = A, B, C$ and $JK = BC, AC, AB$ respectively and where $\sigma_i(\hat{\rho}^{TI})$ are the negative eigenvalues of $\hat{\rho}^{TI}$, the partial transpose of $\hat{\rho}$ with respect to subsystem I. The tripartite negativity fulfills both parts of condition i) for pure states, and ii) and iii) since the bipartite negativities verify them. Moreover this multipartite entanglement measure adds a quantitative appraisal of the full tripartite entanglement of a pure three-qubit states classification explained in detail in [27]. For non-pure states the condition i) may not be verified, mainly because of two different situations. The first one concerns two-party states in dimensions 2×4 where there are entangled states with zero negativity ("bound entangled" states [29]), violating the second part of i). On the other hand, N_{ABC} could be non-zero for generalized biseparable states, violating also the first part of i). The problems related to find a measure that is non-zero for any entangled two-party state in dimension 2×4, and also find a way to discriminate unambiguously between generalized biseparable and fully entangled states of three qubits, are still open. Nevertheless it can be proved that $N_{ABC} > 0$ is a sufficient condition for distillability to a GHZ state (GHZ-*distillability*), a property of central importance in quantum computation. Therefore, tripartite negativity is useful also for non-pure states, even if it does not solve the separability vs. entanglement problem.

Some examples are given for the two representative tripartite entangled states GHZ and W. Respectively we have $N_{ABC}(|GHZ\rangle) = 1$ and $N_{ABC}(|W\rangle) = 0.94$, that introduces a novelty with respect to the 3-tangle measure since it can quantify the amount of tripartite entanglement in the W state. This is better appreciable when GHZ-like or W-like states are considered, as it distinguishes a degree of entanglement for each state, allowing a more detailed classification of states.

CHAPTER 2

Entanglement transfer and state mapping

In this Chapter we treat the problem of the transfer of tripartite quantum correlations and states from radiation to matter qubits. So we are faced with the issue of multipartite entanglement, the effects of entanglement sudden death and birth (ESD and ESB), and open system dynamics in realistic settings.

The general problem of transferring entanglement from bosonic systems to localized qubits for bipartite systems was recently addressed [30] also in the presence of some dissipative effects. In the framework of CQED the Hamiltonian description of entanglement exchange from radiation to two-level atoms was theoretically investigated in [31] and the effect of cavity mode decay was numerically analyzed in [32]. The literature also provides examples of similar investigations in other physical systems such as circuit QED [33] or collective spins of atomic ensembles [34]. In the case of tripartite systems the problem of entanglement transfer was investigated in CQED for unitary dynamics [35, 36]. In turn, tripartite entanglement of radiation in CV systems has been widely investigated both theoretically and experimentally [37, 38, 39, 40, 41, 42] and, recently, photon number multipartite entanglement for qubit-like radiation states was demonstrated [43]. Another scheme for quantum state engineering has been proposed [44] allowing also entanglement purification [45].

Here we provide a full dynamical description of entanglement transfer from three entangled bosonic modes to three localized qubits through the action of a local environment [46]. Our analysis provides a good framework for different physical systems and implementations. In particular, upon exploiting current advances in the optical regime of CQED [47, 43, 48], our scheme could be implemented with three entangled radiation modes, prepared in a qubit-

like state, coupled by optical fibers to three separated optical cavities containing each one a trapped two-level atom.

This chapter is organized as follows. After introducing the physical model (Sec. 2.1), we first describe the whole system dynamics in the Hamiltonian case, showing the occurrence of optimal state mapping and entanglement transfer (Sec. 2.2). In particular, an injected pure entangled state of radiation, carried by single-mode fibers, can be mapped onto the tripartite atomic subsystem, after a suitable interaction time among all nine parties. Switching off the external field at that time, the quantum correlations can be periodically mapped onto the tripartite atomic and cavity mode subsystems, according to a triple Jaynes-Cummings (JC) dynamics [1]. In the case of external radiation prepared in a mixed Werner state we suggest a way to observe the phenomenon of ESD and ESB [49, 50] for tripartite systems. Also we show that, during the time evolution, each subsystem (atoms or cavity modes) can alternatively exhibit different kinds of entanglement, including genuine tripartite GHZ and W entanglement. We also analyze the dynamics including reflectivity losses at input cavity mirrors, showing that it is equivalent to an error in the switching-off time of the interaction between fibers and cavities. Moreover we study the case of multi-mode fiber couplings between the injected field and the cavity modes, highlighting the possibility to get a good state mapping even outside the optimal conditions explained before. In the final part of this section we give a short glance to the possibility of injecting an entangled tripartite CV state of radiation, which has been object of study in interesting experiments [39].

The main dissipative effects are included to obtain a realistic investigation of multipartite entanglement transfer and swapping (Sec. 2.3), that is of interest for quantum interfaces and memories in quantum networks [51, 52]. The effects of dissipation are compared for different initial states and several values of parameters, in order to analyze the robustness against decoherence.

2.1 Model of the physical system

We start describing the general scheme for an entangled three-mode bosonic system (f), prepared in general in a mixed state, interacting with three qubits (a) through their local environments (c). Considering a resonance condition among the three relevant energy frequency of the subsystems and performing the usual RWA in order to obtain a TC model, the system Hamiltonian in the interaction picture takes the form

$$\hat{\mathcal{H}}^I = \sum_{J=A,B,C} \left[\hbar g_J(\hat{c}_J\hat{\sigma}_J^\dagger + \hat{c}_J^\dagger\hat{\sigma}_J)\right] + \sum_{J,K=A,B,C} \left[\hbar\nu_{J,K}(t)(\hat{c}_J\hat{f}_K^\dagger + \hat{c}_J^\dagger\hat{f}_K)\right] \tag{2.1}$$

The operators $\hat{c}_J, \hat{c}_J^\dagger$ ($\hat{f}_J, \hat{f}_J^\dagger$) are the annihilation and creation operators for the local environment (input bosonic) modes, while $\hat{\sigma}_J, \hat{\sigma}_J^\dagger$ are the lowering and raising operators for the target qubits in each subsystem (J =A,B,C). Without loss of generality, we consider real coupling constants g_J for the c-a interaction, whereas $\nu_{J,K}(t)$, f-c coupling, are taken

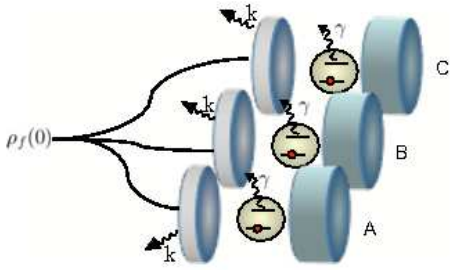

Figure 2.1: Schematic diagram for entanglement transfer in a CQED framework. Three entangled radiation modes are coupled by optical fibers to three cavities each one interacting with an atomic qubit. An open system situation is also taken into account.

real and time dependent in order to simulate the interaction switching-off at a suitable time $t_{\rm off}$. The implementation of our scheme (sketched in Fig. 2.1) may be realized in the optical regime of CQED by choosing a tripartite photon-number entangled field for the bosonic modes (f), guided by optical fibers, and two-level atoms as the target qubits (a). Each qubit is trapped in a one-sided optical cavity, operating as the local environment (c). We consider the optical fibers in the short-fiber limit where radiation is carried by discrete modes [53]. In the following section we shall distinguish the cases of single-mode and multi-mode fibers that couple to the corresponding cavities. As we noticed in the introduction and as will be widened in the next chapter, there exist different physical implementations of this model, in particular in superconducting solid state devices where "artificial atoms" are used as qubits and 1D strip-line resonators as cavities.

If the system is open, it is subjected to several dissipative effects, such as cavity losses at a rate κ_c due to interaction with a thermal bath with a mean photon number $\bar{n}$, the atomic spontaneous emission with a decay rate γ_a, and a leakage of photons from the fibers at a rate κ_f. Hence the time evolution of the whole system can be described by the following master equation (ME) in the Lindblad form for the density operator $\hat{\rho}(t)$:

$$\dot{\hat{\rho}} = -\frac{i}{\hbar}\left(\hat{\mathcal{H}}_e\hat{\rho} - \hat{\rho}\hat{\mathcal{H}}_e^{\dagger}\right) + \sum_{J=A,B,C}\left[\hat{C}_{f,J}\hat{\rho}\hat{C}_{f,J}^{\dagger} + \hat{C}_{c,J}^{(g)}\hat{\rho}\hat{C}_{c,J}^{(g)\dagger} + \hat{C}_{c,J}^{(l)}\hat{\rho}\hat{C}_{c,J}^{(l)\dagger} + \hat{C}_{a,J}\rho\hat{C}_{a,J}^{\dagger}\right] \quad (2.2)$$

where the non-Hermitian effective Hamiltonian is

$$\hat{\mathcal{H}}_e = \hat{\mathcal{H}}^I - \frac{i\hbar}{2}\sum_{J=A,B,C}\left[\hat{C}_{f,J}^{\dagger}\hat{C}_{f,J} + \hat{C}_{c,J}^{(g)\dagger}\hat{C}_{c,J}^{(g)} + \hat{C}_{c,J}^{(l)\dagger}\hat{C}_{c,J}^{(l)} + \hat{C}_{a,J}^{\dagger}\hat{C}_{a,J}\right] \quad (2.3)$$

The jump operators for the qubits are $\hat{C}_{a,J} = \sqrt{\gamma_a}\hat{\sigma}_J$, for the fibers $\hat{C}_{f,J} = \sqrt{\kappa_f}\hat{f}_J$, and for the cavity modes $\hat{C}_{c,J}^{(l)} = \sqrt{\kappa_c(\bar{n}+1)}\hat{c}_J$ (loss of a photon) and $\hat{C}_{c,J}^{(g)} = \sqrt{\kappa_c\bar{n}}\hat{c}_J^{\dagger}$ (gain of a photon). We remark that in optical cavities thermal noise is negligible, spontaneous emission can be effectively suppressed, and single atoms can stay trapped even for several seconds

[47]. From now on we consider dimensionless parameters, all scaled to the coupling constant g_A, and times $\tau = g_A t$, introducing the dimensionless switching-off time $\tau_{\rm off} = g_A t_{\rm off}$. In particular the decay rates will be written in the following as $\tilde{\kappa}_c \equiv \kappa_c/g_A$, $\tilde{\kappa}_f \equiv \kappa_f/g_A$, $\tilde{\gamma}_a \equiv \gamma_a/g_A$.

2.2 Entanglement transfer and state mapping in the Hamiltonian regime

In this section we illustrate analytical and numerical results on the transfer of a quantum state from an entangled radiation, which can be in a pure or mixed state, qubit-like or CV, to localized qubits. In particular we focus on the unitary dynamics of the subsystems, with the conditions ($\{\tilde{\kappa}_f, \tilde{\kappa}_c, \tilde{\gamma}_a\} \ll 1$), and we analyze the effects of a reduced mirror transmittance, of different coupling constants and we differentiate the two cases of single-mode and multi-mode fibers. We consider here only the case of initial GHZ and W states, in order to better understand the mechanism of the transfer protocol, which is the same for all input states. We will introduce later, in the dissipative case, the most general pure tripartite states written in the Generalized Schmidt Decomposition (GSD) form [54], in order to compare their robustness against decoherence. Moreover we study the dynamics of the subsystems in the case of initial mixed states, in particular a GHZ state mixed with white noise and a GHZ state mixed with a w state. We focus on the time evolution of entanglement and we provide a classification of entanglement, showing the effects of ESD and ESB.

2.2.1 Qubit-like external radiation carried by single-mode fibers

Starting from a qubit-like entangled state $\hat{\rho}_{0,f}$ all subsystems (a, c, f) trivially behave as qubits. Since we are interested in the entanglement dynamics and its classification, we combine the information about tripartite negativity [27], entanglement witnesses [55] for the two inequivalent classes GHZ and W [24], and some recently proposed criteria for separability [56] (see Chapter 1). In fact, the tripartite negativity $E^{(\alpha)}(\tau)$ (α=a, c, f), defined as the geometric mean of the three bipartite negativities [57], is an entanglement measure providing only a sufficient condition for entanglement detection, though its positivity guarantees GHZ-distillability. As we will see further on, this becomes important for initial mixed state, while for pure states the tripartite negativity completely describes the entanglement dynamics of the subsystems. For a better and clearer reading we report here the definition of tripartite negativity as the entanglement measure we use throughout this chapter:

$$E^{(\alpha)} \equiv \sqrt[1/3]{N^{(\alpha)}_{A-BC} N^{(\alpha)}_{B-CA} N^{(\alpha)}_{C-AB}} \qquad \alpha = a, c, f \tag{2.4}$$

where $N^{(\alpha)}_{A-BC}$, e.g., is the common bipartite negativity of the bipartition A and BC in every subsystem α = a, c, f.

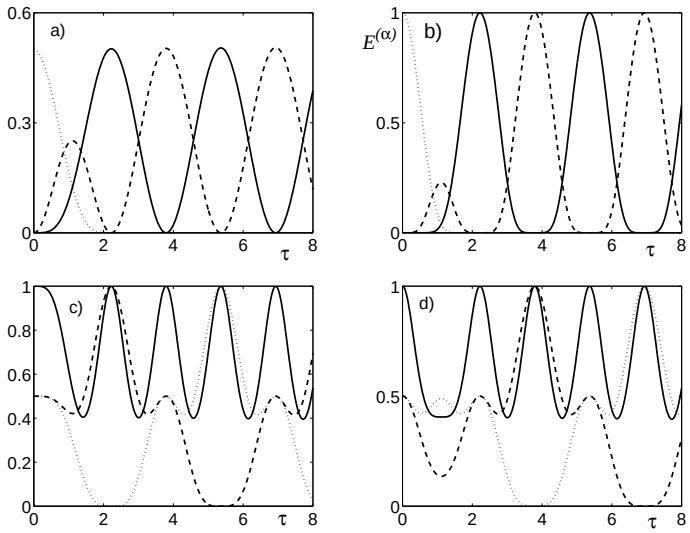

Figure 2.2: Dynamics of the nine-qubit system for the external field initially prepared in a GHZ state. In (a) the average number of photons $N^{(c)}$(dashed), $N^{(f)}$(dotted) and the probability of excited state p_e(solid). In (b) the tripartite negativity $E^{(\alpha)}$ for atoms (solid), cavity modes (dashed) and external field (dotted).In (c) the purity $\mu^{(a)}$ (solid) and the fidelity $F_\phi^{(a)}$ with $\phi = -\frac{\pi}{2}$ (dashed), $\phi = \frac{\pi}{2}$ (dotted). In (d) the purity $\mu^{(c)}$ (solid) and the fidelity $F_\phi^{(c)}$ with $\phi = -\frac{\pi}{2}$ (dashed), $\phi = \frac{\pi}{2} + \pi/2$ (dotted).

We first illustrate the Hamiltonian dynamics for the external field prepared in a qubit-like entangled pure state $|\Psi_0\rangle_f$, atoms prepared in the lower state $|ggg\rangle_a$, and cavities in the vacuum state $|000\rangle_c$. Overall we are dealing with an interacting 9-qubit system where the input field is switched off at the time $\tau_{\rm off}$, when it has completely fed the cavities and the atomic probability of excited state $p_e(\tau)$ reaches the maximum. In practice, the switch off of the injected field can be obtained, e.g., by rotating fiber polarization, interrupting the mode-matching conditions necessary to get the fiber modes and the cavity modes to interact.

In Fig. 2.2 we summarize the dynamics for the external field prepared in the GHZ state $|\Psi_0\rangle_f = (|000\rangle_f + |111\rangle_f)/\sqrt{2}$. The first part of the time evolution is the transient regime $0 < \tau \leq \tau_{\rm off}$, with $\tau_{\rm off} = \pi/\sqrt{2}$, where each input qubit transfers its excitation to the cavity mode, that in turn passes it onto the atom (see Fig. 2.2a). Each cavity mode, simultaneously coupled to the external field and to the atom, exchanges energy according to a Tavis-Cummings dynamics at an effective frequency $\sqrt{2}g_A$ [2, 58] and the mean photon number $N^{(c)}(\tau) \equiv \langle \hat{c}^\dagger \hat{c} \rangle(\tau)$ in each cavity completes a cycle. In Fig. 2.2b we also see that the atomic tripartite negativity is always positive and $E^{(a)}(\tau_{\rm off}) = 1$, that is the value of the injected GHZ state. Until $\tau_{\rm off}$ the dynamics maps the whole initial state $|\Psi_0\rangle_f \otimes |000\rangle_c \otimes |ggg\rangle_a$ onto the pure state $|000\rangle_f \otimes |000\rangle_c \otimes |\tilde{\Psi}\rangle_a$. The state $|\tilde{\Psi}\rangle_a$ is obtained from $|\Psi_0\rangle_f$ by

the substitution $|0\rangle_f \to |g\rangle_a$ and $|1\rangle_f \to \mathrm{i}|e\rangle_a$, that is $|\tilde{\Psi}\rangle_a = (|ggg\rangle_a - \mathrm{i}|eee\rangle_a)/\sqrt{2}$. Thus the mapped state onto the localized qubits is of the same class of the initial state of radiation, unless a local phase factor given by the unitary operator $\hat{U}^{(a)} = \bigotimes_J e^{-i\frac{\pi}{2}\hat{\sigma}_J^\dagger \hat{\sigma}_J}$. Alternately the exact state mapping might be obtained applying $\hat{U}^{\dagger(a)}$ to the atomic state at time $\tau_{\rm off}$, that is $|\Psi_0\rangle_a = \hat{U}^{\dagger(a)}|\tilde{\Psi}\rangle_a$ which is the same quantum state of the injected radiation with the correct substitution $|0\rangle_f \to |g\rangle_a$ and $|1\rangle_f \to |e\rangle_a$, without additional phase factors. This is confirmed by the time evolution of the purity $\mu^{(a)}(\tau) = \mathrm{Tr}_a[\hat{\rho}_a^2(\tau)]$ and of the fidelity to the initial state $F^{(a)}(\tau) = {}_f\langle\Psi_0|\hat{\rho}_a(\tau)|\Psi_0\rangle_f$, where $\hat{\rho}_a(\tau)$ is the atomic reduced density operator. As regards the cavity mode dynamics we note that (see Figs. 2.2b,d) the local maximum of $E^{(c)}(\tau_{\rm off}/2)$ does not correspond to a pure state, i.e. the initial state $|\Psi_0\rangle_f$ cannot be exactly mapped onto the cavity modes during the transient regime. Therefore we have that entanglement is only partially transferred to the cavity modes but nevertheless this is enough for the building up of full atomic entanglement later on. This is quite different with respect to [36].

At the end of the transient regime the external radiation is turned off and the subsequent dynamics is described by a triple JC ruled by oscillations at the vacuum Rabi frequency $2g_A$, hence with a dimensionless period π as shown by cavity mean photon number and atomic probability in Fig. 2.2a. As shown in Fig. 2.2c, the purities oscillate at a double frequency between pure entangled (maximum negativity) and separable (zero negativity) states. In particular, at times $\tau_m = \tau_{\rm off} + m\pi$ $(m = 0, 1, 2...)$ the atoms are in the entangled states $\hat{U}_\phi^{(a)}|\Psi_0\rangle_a$, where $\hat{U}_\phi^{(a)} = \bigotimes_J e^{-i\phi\hat{\sigma}_J^\dagger\hat{\sigma}_J}$ is a generalization of the previous local phase operator, where $\phi = 0$ $(\phi = \pi)$ applies for even (odd) values of m, that are the peaks of $E^{(a)}(\tau)$ in Fig. 2.2b. At times $\tau_n = \tau_{\rm off} + (n + \frac{1}{2})\pi$ $(n = 0, 1, 2...)$ the cavity mode states are obtained by applying $\hat{U}_\phi^{(c)} = \bigotimes_J e^{-i\phi\hat{c}_J^\dagger\hat{c}_J}$, where $\phi = -\frac{\pi}{2}$ $(\phi = \frac{\pi}{2})$ for even (odd) values of n, to the state $|\Psi_0\rangle_c$ derived from $|\Psi_0\rangle_f$ by the substitution $|0\rangle_f \leftrightarrow |0\rangle_c$ and $|1\rangle_f \leftrightarrow |1\rangle_c$.

2.2.2 Effect of cavity mirror transmittance

By choosing to turn off the external field at times $\tau' \leq \tau_{\rm off}$ we find a progressive degradation of the entanglement transfer to the atomic and cavity subsystems. This effect is fully equivalent to the presence of a reduced cavity mirror transmittance, which may be defined as $T(\tau') = 1 - \frac{N^{(f)}(\tau')}{N^{(f)}(0)}$. For several fraction of the initial mean photon number injected in the cavities (see Fig. 2.3a) we analyze the subsequent dynamics of the subsystems. In particular in Fig. 2.3b we show the time evolution of cavity mean photon number $N^{(c)}(\tau)$ and in Fig. 2.3c the atomic excitation probability $p_e(\tau)$. The influence on the entanglement transfer scheme of a reduced intensity of the transmitted radiation is well described by the plots of the tripartite negativity for both the atomic and cavity subsystems in Figs. 2.4(a,b). As expected the lower is the input energy into the local environments, the worse is the entanglement transfer efficiency. Nevertheless even for a 10% changes in the value of $\tau_{\rm off}$, the fidelity remains above 99.9%, i.e. entanglement transfer is robust against fluctuations of

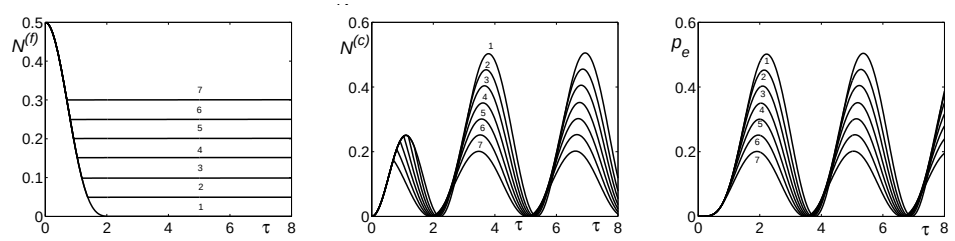

Figure 2.3: Mean photon number of the external radiation and of the cavity modes and atomic excitation probability for different values of mirror transmittance : (1) $T(2.22) = 1.0$, (2) $T(1.38) = 0.9$, (3) $T(1.19) = 0.8$, (4) $T(1.04) = 0.7$, (5) $T(0.92) = 0.6$, (6) $T(0.81) = 0.5$, (7) $T(0.70) = 0.4$.

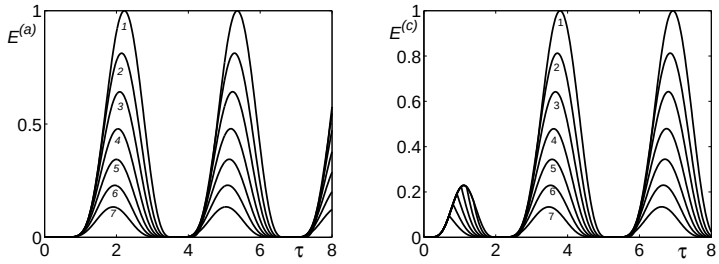

Figure 2.4: Effect of cavity mirror transmittance $T(\tau')$ on the dynamics of atomic and cavity entanglement $E^{(a,c)}$: (1) $T(2.22) = 1.0$, (2) $T(1.38) = 0.9$, (3) $T(1.19) = 0.8$, (4) $T(1.04) = 0.7$, (5) $T(0.92) = 0.6$, (6) $T(0.81) = 0.5$, (7) $T(0.70) = 0.4$.

the switching-off time and this feature is a relevant one in view of possible implementations.

2.2.3 Entanglement sudden death and birth

Let us now consider the injected field excited in a Werner state $\hat{\rho}_f(0) = (1-p)|GHZ\rangle\langle GHZ| + \frac{p}{8}\hat{I}$, $(0 \leq p \leq 1)$, for which it is possible to have full classification of entanglement, making use of the entanglement witnesses [55] $\hat{W}_G = \frac{3}{4}\hat{I} - |GHZ\rangle\langle GHZ|$, $\hat{W}_{W2} = \frac{1}{2}\hat{I} - |GHZ\rangle\langle GHZ|$ and $\hat{W}_{W1} = \frac{2}{3}\hat{I} - |W\rangle\langle W|$. In the range $0 \leq p < \frac{2}{7}$ the state belongs to the GHZ class and to the W class up to $p = \frac{4}{7}$. The tripartite negativity is positive up to $p = 4/5$ whereas the state is clearly inseparable under all bipartitions (from now on we denote this class by INS), i.e. it cannot be written as convex combination of biseparable states and finally, for $4/5 \leq p \leq 1$ it is known that the state is fully separable [59, 56].

The system dynamics can be divided again into a transient and an oscillatory regime, and the state mapping of $\hat{\rho}_f(0)$ onto atoms (cavity modes) still occurs at precise finite times τ_m (τ_n). Out of these times the density matrices of all subsystems lose the form of a GHZ

state mixed with white noise but still preserve invariance under all permutations of the three qubits and present only one non vanishing coherence as in $\hat{\rho}_f(0)$. This greatly helps us in the entanglement classifications in the plane (τ, p) as shown in Fig. 2.5. In fact, in the regions where $E^{(\alpha)}(\tau) > 0$ but out of W class we can exclude the biseparability. The full separability criteria in [56] are violated only where $E^{(a)}(\tau) > 0$ so that if $E^{(a)}(\tau) = 0$ the state may be fully separable or biseparable. Nevertheless, in the latter case the state turns out to be symmetric and biseparable under all bipartitions and hence it is fully separable [60]. For any fixed value of p in the range $0 < p < 4/5$ we thus show the occurrence of entanglement sudden death and birth at the boundaries between fully separable and inseparable states. In particular, for $0 < p < 4/7$ we find genuine tripartite ESD and ESB phenomena. Furthermore note that, for a fixed value of p, the atomic state may exhibit transition from W to GHZ entanglement class and viceversa. The same effect is shown by the cavity modes after the transient (see Fig. 2.5d). The W-GHZ transition is allowed by the non-unitarity of the partial trace over non-atomic degrees of freedom, which implies that the overall map on the initial three qubits is not SLOCC. We also notice that for times $\tau \geq \tau_{\rm off}$ we can solve exactly the triple JC dynamics, thus confirming our numerical results and providing generalization of the results of Ref. [61] to mixed states.

In Fig. 2.5b we see that, for increasing values of p, there is an increase of both the slope of $E^{(a)}(\tau)$ and the time interval of full separability. In Fig. 2.5c we show in detail the transient dynamics of the tripartite negativities $E^{(\alpha)}(\tau, p)$ $(\alpha = a, c, f)$ in the crucial region around $\tau_{\rm off}/2$. We consider some values of p where the atoms exhibit in times different classes of entanglement. We see that for $p = 0.2$, where the input state has GHZ class entanglement, the ESB of subsystems (c),(a) anticipates the ESD of (f),(c), and there is an interval around $\tau_{\rm off}/2$ where all three subsystems are entangled (of INS-type). As p grows, hence the initial state becomes more noisy, the effects of ESD occur earlier and those of ESB later. For $p = 0.4$, involving W-class entanglement, only at most two subsystems are simultaneously entangled (first (f),(c) and then (c),(a)). For $p = 0.6$, involving only entanglement of INS-type, the cavity modes do not entangle at all (see Fig. 2.5d). They physically mediate the discontinuous entanglement transfer from (f) to (a), where for $p \to 4/5$ the time interval without any entanglement increases while the entanglement level vanishes.

Let us now consider the class of mixed qubit-like states for the injected field $\hat{\rho}_f(0) = p|GHZ\rangle\langle GHZ| + (1-p)|W\rangle\langle W|$, $0 \leq p \leq 1$. By analytical and numerical results we show that our scheme for entanglement transfer and swapping is also relevant for the observation of sudden disentanglement and entanglement effects. Since the tripartite negativity $E^{(\alpha)}(\tau)$ with $(\alpha = a, c)$ is an entanglement measure that provides only a sufficient condition for entanglement detection, we cannot properly talk about ESD or ESB for these kind of states in the whole parameter space $\{p, \tau\}$. Nevertheless, we can classify the atomic state by using the entanglement witnesses as above and analyze the discontinuous evolution of entanglement focusing only on the fully tripartite entanglement properties. For negligible dissipation and

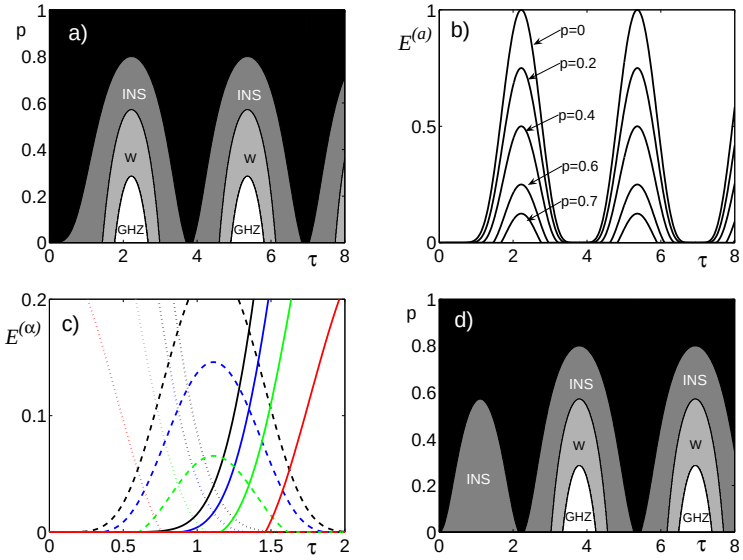

Figure 2.5: ESD/ESB for external field in a GHZ state mixed with white noise. a) Regions in the plain (τ, p) for atomic entanglement of type GHZ, W, INS, and fully separable (black). b) Sections $E^{(a)}(\tau)$ for selected values of p. c) Zoom on $E^{(\alpha)}(\tau_{\rm off}/2)$ for field (dotted), cavity modes (dashed), and atoms (solid) with $p = 0$ (black), $p = 0.2$ (blue), $p = 0.4$ (green), $p = 0.6$ (red). d) Classification for cavity mode entanglement.

at times τ_m, the initial state of radiation is mapped onto the atoms, then the entanglement classification is known. The state is of class GHZ for $\frac{3}{4} \leq p \leq 1$, of class W for $0 \leq p < \frac{1}{3}$ and $\frac{1}{2} \leq p < \frac{3}{4}$, and biseparable (B) for $\frac{1}{3} \leq p < \frac{1}{2}$. Outside times τ_m, we can still make a partial entanglement classification that is shown in Fig. 2.6(a) (Fig. 2.6(b)) for atomic (cavity field) states. Since the tripartite negativity is zero in the black regions of Fig.2.6, we cannot exclude the presence of bound entangled states. With this knowledge on the entanglement properties in parameter space, we can anyway affirm that there is a discontinuity for the full tripartite entanglement. Fixing, for instance, a value of $p < 0.25$ and looking at the time evolution of the atomic state, we can notice that it suddenly acquires a fully tripartite entanglement entering the W region and loses this property after some finite time exiting that region. This effect can be addressed as an ESD and ESB of the fully tripartite inseparability only. Moreover, since the systems share among its subsystems energy and entanglement in a periodic way, we can highlight also that discontinuities in the fully tripartite entanglement are exchanged among them. This occurs after the transient, where the cavity modes do not exhibit genuine tripartite entanglement (see Fig. 2.6(b)) but only support the transfer of quantum correlations from the input field to the atoms.

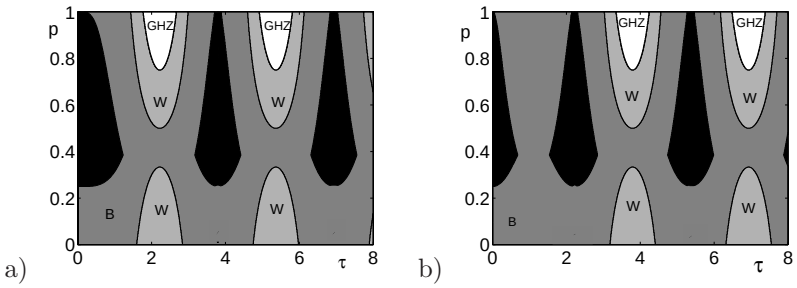

Figure 2.6: Entanglement classification in the parameter space $\{p, \tau\}$ for external field prepared in the mixed GHZ and W state $\hat{\rho}_f(0)$. a) atomic subsystem, b) cavity mode subsystem.

2.2.4 Entanglement transfer for multi-mode fiber coupling

We consider now the case of multi-mode coupling of the external field to each cavity mode. As introduced (Sec. 2.1) in the description of the physical system we are dealing with, if the external radiation is carried by optical fibers in the so-called "short-fiber" limit [53], it propagates with discrete modes. We shall describe here a situation in which the three injected modes can be carried together by a single fiber, allowing the interaction between a cavity mode and a fiber which is not directly connected.

For simplicity we choose equal dimensionless coupling constants $\tilde{\nu}_{J,K} \equiv \nu_{J,K}/g_A \neq 0$ if $K \neq J$ and we consider values up to 1.4. The initial state of the external radiation is always the GHZ state. In the transient regime the dynamics is sharply modified with respect to the case of single-mode fibers shown in Fig. 2.2. By increasing the values of $\tilde{\nu}_{J,K}$ the period of energy exchange decreases from $2\pi/\sqrt{2}$ to $\cong 2.6$. The maximum of cavity mode mean photon number grows up to $N^{(c)} \cong 0.41$ whereas the maximum of atomic excitation probability decreases to $p_e \cong 0.24$. The external field mean photon number does not vanish but it reaches a minimum, that can be always found between the two maxima of $N^{(c)}(\tau)$ and $p_e(\tau)$, such that $0.002 < N^{(f)} < 0.02$ changing $\tilde{\nu}_{J,K}$ from 0.1 to 1.4. We investigate the differences in the entanglement transfer for three selections of the switching-off time τ_{off} corresponding to the maximum of $p_e(\tau)$, the minimum of $N^{(f)}(\tau)$ and the maximum of $N^{(c)}(\tau)$. In Fig. 2.7(a) we show the dependence of τ_{off} on $\tilde{\nu}_{J,K\neq J}$. Switching off the external field at times τ_{off} corresponding to the maxima of $p_e(\tau)$, as in the previous case with single-mode fibers, we find (Fig. 2.7(b,c)) that the maxima of tripartite negativities $E^{(\alpha)}(\tau)$ after the transient regime reduce for increasing values of $\tilde{\nu}_{J,K}$ for both atomic and cavity mode subsystems. If we consider τ_{off} corresponding to the minimum of $N^{(f)}(\tau)$ (Fig. 2.8(a,b)) we observe a small reduction of the peak values of $E^{(\alpha)}(\tau)$. Finally, if we turn off the external field at the first maximum of the cavity mean photon number $N^{(c)}(\tau)$ we note that by increasing the values of $\tilde{\nu}_{J,K}$ it is possible to improve the entanglement transfer (Fig. 2.8(c,d)). The peak value of tripartite negativity grows up to $\cong 0.93$ for

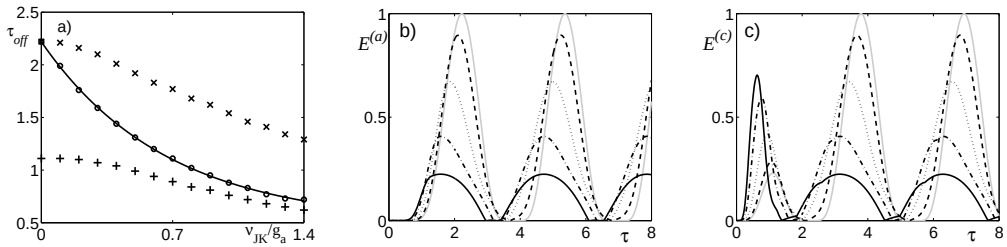

Figure 2.7: Effect of multi-mode coupling. a) Dependence of $\tau_{\rm off}$ on the coupling constants $\tilde{\nu}_{J,K}$ for different choices of switching-off the external field: maximum of $p_e(\tau)$ (o), minimum of $N^{(f)}(\tau)$ (x), and maximum of $N^{(c)}(\tau)$ (+). b,c) Tripartite negativities $E^{(\alpha)}$ ($\alpha = a, c$) for $\tilde{\nu}_{J,K} = 0$ (solid gray), 0.3 (dashed), 0.6 (dotted), 1.0 (dashed-dotted), and 1.4 (solid black) when $\tau_{\rm off}$ corresponds to the maximum of $p_e(\tau)$.

$\tilde{\nu}_{J,K} = 1.4$ and the fidelity up to $\cong 0.95$ for both subsystems (a) and (c). We remark that these values cannot be significantly increased for larger values of $\tilde{\nu}_{J,K}$. In conclusion, for all the above choices of switching-off time $\tau_{\rm off}$ we observe that, by increasing the values of $\tilde{\nu}_{J,K}$, the amount of entanglement that can be transferred to the cavity modes in the transient regime also increases. This is due to the fact that the amount of energy transferred to each cavity mode increases: in fact, the peak value of $N^{(c)}(\tau)$ progressively grows up from $\cong 0.25$ to $\cong 0.41$. Nevertheless, multi-mode coupling for larger values of $\tau_{\rm off}$ results in a less favorite condition for entanglement transfer.

2.2.5 The case of injected CV field

In the previous sections we have considered a qubit-like approximation for the entangled external field, showing, in the unitary case, a perfect state mapping and entanglement transfer of any initial state of this kind. Now, we deal with an example of an experimentally feasible CV field proposed in [62]. It is a Gaussian fully inseparable three-mode radiation generated by two type-I noncollinearly phase-matched interlinked bilinear interactions, that simultaneously couple the three modes. The state has the following representation on the Fock basis:

$$|T\rangle_f = \frac{1}{\sqrt{1+N_A^{(f)}}} \sum_{p,q=0}^{\infty} \left[\frac{N_B^{(f)}}{1+N_A^{(f)}}\right]^{\frac{p}{2}} \left[\frac{N_C^{(f)}}{1+N_A^{(f)}}\right]^{\frac{q}{2}} \left[\frac{(p+q)!}{p!q!}\right]^{\frac{1}{2}} |p+q,p,q\rangle_f \qquad (2.5)$$

where $N_J^{(f)} = \langle \hat{f}_J^\dagger \hat{f}_J \rangle$ (J = A,B,C) is the mean photon number in the J-th mode of external radiation, with $N_A^{(f)} = N_B^{(f)} + N_C^{(f)}$. The generation process of the above state can be described by the following (dimensionless) interaction Hamiltonian:

$$H_{int} = \lambda_1 \hat{f}_A^\dagger \hat{f}_C^\dagger + \lambda_2 \hat{f}_B^\dagger \hat{f}_C + \text{h.c.} \qquad (2.6)$$

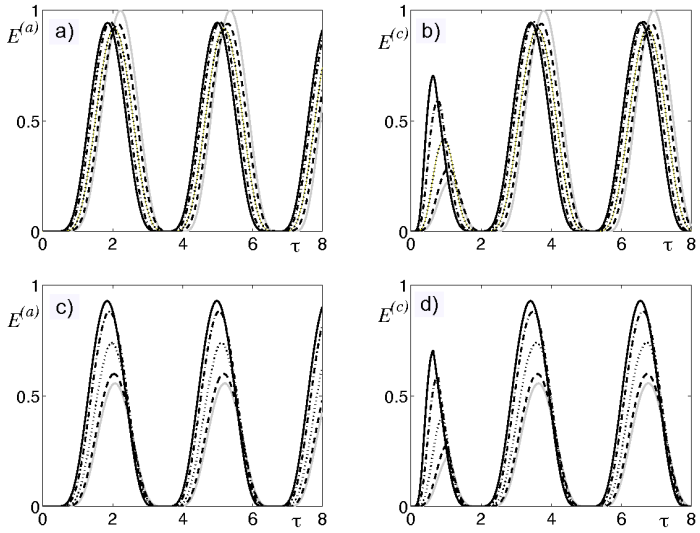

Figure 2.8: Effect of multi-mode coupling on tripartite negativities $E^{(\alpha)}$ ($\alpha = a, c$) for $\tilde{\nu}_{J,K} = 0$ (solid gray), 0.3 (dashed), 0.6 (dotted), 1.0 (dashed-dotted), and 1.4 (solid black): a,b) $\tau_{\rm off}$ in the minimum of $N^{(f)}(\tau)$; c,d) $\tau_{\rm off}$ in the maximum of $N^{(c)}(\tau)$.

The effective dimensionless coupling constants λ_i ($i = 1, 2$) of the two parametric processes are proportional to the nonlinear susceptibilities and the pump intensities. They are also related to the mean photon numbers by

$$\begin{aligned} N_B &= \frac{|\lambda_1|^2|\lambda_2|^2}{(|\lambda_2|^2 - |\lambda_1|^2)^2}\left[1 - \cos^2(\sqrt{|\lambda_2|^2 - |\lambda_1|^2})\right] \\ N_C &= \frac{|\lambda_1|^2}{|\lambda_2|^2 - |\lambda_1|^2}\sin^2(\sqrt{|\lambda_2|^2 - |\lambda_1|^2}) \end{aligned} \tag{2.7}$$

As discussed in [36], the condition for optimal entanglement transfer is such that the photon statistics of state $|T\rangle_f$ must contain mainly three contributions whose probabilities are given by $|b_{110}|^2 = N_B(1+N_B+N_C)^{-2}$, $|b_{101}|^2 = N_C(1+N_B+N_C)^{-2}$ and $|b_{000}|^2 = (1+N_B+N_C)^{-1}$, where $b_{p+q,p,q}$ are the complex coefficients of the state $|T\rangle_f$ corresponding to the Fock states $|p+1, p, q\rangle$. This means that the state $|T\rangle_f$ assumes a qubit-like form. For simplicity, we consider here the case $\lambda_1 = \lambda_2$ so that the mean photon numbers for modes B and C are given by $N_B^{(f)} = \frac{|\lambda_1|^4}{4}$ and $N_C = |\lambda_1|^2$. We investigate the Hamiltonian dynamics in the case $|\lambda_1|^2 = 0.6$, for which the tripartite negativity takes the maximum value at suitable interaction times [36]. In the transient regime the behavior of the energy exchange differs from each subsystem $J = A, B, C$. In particular, the oscillations of the external field mean photon number $N_J^{(f)}(\tau)$ have quite similar periods $T_A^{(f)} \cong T_C^{(f)} \cong 3.5$ and $T_B^{(f)} \cong 3.8$ but different amplitudes because we have $N_A^{(f)}(0) \cong 0.69$, $N_B^{(f)}(0) \cong 0.09$ and $N_C^{(f)}(0) \cong 0.6$. In addition, the functions $N_J^{(f)}(\tau)$ do not vanish and their minimum occurs at times between the maxima of cavity mode mean photon number $N_J^{(c)}(\tau)$ and atomic probability $p_{e,J}(\tau)$.

We choose to turn off the external field at a time $\tau_{\rm off} = T_A^{(f)}/2 \cong 1.74$. In Fig. 2.9 we see that the behavior of cavity field mean photon number $N^c(\tau)$ is similar for subsystems $J = A, C$ while for $J = B$ the oscillations are more regular and have a short period.

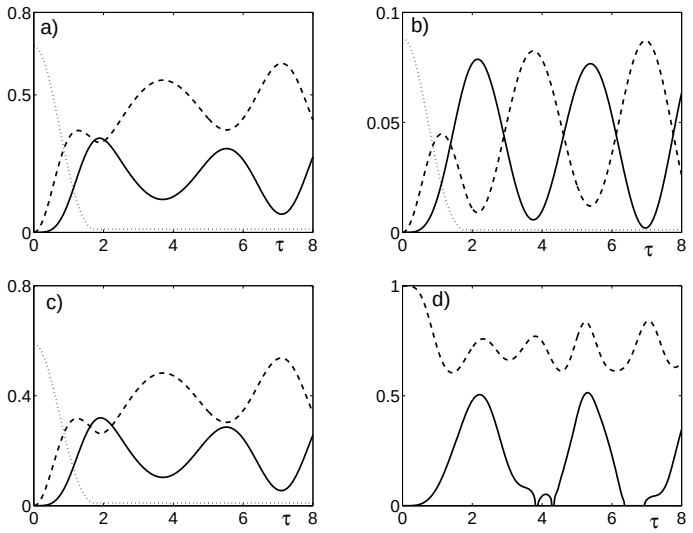

Figure 2.9: Entanglement transfer for external field in a $|T\rangle_f$ state with $|\lambda_i|^2 = 0.6$ $(i = 1, 2)$. $N^{(c)}$(dashed), $N^{(f)}$(dotted) and p_e(solid) for subsystem $J = A$(a), $J = B$ (b), $J = C$ (c). In (d) we show the atomic tripartite negativity $E^{(a)}(\tau)$ (solid) and the purity $\mu^{(a)}(\tau)$(dashed).

2.3 Dissipative effects on the state mapping for qubit-like injected field

In the perspective of an experimental implementation of our scheme, an important problem to be taken into account is the detrimental effect of dissipation on both state mapping and entanglement transfer. Here we consider a Markovian reservoir for which it is possible to derive a ME in the Lindblad form (4.2) where the main noisy channels are the loss of photons from the cavities and from the fibers and the atomic spontaneous emission. As regards the unitary part we will refer to the case of single-mode fibers we have analyzed in Sec. 2.2.1. Since we would like to characterize the effects of dissipation and decoherence on the system and subsystem dynamics, we consider different initial states of the injected radiation, analyzing their behaviour under the influence of the dissipative reservoir. As we noticed at the beginning of Sec.2.2, a three-qubit state can be always written as a GSD and it is known that there exist different types of GSD forms [25]. In fact, it is possible to use several procedures to write a generic state of the whole Hilbert space of three qubit on a five elements basis. For many application of QI the choice of the five elements of the basis it is

not relevant. We consider for the external field state the following GSD forms [54, 63, 27]. The first two are symmetric with respect to the exchange of the three qubits:

$$|\Psi^{GSD}(0)\rangle_f = \alpha|000\rangle_f + \beta|001\rangle_f + \delta|010\rangle_f + \varepsilon|100\rangle_f + \omega|111\rangle_f \tag{2.8}$$

$$|\phi^{GSD}(0)\rangle_f = \alpha|000\rangle_f + \beta|011\rangle_f + \delta|101\rangle_f + \varepsilon|110\rangle_f + \omega|111\rangle_f. \tag{2.9}$$

The last GSD form is symmetric only with respect to the exchange of qubits B and C:

$$|\varphi^{GSD}(0)\rangle_f = \alpha|000\rangle_f + \beta|100\rangle_f + \delta|101\rangle_f + \varepsilon|110\rangle_f + \omega|111\rangle_f \tag{2.10}$$

From these general representations emerge the states $|GHZ\rangle$ and $|W\rangle$ and we provide a wide range comparison among the different dynamics in order to characterize their robustness against decoherence.

First we consider negligible decay of the fiber modes and spontaneous emission ($\tilde{k}_f, \tilde{\gamma}_a \ll 1$) and, as an example, we concentrate on the qubit-like state $|\Psi^{GSD}(0)\rangle_f$ for the external field, with all the coefficients equal to $\frac{1}{\sqrt{5}}$. We can see in Fig. 2.10 the effect of cavity mode dissipation on the atomic probability $p_e(\tau)$, cavity field mean photon number $N^{(c)}(\tau)$ and tripartite negativities $E^{(\alpha)}(\tau)$ for some values of the dimensionless decay rate $\tilde{k}_c$. We see a progressive reduction of the energy and entanglement transferred to the atoms and the cavities by increasing the values of $\tilde{k}_c$. At times $\tau_{m,n}$ with $m = n = 0$, we found that the fidelities $F^{(\alpha)}(\tau_0)$ and the tripartite negativities $E^{(\alpha)}(\tau_0)$ ($\alpha = a, c$) can be well fitted by exponential functions of the type $f^{(\alpha)}(\tilde{k}_c) \propto \exp\{-\beta^{(\alpha)}\tilde{k}_c\}$ whose rates for the atomic subsystem are $\beta_F^{(a)} = 0.75$ and $\beta_E^{(a)} = 1.09$, and for the cavity mode subsystem are $\beta_E^{(c)} = 2.94$ and $\beta_F^{(c)} = 1.80$. We remark that for $\tilde{\kappa}_c = 0.1$ the state mapping onto the atomic (cavity mode) subsystem can be obtained with a fidelity of 95% (88%).

We now add the effect of the atomic decay to the particular case of cavity mode dissipation $\tilde{\kappa}_c = 0.1$ by selecting for $\tilde{\gamma}_a \equiv \gamma_a/g_A$ values up to 0.1. In Fig. 2.11 we show the tripartite negativities $E^{(\alpha)}(\tau)$ for some values of $\tilde{\gamma}_a$ and we see that at least for times $\tau_{m,n}$ with $m = n = 0$ it seems to be not critical. Up to $\tilde{\gamma}_a = 0.03$ we have a reduction on tripartite negativities and fidelities less then 10%. We note that the values of fidelities and tripartite negativities at the first peak $\tau_{m,n}$ with $m = n = 0$ as function of $\tilde{\gamma}_a$ cannot be accurately fitted by exponential functions of the type described before.

Finally, we analyze the effect of dissipation on the fiber mode used to inject the external field into each cavity. Clearly, this effect is relevant only up to $\tau_{\rm off} = 2.22$ and we consider the case of $\tilde{\kappa}_f$ up to 1.0 for negligible atomic and cavity mode decay rates ($\tilde{\kappa}_c \ll 1$, $\tilde{\gamma}_a \ll 1$) (see Fig. 2.11). We evaluate the effect of the parameter $\tilde{\kappa}_f$ on $N^{(c)}(\tau_{\rm off}/2)$ and $p_e(\tau_{\rm off})$ and we see that the amount of energy transferred to the atoms and to the cavity modes decrease exponentially as the value of $\tilde{\kappa}_f$ increase; the decay rates are $\cong 0.53$ and $\cong 0.71$ respectively. Also the behavior of the tripartite negativity $E^{(a)}(\tau_0)$ and the fidelity $F^{(a)}(\tau_0)$ at the first peak can be described by exponential functions whose decay rates are $\cong 1.93$ and $\cong 0.69$.

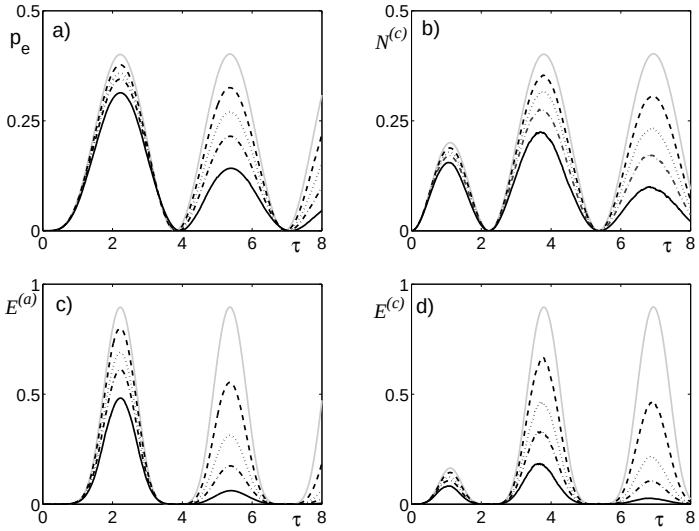

Figure 2.10: Effect of cavity mode dissipation for the external field in the qubit-like state $|\Psi^{GSD}(0)\rangle_f$ as in Eq. (2.8). $\tilde{k}_c = 0$ (solid gray), 0.1 (dash), 0.2 (dot), 0.3 (dash-dot), 0.5 (solid). (a) atomic probability p_e, (b) cavity mean photon number $N^{(c)}$; (c) $E^{(a)}$; (d) $E^{(c)}$.

2.3.1 Robustness to dissipation of external radiation in different GSD states

Here we evaluate the goodness of the entanglement transfer protocol for other GSD forms of the input radiation field state, in the presence of cavity mode dissipation ($\tilde{\kappa}_c$). We briefly remind that, as regards the unitary case, the transfer process is optimal and this means that all the initial features of the radiation quantum state (mean photon number,entanglement) are perfectly mapped onto the atomic degrees of freedom. For instance if we choose the initial state in the form (2.9) with all coefficients equal to $\frac{1}{\sqrt{5}}$ the peaks values for $N^c(\tau)$ and $p_e(\tau)$ are different to those of a GSD state in the form (2.8), but the values of tripartite negativities $E^{(\alpha)}(\tau_{m,n}) =$ are the same. In the case of an initial state in the GSD form (2.10) with all the coefficients equal to $\frac{1}{\sqrt{5}}$ the peaks values of $N^c(\tau)$ and $p_e(\tau)$ for subsystem A are different from those of subsystem B and C. In addition, we have a lower value of the maxima for the tripartite negativities $E^{(\alpha)}(\tau_{m,n}) \cong 0.61$.

What is really interesting is to compare the three GSD forms from the point of view of their robustness against dissipative effects. We evaluate the fidelities $F^{(\alpha)}(\tau_0)$ and the tripartite negativities $E^{(\alpha)}(\tau_0)$ at the first peaks $\tau_{m,n}$ (with $m = n = 0$) in function of $\tilde{\kappa}_c$. We find for all quantities an exponential decay behaviour and in Table 2.1 we report the respective values of the decay rates β. We note that the state $|\Psi^{GSD}(0)\rangle_f$ is less affected by dissipation than the other two GSD forms and this result can be explained in terms of the mean photon number of the initial state that is equal to 1.2 for $|\Psi^{GSD}(0)\rangle_f$, 1.4 for $|\varphi^{GSD}(0)\rangle_f$ and 1.8

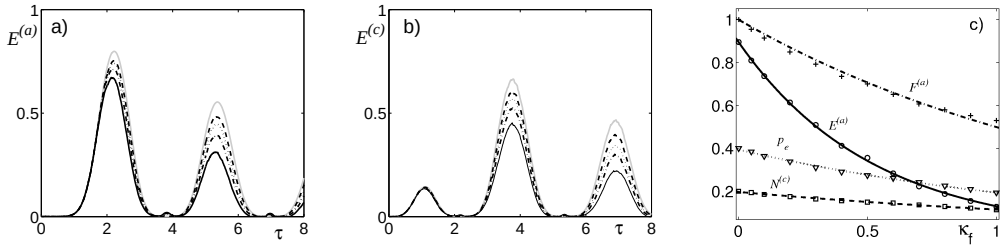

Figure 2.11: Effect of atomic decay and cavity mode dissipation ($\tilde{\kappa}_c = 0.1$) for the external field in the qubit-like state $|\Psi^{GSD}(0)\rangle_f$ as in Eq. (2.8). We consider $\tilde{\gamma_a} = 0.0001$(solid gray), 0.03 (dash), 0.05 (dot), 0.07 (dash-dot), 0.1 (solid) and we show (a) $E^{(a)}(\tau)$ and (b) $E^{(c)}(\tau)$. Effect of fiber mode decay rate $\tilde{\kappa}_f$ for the external field in the qubit-like state $|\Psi^{GSD}(0)\rangle_f$ as in Eq. (2.8) for $\tilde{\kappa}_c \ll 1$, $\tilde{\gamma}_a \ll 1$. Plots of the atomic tripartite negativity (solid), the fidelity(dash-dot), and the atomic probability (dot) at time $\tau_{\rm off}$, and of the cavity mean photon number (dash) at time $\tau_{\rm off}/2$.

for $|\phi^{GSD}(0)\rangle_f$. Even at a first glance to Eqs. (2.8), (2.9), (2.10) one realizes that, apart from the common basis elements $|000\rangle_f$ and $|111\rangle_f$, the $|\Psi^{GSD}(0)\rangle_f$ state contains terms with only one mode populated with one photon and, consequently, it has a lower probability to decay.

Table 2.1: Comparison between different GSD forms of the external field with respect to the effect of cavity mode decay rate $\tilde{\kappa}_c$.

β	$\lvert\Psi^{GSD}(0)\rangle_f$	$\lvert\varphi^{GSD}(0)\rangle_f$	$\lvert\phi^{GSD}(0)\rangle_f$
$E^{(a)}(\tau_0)$	1.26	1.42	1.44
$F^{(a)}(\tau_0)$	0.55	0.64	0.88
$E^{(c)}(\tau_0)$	3.35	3.86	3.95
$F^{(c)}(\tau_0)$	1.32	1.58	2.14

2.3.2 Robustness to dissipation of the external field in a state W and GHZ

Many applications to QI are based on the well known tripartite states W and GHZ. The W state can be obtained from the GSD state in Eq. (2.8) by setting $\alpha = \omega = 0$ and $\beta = \delta = \epsilon = \frac{1}{\sqrt{3}}$ while the state GHZ with the choice $\alpha = \omega = \frac{1}{\sqrt{2}}$ and $\beta = \delta = \epsilon = 0$. From the point of view of the entanglement classification these states are genuine tripartite entangled states and they represent two inequivalent classes [24]. We first consider the effect of cavity mode dissipation ($\tilde{\kappa}_c$), for negligible values of $\tilde{\gamma}_a$ and $\tilde{\kappa}_f$, on the entanglement transfer process starting by external field prepared in the states $|GHZ\rangle_f = (|000\rangle_f + |111\rangle_f)/\sqrt{2}$

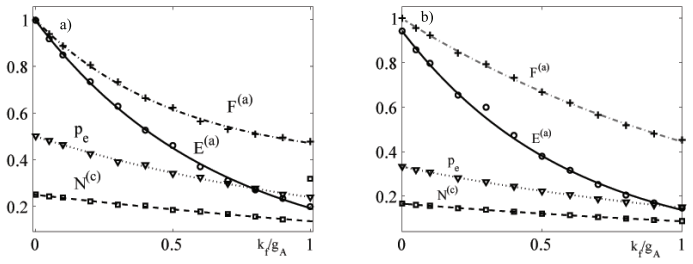

Figure 2.12: Effect of fiber mode decay rate $\tilde{\kappa}_f$ for the external field in the GHZ state (a) and in the W state (b), for $\tilde{\kappa}_c \ll 1$, $\tilde{\gamma}_a \ll 1$. We evaluate at time $\tau_{\rm off}$ the atomic tripartite negativity (solid), the fidelity(dash-dot), and the atomic probability (dot), and at time $\tau_{\rm off}/2$ the cavity mean photon number (dash).

and $|W\rangle_f = (|001\rangle_f + |010\rangle_f + |100\rangle_f)/\sqrt{3}$. We consider tripartite negativities $E^{(\alpha)}(\tau_0)$ and fidelities $F^{(\alpha)}(\tau_0)$ at the first peak ($\tau_{m,n}$ with $m = n = 0$) and we report in Table 2.2 the values of the decay rates β obtained for the exponential functions used to fit the numerical results. We note that in the Hamiltonian regime the maximum value for the tripartite negativity is $E^{(\alpha)}(\tau_{m,n}) = 1$ for the GHZ state and $E^{(\alpha)}(\tau_{m,n}) \cong 0.94$ for the W state. We can affirm that the results are quite similar but the GHZ state seems to be slightly more robust as regards the entanglement transfer ($E^{(\alpha)}(\tau_0)$), while the state W behaves better in the state mapping ($F^{(\alpha)}(\tau_{m,n})$) .

We consider now the effect of the atomic decay by setting the cavity dissipation rate

Table 2.2: Comparison between W and GHZ initial states of the external field with respect to the effect of cavity mode decay rate $\tilde{\kappa}_c$.

β	$\|W\rangle_f$	$\|GHZ\rangle_f$
$E^{(a)}(\tau_0)$	1.19	1.09
$F^{(a)}(\tau_0)$	0.55	0.75
$E^{(c)}(\tau_0)$	3.20	2.94
$F^{(c)}(\tau_0)$	1.40	1.80

$\tilde{\kappa}_c = 0.1$. We always look at the decrease of the first peak value ($\tau_{m,n}$ with $m = n = 0$) for the fidelity and the tripartite negativity, but the exponential function fit is less precise in this case. We can only show percentages for the peak value reductions up to $\tilde{\gamma}_a = 0.03$. For the GHZ state $E^{(a)}(\tau_0)$ ($E^{(c)}(\tau_0)$) reduces of 6% (12%) while $F^{(a)}(\tau_0)$ ($F^{(c)}(\tau_0)$) reduces of 5% (9%). On the other side the state W seems to be less affected because $E^{(a)}(\tau_0)$ ($E^{(c)}(\tau_0)$) reduces of 5% (9%) while $F^{(a)}(\tau_0)$ ($F^{(c)}(\tau_0)$) reduces of 3% (4%).

Finally, we evaluate the effect of photon leakeges in the fibers for a range of values $0 < \tilde{\kappa}_f \leq 1.0$ and negligible atomic and cavity decay rates ($\tilde{\kappa}_c \ll 1$, $\tilde{\gamma}_a \ll 1$) (see Fig. 2.12).

We evaluate the effect of parameter $\tilde{\kappa}_f$ on $N^{(c)}(\tau_{\rm off}/2)$ and on $p_e(\tau_{\rm off})$ and we see that the amount of energy transferred to the atoms and to the cavity modes decays exponentially by increasing the value of $\tilde{\kappa}_f$; the decay rates for GHZ (W) state are $\cong 0.42$ ($\cong 0.54$) and $\cong 0.82$ ($\cong 0.77$) respectively. Also the behavior of tripartite negativity $E^{(a)}(\tau_0)$ and fidelity $F^{(a)}(\tau_0)$ at the first peak can be described as function of $\tilde{\kappa}_f$ by an exponential fit whose decay rates for GHZ (W) states are given respectively by $\cong 1.51$ ($\cong 1.67$) and $\cong 1.95$ ($\cong 0.76$).

CHAPTER 3

Open dynamics of N driven qubits inside an optical cavity

We describe the dynamics of a system where N two-level atoms, strongly driven by an external coherent field, are resonantly coupled to a cavity field mode that is in contact with an environment. There are different available or forthcoming routes to the implementation of our model. In the microwave regime of cavity QED atoms excited to Rydberg levels cross a high-Q superconductive cavity with negligible spontaneous emission during the interaction [2]. Difficulties may arise due to the (ideal) requirements on atomic simultaneous injection, equal velocity, and equal coupling rate to the cavity mode. In the optical regime the application of cooling and trapping techniques in cavity QED allows the deterministic loading of single atoms in a high-finesse cavity, with accurate position control and trapping times of many seconds [47]. In this regime laser-assisted three-level atoms can behave as effective two-level atoms with negligible spontaneous emission [64]. On the other hand, trapped atomic ions can remain in an optical cavity for an indefinite time in a fixed position, where they can couple to a single mode without coupling rate fluctuations [48]. These systems are quite promising to our purposes and could become almost ideal in case of achievement of the strong coupling regime.

Under full resonance conditions and starting from the vacuum state of the cavity field, and for negligible thermal fluctuations, we solved exactly the system dynamics for any initial preparation of the atom pair, thus deriving a number of analytical results on the whole system as well as the different subsystems. These results are confirmed and extended by numerical simulations, e.g. investigating regimes under weaker driving conditions. In particular we show the existence of both global (field-atoms) and atomic decoherence-free

subspaces (DFSs) [65] where an initial N-qubit entanglement remains preserved and available e.g. for quantum memories or quantum processors [66]. Furthermore, the structure of the general solution allows predicting a way to monitor the decay of quantum coherence, as well as of purity, by measurements of atomic probabilities.
The chapter is organized as follows. We firstly introduce the general physical model (Sec. 3.1), deriving an effective master equation (ME) for the open system dynamics of N strongly driven qubits interacting with a single cavity mode. Then we focus our attention on the 2-qubit case (Sec. 3.2), in order to understand the mathematical method of characteristics [67] to obtain an analytical solution and also to highlight the main features of the dynamics of the system and the subsystems, neglecting the atomic spontaneous emission [68]. Here we analyze the dynamics of entanglement and the conditional generation of cat-like states for the cavity field. It is, thus, straightforward the derivation of the solution for the N-qubit case (Sec. 3.3), including the dissipative channel of the spontaneous emission of the excited atomic level [69]. At this point DFSs come out naturally from the general solution and some examples are provided for the particular cases of $N = 3$ and $N = 4$ atoms [70].
We point out that the basic example of $N = 1$ qubit is widely treated elsewhere [64] and that, for a more general understanding of the qubit entanglement dynamics and its protection against decoherence in DFSs, it is more instructive to start from the $N = 2$ case.

3.1 The physical model

The system we are considering is made of N classically driven two-level atoms interacting with a single cavity field mode, in contact with a dissipative environment. In this section we derive an effective Hamiltonian for the system, in the strongly driven regime, that encompasses both JC and anti-JC terms simultaneously. Since we are dealing with an open system, its dynamics is described by a master equation (ME) that will be written in the standard Lindblad form. All the unitary transformations and approximations used for the interaction Hamiltonian will be accordingly adapted to the ME and we will find that such a model can be analytically solved in the phase space through the method of characteristics.

3.1.1 Interaction Hamiltonian

A coherent external field of frequency ω_D drives the atoms during the interaction with the cavity mode of frequency ω [71, 72]. The transition frequency ω_0 between excited and ground states, $|e\rangle_j$ and $|g\rangle_j$ ($j = 1, 2, \ldots N$) respectively, is the same for all the qubits. The starting point is the Hamiltonian describing the whole system unitary dynamics, which can be written as the sum of four contributions $\hat{\mathcal{H}}(t) = \hat{\mathcal{H}}_f + \hat{\mathcal{H}}_a + \hat{\mathcal{H}}_{af} + \hat{\mathcal{H}}_{aD}(t)$. Thes terms correspond to the free energy of the atomic and cavity subsystems, to the JC interaction between each atom with the cavity mode and to the coupling of the qubits to a classical

external driving field. The basic Hamiltonian reads:

$$\hbar\omega\hat{a}^\dagger\hat{a} + \hbar\sum_{l=1}^{N}\Big[\frac{\omega_0}{2}\hat{\sigma}_{z,l} + g(\hat{\sigma}_l^\dagger\hat{a} + \hat{\sigma}_l\hat{a}^\dagger) + \Omega(e^{-\mathrm{i}\omega_D t}\hat{\sigma}_l^\dagger + e^{\mathrm{i}\omega_D t}\hat{\sigma}_l)\Big], \tag{3.1}$$

where Ω is the Rabi frequency associated with the coherent driving field amplitude, g the atom-cavity mode coupling constant (taken equal for all atoms), $\hat{a}$ ($\hat{a}^\dagger$) the field annihilation (creation) operator, $\hat{\sigma}_j = |g\rangle_j\langle e|$ ($\hat{\sigma}_j^\dagger = |e\rangle_j\langle g|$) the atomic lowering (raising) operator, and $\hat{\sigma}_j^z = |e\rangle_j\langle e| - |g\rangle_j\langle g|$ the inversion operator.
In order to eliminate the time dependence in the Hamiltonian (3.1), by adding and subtracting the term $\omega_0\hat{a}^\dagger\hat{a}$ we obtain

$$\hat{\mathcal{H}}(t) = \hbar\omega_{\mathbf{0}}\hat{\mathbf{a}}^\dagger\hat{\mathbf{a}} + \hbar\delta\hat{\mathbf{a}}^\dagger\hat{\mathbf{a}} + \hbar\sum_{l=1}^{N}\Big[\frac{\omega_0}{2}\hat{\sigma}_{z,l} + g(\hat{\sigma}_l^\dagger\hat{a} + \hat{\sigma}_l\hat{a}^\dagger) + \Omega(e^{-\mathrm{i}\omega_D t}\hat{\sigma}_l^\dagger + e^{\mathrm{i}\omega_D t}\hat{\sigma}_l)\Big]$$

with a *detuning* parameter $\delta = \omega - \omega_0$. Now we define

$$\begin{aligned}\hat{\mathcal{H}}_0 =& \hbar\omega_0\hat{a}^\dagger\hat{a} + \hbar\sum_{l=1}^{N}\frac{\omega_0}{2}\hat{\sigma}_{z,l}\\ \hat{\mathcal{H}}_1 =& \hbar\delta\hat{a}^\dagger\hat{a} + \hbar\sum_{l=1}^{N}\Big[g(\hat{\sigma}_l^\dagger\hat{a} + \hat{\sigma}_l\hat{a}^\dagger) + \Omega(e^{-\mathrm{i}\omega_D t}\hat{\sigma}_l^\dagger + e^{\mathrm{i}\omega_D t}\hat{\sigma}_l)\Big]\end{aligned}$$

and we perform the unitary transformation $\hat{\mathcal{H}}^I = \hat{U}_1\hat{\mathcal{H}}_1\hat{U}_1^\dagger$ under the resonance condition $\omega_0 = \omega_D$, where $\hat{U}_1 = \mathrm{e}^{\frac{\mathrm{i}}{\hbar}\hat{\mathcal{H}}_0 t}$. In this way, the Pauli operators become $\hat{\sigma}_l \to \hat{\sigma}_l\mathrm{e}^{-\mathrm{i}\omega_0 t}$ and the cavity mode annihilation operator $\hat{a} \to \hat{a}\mathrm{e}^{-\mathrm{i}\omega_0 t}$ and we get a new Hamiltonian operator

$$\hat{\mathcal{H}}^I = \hbar\delta\hat{a}^\dagger\hat{a} + \hbar g\sum_{l=1}^{N}\Big[(\hat{\sigma}_l^\dagger\hat{a} + \hat{\sigma}_l\hat{a}^\dagger) + \hbar\Omega(\hat{\sigma}_l^\dagger + \hat{\sigma}_l)\Big]. \tag{3.2}$$

A second unitary transformation is applied to (3.2) through the operator $\hat{U}_2 = \mathrm{e}^{\frac{\mathrm{i}}{\hbar}\hat{\mathcal{H}}_0^I t}$ with $\hat{\mathcal{H}}_0^I = \hbar\delta\hat{a}^\dagger\hat{a} + \hbar\Omega\sum_{l=1}^{N}(\hat{\sigma}_l^\dagger + \hat{\sigma}_l)$. As before, this operation trasnforms the cavity annihilation operator as $\hat{a} \to \hat{a}\mathrm{e}^{-\mathrm{i}\delta t}$ and the raising operator becomes $\hat{\sigma}_l^\dagger \to \frac{1}{2}\Big(\hat{\sigma}_{x,l} + |+\rangle_l\langle -|\mathrm{e}^{2\mathrm{i}\Omega t} - |-\rangle_l\langle +|\mathrm{e}^{-2\mathrm{i}\Omega t}\Big)$, where $\hat{\sigma}_{x,l} = \hat{\sigma}_l^\dagger + \hat{\sigma}_l$ and $|\pm\rangle_l = \frac{1}{\sqrt{2}}(|g\rangle_l \pm |e\rangle_l)$ is the rotated basis.
In the strong driving regime for the interaction between the atoms and the external coherent field $\Omega \gg g$, we are allowed to apply a rotating-wav approximation (RWA) obtaining the effective Hamiltonian:

$$\hat{\mathcal{H}}_{\mathrm{eff}}(t) = \frac{\hbar g}{2}\sum_{l=1}^{N}\hat{\sigma}_{x,l}(\hat{a}\mathrm{e}^{\mathrm{i}\delta t} + \hat{a}^\dagger\mathrm{e}^{-\mathrm{i}\delta t}) \tag{3.3}$$

which outlines the presence of JC ($\hat{\sigma}_l^\dagger\hat{a} + \hat{\sigma}_l\hat{a}^\dagger$) and anti-JC ($\hat{\sigma}_l^\dagger\hat{a}^\dagger + \hat{\sigma}_l\hat{a}$) terms.

3.1.2 Open system master equation

In the perspective of experimental implementation of our scheme, we take into account the loss of energy to the environment via both the cavity mode dissipation and the atomic

spontaneous emission channels. The system time evolution is then described by the density operator $\rho'(t)$ as a solution of the following master equation (ME):

$$\dot{\hat{\rho}}' = -\frac{\mathrm{i}}{\hbar}[\hat{\mathcal{H}}(t), \hat{\rho}'] + \hat{\mathcal{L}}_f\hat{\rho}' + \hat{\mathcal{L}}_a\hat{\rho}', \tag{3.4}$$

where

$$\hat{\mathcal{L}}_f\hat{\rho}' = \frac{\kappa}{2}[2\hat{a}\hat{\rho}'\hat{a}^\dagger - \hat{a}^\dagger\hat{a}\hat{\rho}' - \hat{\rho}'\hat{a}^\dagger\hat{a}] \tag{3.5}$$

$$\hat{\mathcal{L}}_a\hat{\rho}' = \frac{\gamma}{2}\sum_{l=1}^{N}[2\hat{\sigma}_l\hat{\rho}'\hat{\sigma}_l^\dagger - \hat{\sigma}_l^\dagger\hat{\sigma}_l\hat{\rho}' - \hat{\rho}'\hat{\sigma}_l^\dagger\hat{\sigma}_l]. \tag{3.6}$$

$\hat{\mathcal{L}}_f$ and $\hat{\mathcal{L}}_a$ are the standard Liouville superoperators describing, respectively, the dissipative decay of the cavity field at a rate κ and of the atomic excited level at a rate γ. We assume that both reservoirs are at zero temperature.

As formerly we must apply the same unitary tranformation to the density operator $\hat{\rho}'$, in order to obtain a correct ME that includes the effective Hamiltonian (3.3). The first step is to use the operator $\hat{U}_1 = \mathrm{e}^{\frac{\mathrm{i}}{\hbar}\hat{\mathcal{H}}_0 t}$ and, since the Liouvillean parts do not change under this transformation, the ME for the new density operator $\hat{\rho}^I = \hat{U}_1\hat{\rho}'\hat{U}_1^\dagger$ is

$$\dot{\hat{\rho}}^I = -\frac{\mathrm{i}}{\hbar}[\hat{\mathcal{H}}^I, \hat{\rho}^I] + \hat{\mathcal{L}}_f\hat{\rho}^I + \hat{\mathcal{L}}_a\hat{\rho}^I. \tag{3.7}$$

A second unitary operation must applied to the ME (3.7) through the operator $\hat{U}_2 = \mathrm{e}^{\frac{\mathrm{i}}{\hbar}\hat{\mathcal{H}}_0^I t}$. As before the cavity mode operators change in such a way they do not modify the formal structure of the Liouville superoperator $\hat{\mathcal{L}}_f$, but as regards the atomic spontaneous emission, $\hat{\mathcal{L}}_a$ is modified by the unitar transformation. As we noted before that if we consider a strong driving regime for the external field $\{\Omega \gg g, \kappa, \gamma\}$, we can apply the RWA obtaing the approximated expression for the transformed Pauli operator $(\hat{\sigma}_l^\dagger)_{\mathrm{eff}} = \hat{\sigma}_{x,l}/2$. This brings to an effective description of the superoperator $\hat{\mathcal{L}}_a$ that corresponds to have a dephasing noise acting on the qubits, since it can be written as follows:

$$\hat{\mathcal{L}}_a^{\mathrm{eff}}\hat{\rho} = \frac{\gamma}{4}\sum_{l=1}^{N}[\hat{\sigma}_{x,l}\hat{\rho}\hat{\sigma}_{x,l} - \hat{\rho}]. \tag{3.8}$$

Thus the final ME can be written as:

$$\dot{\hat{\rho}} = -\frac{\mathrm{i}}{\hbar}[\hat{\mathcal{H}}_{\mathrm{eff}}, \hat{\rho}] + \hat{\mathcal{L}}_f\hat{\rho} + \hat{\mathcal{L}}_a^{\mathrm{eff}}\hat{\rho} \tag{3.9}$$

that is the correct one for the Hamiltonian (3.3) and the dissipative environment.

This is the complete description of our physical model that includes a multi-qubit system strongly driven by a classical coherent field interacting with a single cavity mode, in the presence of a dissipative bath for the cavity and the two-level atoms. In the following we will show how to get an analytical solution of (3.9) and we will describe the dynamics of this kind of system and of entanglement.

3.2 Two-qubit case

In this section we consider the solution of the ME (3.9) in the case of exact resonance $\delta = 0$, cavity field initially in the vacuum state, and a generic superposition pure state for the atoms. As regards the dissipative channel, in this treatment we will consider only the leakage of photons from the cavity in the analytical treatment, leaving the effect of spontaneous emission for the atoms to numerical simulations. This because we want to highlight the main features of the analyical methods in the two-qubit case, making it as simple and clear as possible. We will study the dynamics of the system at all times, showing the transient and the steady state and the properties of every term of the analytical solution. The dynamics of the subsystems is also analyzed in detail, in order to study the effect of decoherence on the atom-atom entanglement, to be distinguished from classical correlation functions. A first hint for the existence of DFSs for particular initial states of the atoms is given in this case. Then we will enter into the details of the conditional generation of cat-like (entangled) states for the cavity field. Finally we treat the dynamics with numerical simulations, which confirm our theoretical analysis and extend it to analytical unsolvable situations, such as the weak driving condition.

3.2.1 The analytical solution

The exact solution of the ME is based on the following decomposition for the density operator $\hat{\rho}(t)$ of the whole system:

$$\hat{\rho}(t) = \sum_{i,j=1}^{4} \langle i|\hat{\rho}(t)|j\rangle |i\rangle\langle j| = \sum_{i,j=1}^{4} \hat{\rho}_{ij}(t)|i\rangle\langle j| \tag{3.10}$$

where $\{|i\rangle\}_{i=1}^{4} = \{|++\rangle, |+-\rangle, |-+\rangle, |--\rangle\}$ is the rotated basis of the atomic Hilbert space. This means that the ME is equivalent to the following set of uncoupled equations for the field operators $\hat{\rho}_{ij}(t)$:

$$\begin{aligned}
\dot{\hat{\rho}}_{11} &= -ig[\hat{a}^\dagger + \hat{a}, \hat{\rho}_{11}] + \hat{\mathcal{L}}_f \hat{\rho}_{11} \\
\dot{\hat{\rho}}_{12,13} &= -ig(\hat{a}^\dagger + \hat{a})\hat{\rho}_{12,13} + \hat{\mathcal{L}}_f \hat{\rho}_{12,13} \\
\dot{\hat{\rho}}_{14} &= -ig\{\hat{a}^\dagger + \hat{a}, \hat{\rho}_{14}\} + \hat{\mathcal{L}}_f \hat{\rho}_{14} \\
\dot{\hat{\rho}}_{22,23,33} &= \hat{\mathcal{L}}_f \hat{\rho}_{22,23,33} \\
\dot{\hat{\rho}}_{24,34} &= -ig\hat{\rho}_{24,34}(\hat{a}^\dagger + \hat{a}) + \hat{\mathcal{L}}_f \hat{\rho}_{24,34} \\
\dot{\hat{\rho}}_{44} &= ig[\hat{a}^\dagger + \hat{a}, \hat{\rho}_{44}] + \hat{\mathcal{L}}_f \hat{\rho}_{44}
\end{aligned} \tag{3.11}$$

where the brackets [,] and braces { , } denote the standard commutator and anti-commutator symbols and $\dot{\hat{\rho}}_{j,i}(t) = [\dot{\hat{\rho}}_{i,j}(t)]^\dagger$. In the phase space associated to the cavity field we introduce the functions $\chi_{ij}(\beta, t) = Tr_f[\hat{\rho}_{ij}(t)\hat{\mathcal{D}}(\beta)]$. We note that the functions $\chi_{ij}(\beta, t)$ cannot be interpreted as characteristic functions [73] for the cavity field, because

the operators $\hat{\rho}_{ij}$ do not exhibit all required properties of a density operator. As a consequence the functions $\chi_{ij}(\beta,t)$ do not fulfill all conditions for quantum characteristic functions. Nevertheless, they are continuous and square-integrable, which is enough for our purposes. Now we present a short list of the main properties of trace operation, commutator and anti-commutator together with the displacement operator $\hat{\mathcal{D}}(\beta)$ and the operators $\hat{a}$ and $\hat{a}^\dagger$:

$$\begin{aligned}
&\hat{\mathcal{D}}(\beta)\hat{a}^\dagger = \hat{a}^\dagger\hat{\mathcal{D}}(\beta) - \beta^*\hat{\mathcal{D}}(\beta) \qquad , \qquad \hat{\mathcal{D}}(\beta)\hat{a} = \hat{a}\hat{\mathcal{D}}(\beta) - \beta\hat{\mathcal{D}}(\beta) \\
&Tr_F[\hat{a}^\dagger\hat{\mathcal{D}}(\beta)\rho] = \left(\frac{\partial}{\partial\beta} + \frac{\beta^*}{2}\right)\chi \qquad , \qquad Tr_F[\hat{a}\hat{\mathcal{D}}(\beta)\rho] = \left(-\frac{\partial}{\partial\beta^*} + \frac{\beta}{2}\right)\chi
\end{aligned} \tag{3.12}$$

With these tools at hand Eqs. (3.11) become in phase space

$$\begin{aligned}
\dot{\chi}_{11} &= ig(\beta+\beta^*)\chi_{11} - \frac{\kappa}{2}\left(\beta\frac{\partial}{\partial\beta} - \beta^*\frac{\partial}{\partial\beta^*} + |\beta|^2\right)\chi_{11} \\
\dot{\chi}_{12,13} &= -ig\left[\frac{\partial}{\partial\beta} - \frac{\partial}{\partial\beta^*} - \frac{1}{2}(\beta+\beta^*)\right]\chi_{12,13} - \frac{\kappa}{2}\left(\beta\frac{\partial}{\partial\beta} - \beta^*\frac{\partial}{\partial\beta^*} + |\beta|^2\right)\chi_{12,13} \\
\dot{\chi}_{14} &= -2ig\left[\frac{\partial}{\partial\beta} - \frac{\partial}{\partial\beta^*}\right]\chi_{14} - \frac{\kappa}{2}\left(\beta\frac{\partial}{\partial\beta} - \beta^*\frac{\partial}{\partial\beta^*} + |\beta|^2\right)\chi_{14} \\
\dot{\chi}_{22,23,33} &= -\frac{\kappa}{2}\left(\beta\frac{\partial}{\partial\beta} - \beta^*\frac{\partial}{\partial\beta^*} + |\beta|^2\right)\chi_{22,23,33} \\
\dot{\chi}_{24,34} &= -ig\left[\frac{\partial}{\partial\beta} - \frac{\partial}{\partial\beta^*} + \frac{1}{2}(\beta+\beta^*)\right]\chi_{24,34} - \frac{\kappa}{2}\left(\beta\frac{\partial}{\partial\beta} - \beta^*\frac{\partial}{\partial\beta^*} + |\beta|^2\right)\chi_{24,34} \\
\dot{\chi}_{44} &= -ig(\beta+\beta^*)\chi_{11} - \frac{\kappa}{2}\left(\beta\frac{\partial}{\partial\beta} - \beta^*\frac{\partial}{\partial\beta^*} + |\beta|^2\right)\chi_{44}.
\end{aligned} \tag{3.13}$$

We consider as initial state of the system

$$\begin{aligned}
&|\Psi(0)\rangle = |\Psi(0)\rangle_a \otimes |\Psi(0)\rangle_f \\
&\quad\begin{cases} |\Psi(0)\rangle_a = \sum_{i=1}^{4} a_i|i\rangle & \text{atomic subsystem} \\ |\Psi(0)\rangle_f = |0\rangle & \text{cavity field subsystem} \end{cases}
\end{aligned} \tag{3.14}$$

where the for the atomic subsystem we use a general superposition state in the rotated basis, while the cavity field is in the vacuum state. This initial condition, for each cavity field operator becomes $\hat{\rho}(0)_{ij} = a_i^* a_j \otimes |0\rangle\langle 0|$ that corresponds in the phase space to the characteristic functions

$$\chi_{ij}(\beta,0) = a_i^* a_j \mathrm{e}^{-\frac{|\beta|^2}{2}}. \tag{3.15}$$

Introducing the real and imaginary part of the variable $\beta = x + \mathrm{i}y$ we can derive from Eq.(3.13) a system of uncoupled equations such that each of them can be solved by applying the method of characteristics [67]. Then, rearranging the complex variables β and β^*, we

group in the following the solutions with similar expressions

$$\begin{aligned}
\chi_{11,44}(\beta,t) &= a^*_{1,4}a_{1,4}\exp\left\{-\frac{|\beta|^2}{2}\pm 2\alpha^*(t)\beta\mp 2\alpha(t)\beta^*\right\}\\
\chi_{12,13}(\beta,t) &= a^*_{1,2}a_{1,3}f_1(t)\exp\left\{-\frac{|\beta|^2}{2}+2\alpha(t)^*\beta\right\}\\
\chi_{14}(\beta,t) &= a^*_1a_4f_2(t)\exp\left\{-\frac{|\beta|^2}{2}-2\alpha(t)^*\beta-2\alpha(t)\beta^*\right\}\\
\chi_{22,33}(\beta,t) &= a^*_{2,3}a_{2,3}\exp\left\{-\frac{|\beta|^2}{2}\right\}\\
\chi_{23}(\beta,t) &= a^*_2a_3\exp\left\{-\frac{|\beta|^2}{2}\right\}\\
\chi_{24,34}(\beta,t) &= a^*_{2,3}a_{4,4}f_1(t)\exp\left\{-\frac{|\beta|^2}{2}+2\alpha(t)\beta^*\right\}
\end{aligned}\tag{3.16}$$

Since the relation between these characteristic functions and the field operators is unambiguous, there is only one solution for the operators $\hat{\rho}_{ij}(t)$:

$$\begin{aligned}
\hat{\rho}_{(11,44)}(t) &= a^*_{1,4}a_{1,4}|\pm 2\alpha(t)\rangle\langle\pm 2\alpha(t)|\\
\hat{\rho}_{(12,13)}(t) &= a^*_{1,1}a_{2,3}f_1(t)\mathrm{e}^{2|\alpha(t)|^2}|2\alpha(t)\rangle\langle 0|\\
\hat{\rho}_{14}(t) &= a^*_1a_4f_2(t)\mathrm{e}^{2|\alpha(t)|^2}|2\alpha(t)\rangle\langle -2\alpha(t)|\\
\hat{\rho}_{(22,23,33)}(t) &= a^*_{2,2,3}a_{2,3,3}|0\rangle\langle 0|\\
\hat{\rho}_{(24,34)}(t) &= a^*_{2,3}a_{4,4}f_1(t)\mathrm{e}^{2|\alpha(t)|^2}|0\rangle\langle -2\alpha(t)|,
\end{aligned}\tag{3.17}$$

where we introduced the time dependent coherent field amplitude

$$\alpha(t) = i\frac{g}{\kappa}\left(e^{-\frac{\kappa}{2}t}-1\right),\tag{3.18}$$

and the decoherence function

$$f_1(t) = \exp\left\{-\frac{2g^2}{\kappa}t+\frac{4g^2}{\kappa^2}\left(1-e^{-\frac{\kappa}{2}t}\right)\right\}.\tag{3.19}$$

We recall that $\hat{\rho}_{ji}(t) = \hat{\rho}^\dagger_{ij}(t)$ and that the reconstruction of the whole system density operator is made simply with Eq. (3.10). We notice the presence of single atom-cavity field coherences whose evolution is ruled by the function $f_1(t)$ [64], as well as full atom-atom-field coherences ruled by $f_2(t) = f_1^4(t)$, that we shall discuss later on. There are also two one-atom coherences, and two diagonal terms, which do not evolve in time, corresponding to a pure state

$$|0\rangle\otimes(|+-\rangle+|-+\rangle) = |0\rangle\otimes(|gg\rangle-|ee\rangle),\tag{3.20}$$

where we recognize (up to normalization) a Bell atomic state $|\Phi^-\rangle$. The explanation goes as follows. First of all, if we start with atoms prepared in states of the rotated basis used in the decomposition of (3.10), we obtain much simpler results due to the structure of Hamiltonian (3.3) on resonance and the obvious uninfluence of dissipation on the cavity vacuum. Actually,

either the field states are coherent, $|0\rangle \otimes |\pm\pm\rangle \mapsto |\mp 2\alpha(t)\rangle \otimes |\pm\pm\rangle$, or there is no evolution at all for the states $|0\rangle \otimes |\pm\mp\rangle$, showing the presence of an invariant subspace for system dynamics. It is the component of the initial state $|0\rangle \otimes |gg\rangle$ in that subspace, (3.20), which does not evolve.
In the following we will consider, for simplicity, the atoms initially prepared in their ground state $|\Psi(0)\rangle_a = |gg\rangle$, that corresponds to take $a_i = \frac{1}{4}\ \forall i = 1, \ldots, 4$.

The transient-regime state

In the transient regime ($\kappa t \ll 1$), the decoherence function can be approximated by $f_1(t) \simeq e^{-2|\tilde{\alpha}(t)|^2}$ where $\tilde{\alpha}(t) = -igt$, and the whole system is described by a pure Schrödinger-cat-like state

$$|\tilde{\psi}(t)\rangle = \frac{1}{2}\Big[|2\tilde{\alpha}(t)\rangle \otimes |++\rangle + |0\rangle \otimes (|+-\rangle + |-+\rangle) + |-2\tilde{\alpha}(t)\rangle \otimes |--\rangle\Big]. \tag{3.21}$$

If we rewrite this result in the standard atomic basis

$$\begin{aligned}|\tilde{\psi}(t)\rangle =& \frac{1}{4}\Big[\big(|2\tilde{\alpha}(t)\rangle - 2|0\rangle + |-2\tilde{\alpha}(t)\rangle\big) \otimes |ee\rangle + \big(|2\tilde{\alpha}(t)\rangle - |-2\tilde{\alpha}(t)\rangle\big) \otimes (|eg\rangle + |ge\rangle) \\ &+ \big(|2\tilde{\alpha}(t)\rangle + 2|0\rangle + |-2\tilde{\alpha}(t)\rangle\big) \otimes |gg\rangle\Big]\end{aligned} \tag{3.22}$$

showing the onset of correlations between atomic states and cavity field cat-like states. This will be important for the discussion on the generation of field cat-like states later on. For the terms related to the field subsystem we recover expressions analogous to those derived in [74] for a strongly driven micromaser system. Unlike the present system, in that case the atoms pump the cavity mode with a Poissonian statistics, interacting for a very short time such that the cavity dissipation is relevant only in the time intervals between atomic injections. Furthermore, the cavity field states are conditioned on atomic measurements.

The steady state

At steady state ($\kappa t \to \infty$) the density operator is a statistical mixture and it is given by:

$$\begin{aligned}\hat{\rho}^{SS} =& \frac{1}{4}\Big[|-2\alpha^{SS}\rangle\langle -2\alpha^{SS}| \otimes |++\rangle\langle ++| + |2\alpha^{SS}\rangle\langle 2\alpha^{SS}| \otimes |--\rangle\langle --| \\ &+ |0\rangle\langle 0| \otimes (|+-\rangle\langle +-| + |+-\rangle\langle -+| + |-+\rangle\langle +-| + |-+\rangle\langle -+|)\Big]\end{aligned}$$

with $\alpha^{SS} = i\frac{g}{\kappa}$. Interestingly, the steady state has not a fully diagonal structure, i.e., it is not completely mixed, in agreement with the previous discussion on the time-dependent solution. The change from a pure state to a mixed one and the degree of mixedness can be we evaluated by the purity of the whole system $\mu(t) = Tr[\hat{\rho}^2(t)]$:

$$\mu(t) = \frac{1}{8}\left[3 + 4\frac{f_1^2(t)}{e^{-4|\alpha(t)|^2}} + \frac{f_2^2(t)}{e^{-16|\alpha(t)|^2}}\right]. \tag{3.23}$$

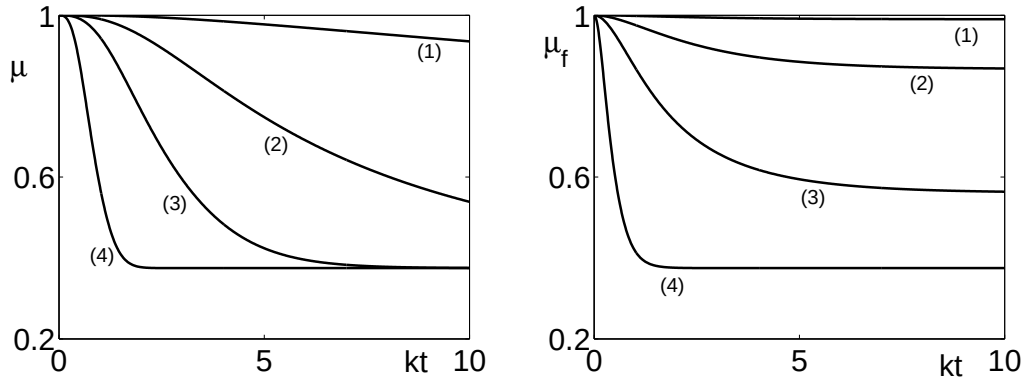

Figure 3.1: Purities $\mu(t)$ and $\mu_f(t)$ of the whole system density operator and of the cavity field subsystem vs. dimensionless time κt for dimensionless coupling constant g/κ: (1) 0.05, (2) 0.2, (3) 0.5, (4) 2.

In Fig. 3.1 we show $\mu(t)$ as a function of the dimensionless time κt for different values of the dimensionless coupling constant g/κ. We see that the purity decays rather fast in the strong coupling regime $g/\kappa \gtrsim 1$.

3.2.2 Subsystems dynamics

Now we consider the time evolution of the atomic and cavity field subsystems in the case of both atoms initially prepared in the ground state and the cavity in the vacuum. The operation that provides the density operator for one subsystem is the partial trace over the degrees of freedom of the other one. We will show the steady state of the cavity mode only and the stationary mean photon number, the joint probabilities for the two atoms and their correlation functions.

Cavity field

The cavity field reduced density operator $\hat{\rho}_f(t) = Tr_a[\hat{\rho}(t)]$ can be derived by tracing over both atoms:

$$\hat{\rho}_f(t) = \frac{1}{4}\Big[|2\alpha(t)\rangle\langle 2\alpha(t)| + 2|0\rangle\langle 0| + |-2\alpha(t)\rangle\langle -2\alpha(t)|\Big]. \tag{3.24}$$

Hence the cavity field mean photon number is $\langle\hat{N}\rangle = 2|\alpha(t)|^2$ and its steady state value $\langle\hat{N}\rangle_{SS} = 2\frac{g^2}{\kappa^2}$. These results hold for atoms prepared in any state of the standard basis. At any time Eq. (3.24) describes a mixed state, whose purity $\mu_f(t) = Tr_f[\hat{\rho}_f^2(t)]$ is:

$$\mu_f(t) = \frac{1}{8}\left[3 + 4e^{-4|\alpha(t)|^2} + e^{-16|\alpha(t)|^2}\right]. \tag{3.25}$$

In Fig. 3.1 we show the purity $\mu_f(t)$ as a function of dimensionless time κt for different values of the ratio g/κ, showing a better survival of the purity than for the global state of

Fig. 3.1 except in the strong coupling regime.

Atoms

The reduced atom-atom density operator $\hat{\rho}_a(t)$ can be obtained by tracing over the field variables. In the rotated basis $\{|++\rangle, |+-\rangle, |-+\rangle, |--\rangle\}$, we obtain

$$\rho_a^{\pm}(t) = \frac{1}{4}\begin{pmatrix} 1 & f_1(t) & f_1(t) & f_2(t) \\ f_1(t) & 1 & 1 & f_1(t) \\ f_1(t) & 1 & 1 & f_1(t) \\ f_2(t) & f_1(t) & f_1(t) & 1 \end{pmatrix}. \tag{3.26}$$

The presence of six time-independent matrix elements is in agreement with the remarks below Eq.(3.20). The purity $\mu_a(t) = Tr_a[\hat{\rho}_a^2(t)]$ of the bi-atomic subsystem is:

$$\mu_a(t) = \frac{1}{8}\left[3 + 4f_1^2(t) + f_2^2(t)\right]. \tag{3.27}$$

Its behavior is quite similar to the one of Fig. 3.1 (left) for the whole system purity. From Eq. (3.26) we can derive the single-atom density matrices and evaluate the probability to measure one atom in the excited or ground state

$$P_{e,g}(t) = \frac{1}{2}\left[1 \mp f_1(t)\right]. \tag{3.28}$$

Quite similar expressions hold for atoms prepared in any state of the standard basis. We see that from measurements of the atomic inversion $I(t) = p_g(t) - p_e(t)$ we can monitor the one-atom decoherence function $f_1(t)$ as in [64]. By rewriting the atomic density matrix (3.26) in the standard basis we evaluate the joint probabilities $P_{lm}(t) = \langle lm|\hat{\rho}_a^{(e,g)}(t)|lm\rangle$ with $\{l, m\} = \{e, g\}$. The corresponding correlation functions at a given time t are:

$$\begin{aligned} C_{ee}(t) &= \frac{3 - 4f_1(t) + f_2(t)}{2[1 - f_1(t)]^2} \\ C_{eg}(t) &= C_{ge}(t) = \frac{1 - f_2(t)}{2[1 - f_1^2(t)]} \\ C_{gg}(t) &= \frac{3 + 4f_1(t) + f_2(t)}{2[1 + f_1(t)]^2} \end{aligned} \tag{3.29}$$

In Figs. 3.2(a-c) we show the correlation functions $C_{lm}(t)$ versus dimensionless time kt and coupling constant $\frac{g}{k}$. At steady-state we see that $C_{gg}(t), C_{ee}(t) \to 3/2$, that is positive atom-atom correlation or bunching, whereas $C_{eg}(t) \to 1/2$, indicating negative correlation or anti-bunching. These results generalize those in [74], which can be derived from Eqs.(3.29) in the limit of negligible dissipation $kt \ll 1$. We notice that from the joint atomic probability $P_{eg}(t) = P_{ge}(t) = \frac{1}{8}[1 - f_2(t)]$ one can monitor the two-atom decoherence described by $f_2(t)$.

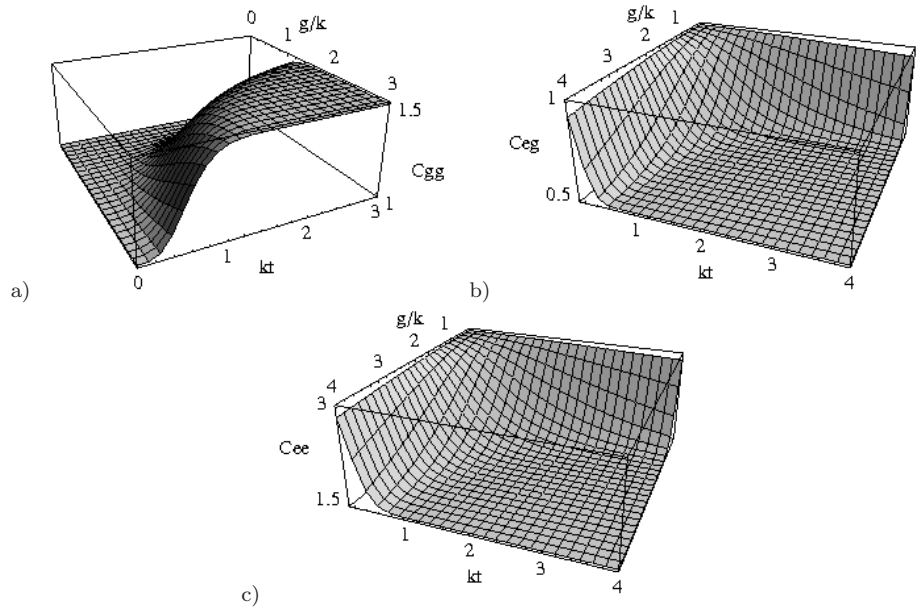

Figure 3.2: Correlation functions (a) C_{gg}, (b) C_{eg}, (c) C_{ee} vs. dimensionless time kt and coupling constant g/k, showing atomic bunching and anti-bunching.

3.2.3 Dynamics of qubit-qubit entanglement

Until now we have discussed the solution of the ME (3.9) for both atoms prepared in the ground state as an example of separable state. In order to describe also initially entangled atoms now we consider the general solution for atoms prepared in a superposition of Bell states $|\psi_a(0)\rangle = \sum_{i=1}^{4} c_i|\nu_i\rangle$, where the coefficients c_i are normalized as $\sum_{i=1}^{4}|c_i|^2 = 1$, and $\{|\nu_i\rangle\}_{i=1,..,4} = \{|\Phi^+\rangle, |\Phi^-\rangle, |\Psi^+\rangle, |\Psi^-\rangle\}$ is the Bell basis where

$$\begin{aligned}
|\Phi^+\rangle &= \frac{|ee\rangle + |gg\rangle}{\sqrt{2}} = \frac{|++\rangle + |--\rangle}{\sqrt{2}} \\
|\Phi^-\rangle &= \frac{|ee\rangle - |gg\rangle}{\sqrt{2}} = -\frac{|+-\rangle + |-+\rangle}{\sqrt{2}} \\
|\Psi^+\rangle &= \frac{|eg\rangle + |ge\rangle}{\sqrt{2}} = \frac{|++\rangle - |--\rangle}{\sqrt{2}} \\
|\Psi^+\rangle &= \frac{|eg\rangle - |ge\rangle}{\sqrt{2}} = \frac{|+-\rangle - |-+\rangle}{\sqrt{2}}
\end{aligned} \tag{3.30}$$

Tracing over the atomic variables the solution for the whole density operator (3.10), we derive the cavity field density operator generalizing Eq. (3.24):

$$\begin{aligned}
\hat{\rho}_f(t) \quad &= \frac{1}{2}\Big[|c_1 + c_3|^2|-2\alpha(t)\rangle\langle -2\alpha(t)| + \\
&+2(|c_2|^2 + |c_4|^2)|0\rangle\langle 0| + |c_1 - c_3|^2|2\alpha(t)\rangle\langle 2\alpha(t)|\Big].
\end{aligned} \tag{3.31}$$

For the mean photon number we obtain $\langle\hat{N}\rangle(t) = (|c_1|^2 + |c_3|^2)2|\alpha(t)|^2$ that is independent of the coefficients of states $|\Phi^-\rangle$ and $|\Psi^-\rangle$, in agreement with the fact that these states are correlated to the vacuum of the cavity field. On the other hand, tracing over the field variables we obtain the atomic density matrix. We report the solution in the so called *magic basis* [22]:

$$\rho_a^{mB} = \begin{pmatrix} \frac{[1+f_2]|c_1|^2+[1-f_2]|c_3|^2}{2} & -\mathrm{i}f_1c_1c_2^* & -\mathrm{i}\frac{[1+f_2]c_1c_3^*+[1-f_2]c_1^*c_3}{2} & f_1c_1c_4^* \\ \mathrm{i}f_1c_1^*c_2 & |c_2|^2 & f_1c_2c_3^* & \mathrm{i}c_2c_4^* \\ \mathrm{i}\frac{[1+f_2]c_1^*c_3+[1-f_2]c_1c_3^*}{2} & f_1c_2^*c_3 & \frac{[1-f_2]|c_1|^2+[1+f_2]|c_3|^2}{2} & \mathrm{i}f_1c_3c_4^* \\ f_1c_1^*c_4 & -\mathrm{i}c_2^*c_4 & -\mathrm{i}f_1c_3^*c_4 & |c_4|^2 \end{pmatrix}, \tag{3.32}$$

where we omitted the time dependence for brevity. To evaluate the entanglement properties of the atomic subsystem we consider the entanglement of formation $\epsilon_F(t)$ [21] defined as

$$\begin{aligned} \epsilon_F(t) &= -\frac{1-\sqrt{1-C^2(t)}}{2}\log_2\frac{1-\sqrt{1-C^2(t)}}{2} + \\ &- \frac{1+\sqrt{1-C^2(t)}}{2}\log_2\frac{1+\sqrt{1-C^2(t)}}{2}, \end{aligned} \tag{3.33}$$

where $C(t)$ is the concurrence that can be evaluated as $C(t) = \max\{0, \Lambda_4(t) - \Lambda_3(t) - \Lambda_2(t) - \Lambda_1(t)\}$ (Λ_i are the square roots of the eigenvalues of the non hermitian matrix $\rho_a^{mB}(t)(\rho_a^{mB}(t))^*$ taken in decreasing order). From Eq. (3.32) we can derive the probabilities for joint atomic measurements in the standard basis

$$\begin{aligned} P_{ee,gg}(t) &= \frac{1}{4}\big[|c_1|^2(1+f_2(t)) + 2|c_2|^2 \\ &+ |c_3|^2(1-f_2(t)) \pm 4f_1(t)Re(c_1c_2^*)\big] \\ P_{eg,ge}(t) &= -\frac{1}{4}\big[|c_1|^2(1-f_2(t)) + 2|c_4|^2 \\ &+ |c_3|^2(1+f_2(t)) \pm 4f_1(t)Re(c_3c_4^*)\big]. \end{aligned} \tag{3.34}$$

Also, we can derive the density matrix corresponding to a single atom and obtain the atomic probabilities generalizing Eq. (3.28):

$$P_{e,g}(t) = \frac{1}{2}\left[1 \pm 2f_1(t)Re(c_1^*c_2 + c_3^*c_4)\right]. \tag{3.35}$$

First we consider the case of a superposition of Bell states $|\Phi^\pm\rangle$ (i.e., $c_1 = a, c_2 = be^{i\theta}, c_3 = c_4 = 0$ with a, b real numbers). The initial atomic state $|gg\rangle$ ($|ee\rangle$) can be obtained if $a = b = \frac{1}{\sqrt{2}}$ and $\theta = \pi$ ($\theta = 0$). We find that the concurrence $C(t)$ vanishes for any time and every value of g/k, so that it is not possible to entangle the atoms. In the case of atoms prepared in a partially entangled state we find that the entanglement of formation can only decrease during the system evolution as shown for example in Fig. 3.3(a) in the case $a = b = \frac{1}{\sqrt{2}}$ and $\theta = \pi/4$. We also see that the progressive loss of entanglement is faster for large values of the parameter g/k. For atoms prepared in the maximally entangled state

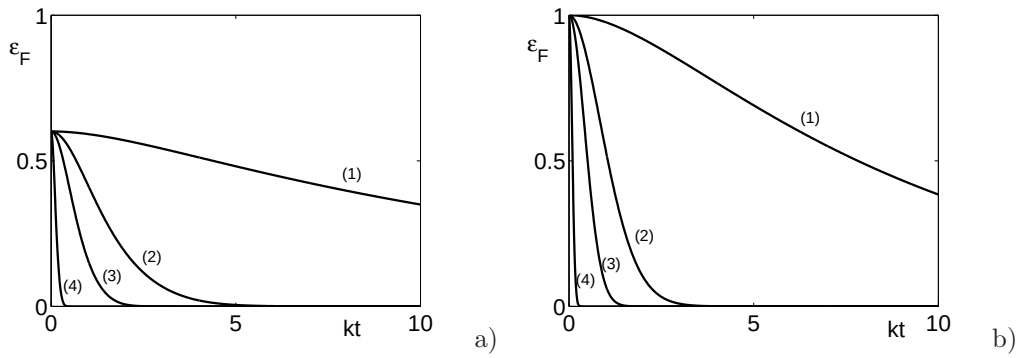

Figure 3.3: Entanglement of formation $\epsilon_F(t)$ as a function of kt and for different values of g/k: 0.1 (1), 0.5 (2), 1 (3), 5 (4). (a) atoms prepared in a partially entangled state $\frac{|\Phi^+\rangle+e^{i\pi/4}|\Phi^-\rangle}{\sqrt{2}}$, (b) atoms prepared in the Bell states $|\Phi^+\rangle$.

$|\Phi^+\rangle$ (i.e., $\theta = 0, a = 1, b = 0$) we derive that the concurrence simply reduces to $f_2(t)$ that also describes the whole system decoherence. This important point will be discussed later. In Fig. 3.3(b) we show the entanglement of formation as a function of dimensionless time kt. For atoms prepared in the maximally entangled state $|\Phi^-\rangle$ (i.e., $\theta = 0, a = 0, b = 1$) the concurrence is always maximum ($C(t) = 1$). In fact, we can see from Eq. (3.32) that the atomic density matrix is always the one of the initial state, as expected because $|\Phi^-\rangle$ is a linear combination of the invariant states $|+-\rangle$ and $|-+\rangle$.

Starting from a superposition of Bell states $|\Psi^\pm\rangle$ (i.e., $c_3 = a, c_4 = be^{i\theta}, c_1 = c_2 = 0$) we obtain analogous results. In particular entanglement cannot be generated for atoms prepared in states $|eg\rangle$ and $|ge\rangle$, for the state $|\Psi^+\rangle$ the concurrence is given by $f_2(t)$, and the entanglement of state $|\Psi^-\rangle$ is preserved during system evolution. We find analogous results also for the concurrence of atoms prepared in a superposition of $|\Phi^-\rangle$ and $|\Psi^+\rangle$ (i.e., $c_2 = a, c_3 = be^{i\theta}, c_1 = c_4 = 0$) or in a superposition of $|\Phi^+\rangle$ and $|\Psi^-\rangle$ (i.e., $c_1 = a, c_4 = be^{i\theta}, c_2 = c_3 = 0$).

Let us summarize and discuss the main results in the case of atoms prepared in entangled states. If we consider a superposition of states $|\Phi^-\rangle$ and $|\Psi^-\rangle$ (i.e., $c_2 = a, c_4 = be^{i\theta}, c_1 = c_3 = 0$) we find that the atomic density matrix of Eq. (3.32) does not evolve. Actually, the atomic subspace spanned by $|\Phi^-\rangle$ and $|\Psi^-\rangle$ coincides with the time-invariant subspace spanned by $|+-\rangle$ and $|-+\rangle$, so that it remains protected from dissipation during the system evolution. It provides an example of Decoherence Free Subspace (DFS) [65]. Atomic entanglement injected in the system can thus remain available for long storage times for applications in quantum information processing [75].

If we consider a superposition of states $|\Phi^+\rangle$ and $|\Psi^+\rangle$ (i.e., $c_1 = a, c_3 = be^{i\theta}, c_2 = c_4 = 0$) the concurrence is given by:

$$C(t) = \sqrt{a^4 + b^4 - 2a^2b^2\cos(2\theta)}f_2(t) \tag{3.36}$$

and we find the remarkable result that the initial entanglement is progressively reduced by the decoherence function $f_2(t)$. Note that $C(t) = f_2(t)$ for states $|\Phi^+\rangle$, $|\Psi^+\rangle$, and any superposition as $a|\Phi^+\rangle \pm ib|\Psi^+\rangle$. To understand this point let us consider the specific example of the initial state $|0\rangle \otimes |\Phi^+\rangle$. The evolved density operator of the whole system is

$$\begin{aligned}\hat{\rho}(t) = \frac{1}{2}\big\{&|-2\alpha(t)\rangle\langle -2\alpha(t)| \otimes |++\rangle\langle ++| + |2\alpha(t)\rangle\langle 2\alpha(t)| \otimes |--\rangle\langle --| + \\ &\frac{f_2(t)}{e^{-8|\alpha(t)|^2}}\big[|-2\alpha(t)\rangle\langle 2\alpha(t)| \otimes |++\rangle\langle --| + |2\alpha(t)\rangle\langle -2\alpha(t)| \otimes |--\rangle\langle ++|\big]\big\}.\end{aligned} \tag{3.37}$$

In the limit, $kt \ll 1$, of short time and/or negligible dissipation, where $f_2(t) \simeq e^{-8|\tilde{\alpha}(t)|^2}$ with $\tilde{\alpha}(t) = \mathrm{i}\frac{gt}{2}$, the system evolves into a pure cat-like state where the atoms are correlated with coherent states

$$|0\rangle \otimes \frac{|++\rangle + |--\rangle}{\sqrt{2}} \mapsto \frac{|-2\tilde{\alpha}\rangle \otimes |++\rangle + |2\tilde{\alpha}\rangle \otimes |--\rangle}{\sqrt{2}}. \tag{3.38}$$

For longer times/larger dissipation, the system coherence decays as described by the function $f_2(t)$. Let us now consider the atomic dynamics disregarding the field subsystem. The reduced atomic density operator is

$$\begin{aligned}\hat{\rho}_a(t) = \frac{1}{2}\big[&|++\rangle\langle ++| + |--\rangle\langle --| \\ &+f_2(t)\big(|++\rangle\langle --| + |--\rangle\langle ++|\big)\big].\end{aligned} \tag{3.39}$$

Hence, as the quantum coherence reduces, simultaneously the atoms lose their inseparability, and the state becomes maximally mixed (in the relevant subspace). In fact, the atomic purity is given by $\mu_a(t) = \frac{1+f_2^2(t)}{2}$. Hence the time evolution of decoherence, concurrence, and purity is described by the function $f_2(t)$, which can be monitored via a measurement of joint atomic probabilities (see Eq. (3.34))

$$\begin{aligned}P_{ee}(t) &= P_{gg}(t) = \frac{1}{4}\left[1 + f_2(t)\right] \\ P_{eg}(t) &= P_{ge}(t) = \frac{1}{4}\left[1 - f_2(t)\right].\end{aligned} \tag{3.40}$$

The probability $P_{ee}(t)$ is shown in Fig. 3.4 as a function of kt for different values of the ratio g/k. For $kt \ll 1$, when the whole system is in the cat-like state (3.38), $f_2(t)$ quadratically decreases as $\exp(-2g^2t^2)$, independent of the dissipative rate k. The subsequent behavior is approximately an exponential decay whose start and rate depend on the atom-cavity field coupling. For $g/k \gtrsim 0.5$, that is also below the strong coupling regime, we can introduce a decoherence and disentanglement rate

$$\gamma_D \simeq k|\alpha^{SS}| = g, \tag{3.41}$$

that is again independent of (and faster than) k. A physical interpretation of this result is that the more coupled the two atoms are to the dissipative cavity mode, the more effective

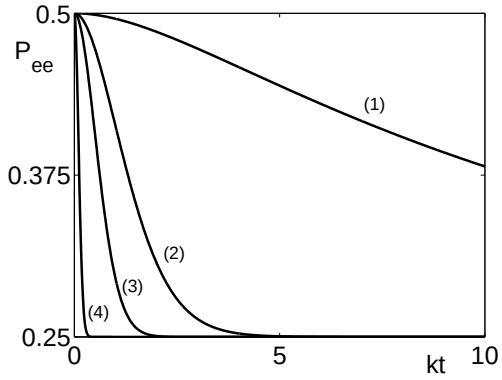

Figure 3.4: Atoms prepared in the Bell state $|\Phi^+\rangle$: joint atomic probability $P_{ee}(t)$ vs. kt for different values of g/k: 0.1 (1), 0.5 (2), 1 (3), 5 (4).

becomes the decay of both the environment-induced decoherence and the initial entanglement. For $g/k \ll 1$, that is in a weak coupling regime, the exponential decay of coherence and concurrence starts later and its rate, $\gamma_D \simeq 8g^2/k$, is slower than the dissipative rate k.

We have shown that under full resonance conditions it is not possible to generate or increase the initial atomic entanglement. This can be explained looking at the initial requirements that allow us to write Eq. (3.11). In particular, the strong driving condition $\Omega \gg g$, the resonance condition $\delta = 0$ and the choice of negligible atomic decays $\gamma = 0$ are necessary to obtain an independent set of equations for the operators $\hat{\rho}_{ij}$ and to exactly solve the system dynamics. In the following we will show that removing the strong driving condition it is possible to slightly entangle the atoms. On the other hand, it can be shown [76] that with off-resonant atoms-cavity field interaction it is possible to generate maximally entangled atomic states also under strong driving conditions. Also we recall that, in the resonant case and without driving field, two atoms prepared in a separable state can partially entangle by coupling to a thermal cavity field [77].

3.2.4 Conditional generation of entangled states

In this section we seek information about the states of one of the two subsystems conditioned by a projective measurement on the other one.

If the system is implemented in the optical domain and the cavity field is accessible to measurements, a null measurement by a on/off detector implies the generation of a maximally entangled atomic Bell state [72]. In the case of atoms prepared in state $|gg\rangle$ (or $|ee\rangle$), the atomic conditioned state will be the Bell state $|\Phi^-\rangle$ (see (3.20)). Analogously, for initial atomic state $|eg\rangle$ or $|ge\rangle$ the atomic conditioned state will be $|\Psi^-\rangle$.

Now we consider the evolution of the field subsystem conditioned by a projective atomic

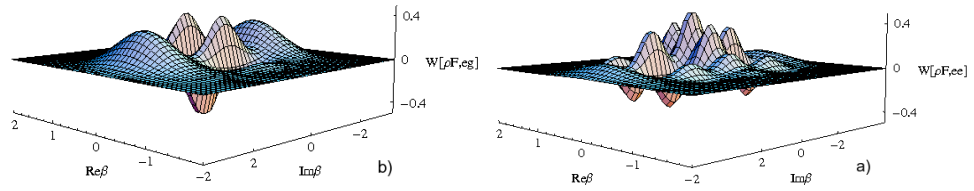

Figure 3.5: Wigner function of the cavity field $W[\hat{\rho}_{f,(ee)}]$ (a) and $W[\hat{\rho}_{f,(eg)}]$ (b), for $\kappa t = 0.05$, and for $\frac{g}{\kappa} = 80$ (a) and $\frac{g}{\kappa} = 40$ (b).

measurement on the bare basis $\{|ee\rangle, |eg\rangle, |ge\rangle, |gg\rangle\}$. Starting e.g. from the initial state $|0\rangle \otimes |gg\rangle$, the cavity field will be in the conditioned states at a given time t (omitted for brevity in this section):

$$\begin{aligned}\hat{\rho}_{f,(ee,gg)} = \frac{1}{2(3 + f_2 \mp 4f_1)}\Big[&|-2\alpha\rangle\langle -2\alpha| + |2\alpha\rangle\langle 2\alpha| + 4|0\rangle\langle 0| \\ &+ f_2 e^{8|\alpha|^2}\Big(|2\alpha\rangle\langle -2\alpha| + |-2\alpha\rangle\langle 2\alpha|\Big) \\ &\mp 2f_1 e^{2|\alpha|^2}\Big(|0\rangle\langle -2\alpha| + |0\rangle\langle 2\alpha| + |-2\alpha\rangle\langle 0| + |2\alpha\rangle\langle 0|\Big)\Big]\end{aligned} \tag{3.42}$$

$$\hat{\rho}_{f,(eg,ge)} = \frac{1}{2(1 - f_2)}\Big[|-2\alpha\rangle\langle -2\alpha| + |2\alpha\rangle\langle 2\alpha| - f_2 e^{8|\alpha|^2}\Big(|2\alpha\rangle\langle -2\alpha| + |-2\alpha\rangle\langle 2\alpha|\Big)\Big]. \tag{3.43}$$

Note that in the limit $\kappa t \ll 1$, the transient regime, the conditioned field state is a Schrödinger-cat-like state

$$|\psi\rangle_{f,(ee,gg)} = \frac{|-2\tilde{\alpha}\rangle \mp 2|0\rangle + |2\tilde{\alpha}\rangle}{\sqrt{2(e^{-8|\tilde{\alpha}|^2} \mp 4e^{-2|\tilde{\alpha}|^2} + 3)}} \tag{3.44}$$

$$|\psi\rangle_{f,(eg,ge)} = \frac{|-2\tilde{\alpha}\rangle - |2\tilde{\alpha}\rangle}{\sqrt{2(1 - e^{-8|\tilde{\alpha}|^2})}} \tag{3.45}$$

where $\tilde{\alpha}(t) = \mathrm{i}\frac{gt}{2}$.

It is possible to calculate the Wigner function for the conditional cavity field state. It describes in the phase space the properties of a quantum state since, even though it is a regular and normalized function, can assume negative values and for this reason it is sometimes called *quasi-probability function*. The Wigner function can be written in the form [78]:

$$W[\rho](\beta) = \frac{2}{\pi} Tr\left[\rho\hat{\mathcal{D}}(2\beta)\hat{\Pi}\right] \tag{3.46}$$

where $\hat{\mathcal{D}}$ is the usual displacement operator and $\hat{\Pi} = (-)^{\hat{a}^\dagger \hat{a}} = \sum_n (-)^n |n\rangle\langle n|$ is the parity operator. Since the trace operation is linear it is possible to calculate the single terms composing the operators in 3.44 by using the following properties of displacement and parity

operators:

$$\hat{\mathcal{D}}^{\dagger}(\lambda) = \hat{\mathcal{D}}(-\lambda) \tag{3.47a}$$

$$\hat{\mathcal{D}}(\lambda_1)\hat{\mathcal{D}}(\lambda_2) = \hat{\mathcal{D}}(\lambda_1+\lambda_2)exp\left\{\frac{1}{2}\left(\lambda_1\lambda_2^* - \lambda_1^*\lambda_2\right)\right\} \tag{3.47b}$$

$$\hat{\mathcal{D}}^{\dagger}(\lambda)\hat{\mathcal{D}}(z)\hat{\mathcal{D}}(\lambda) = \hat{\mathcal{D}}(z)exp\{z\lambda^* - z^*\lambda\} \tag{3.47c}$$

$$\hat{\mathcal{D}}(\lambda)\hat{\mathcal{D}}(z)\hat{\mathcal{D}}(\lambda) = \hat{\mathcal{D}}(z+2\lambda) \tag{3.47d}$$

$$\hat{\Pi}|\alpha\rangle = |-\alpha\rangle \tag{3.47e}$$

We thus obtain for each term:

$$\begin{aligned}
W[|\pm 2\alpha\rangle\langle\pm 2\alpha|](\beta) &= \frac{2}{\pi}exp\{-2|\beta|^2 - 8|\alpha|^2 \pm 8|\alpha|\mathrm{Im}\beta\}\\
W[|\pm 2\alpha\rangle\langle\mp 2\alpha|](\beta) &= \frac{2}{\pi}exp\{-2|\beta|^2 \pm 8\mathrm{i}|\alpha|\mathrm{Re}\beta\}\\
W[|0\rangle\langle 0|](\beta) &= \frac{2}{\pi}exp\{-2|\beta|^2\}\\
W[|0\rangle\langle\pm 2\alpha|](\beta) &= \frac{2}{\pi}exp\{-2|\beta|^2 - 2|\alpha|^2 \mp 4|\alpha|\mathrm{Im}\beta \pm 4\mathrm{i}|\alpha|\mathrm{Re}\beta\}\\
W[|\pm 2\alpha\rangle\langle 0|](\beta) &= \frac{2}{\pi}exp\{-2|\beta|^2 - 2|\alpha|^2 \pm 4|\alpha|\mathrm{Im}\beta \pm 4\mathrm{i}|\alpha|\mathrm{Re}\beta\}
\end{aligned}$$

By recombining these terms we obtain the Wigner function corresponding to the states (3.44):

$$\begin{aligned}
W_{f,(ee,gg)}(\beta) = \frac{2e^{-2|\beta|^2}}{\pi(3+f_2\mp 4f_1)}\Big[&2 + e^{-8|\alpha|^2}\cosh(8|\alpha|Im\beta)\\
&+ f_2 e^{8|\alpha|^2}\cos(2|\alpha|Re\beta) \mp 4f_1\cosh(4|\alpha|Im\beta)\cos(4|\alpha|Re\beta)\Big]
\end{aligned} \tag{3.48}$$

$$W_{f,(eg,ge)}(\beta) = \frac{2e^{-2|\beta|^2}}{\pi(1-f_2)}\Big[e^{-8|\alpha|^2}\cosh(8|\alpha|Im\beta) - f_2 e^{8|\alpha|^2}\cos(8|\alpha|Re\beta)\Big]. \tag{3.49}$$

In Fig. 3.5 we illustrate two of the Wigner functions (3.48) in the transient $\kappa t \ll 1$ and in the strong coupling regime $g \gg \kappa$. At steady state the Wigner functions are positive, corresponding to the states:

$$\begin{aligned}
\hat{\rho}^{SS}_{F,(ee,gg)} &= \frac{1}{6}\left[|-2\alpha^{SS}\rangle\langle -2\alpha^{SS}| + |2\alpha^{SS}\rangle\langle 2\alpha^{SS}| + 4|0\rangle\langle 0|\right]\\
\hat{\rho}^{SS}_{F,(eg,ge)} &= \frac{1}{2}\left[|-2\alpha^{SS}\rangle\langle -2\alpha^{SS}| + |2\alpha^{SS}\rangle\langle 2\alpha^{SS}|\right]
\end{aligned} \tag{3.50}$$

where $\alpha^{SS} = \mathrm{i}\frac{g}{\kappa}$.

3.2.5 Numerical results

To confirm our theoretical analysis, as well as to investigate system dynamics without the strong driving condition, where analytical results are not available, and to include atomic

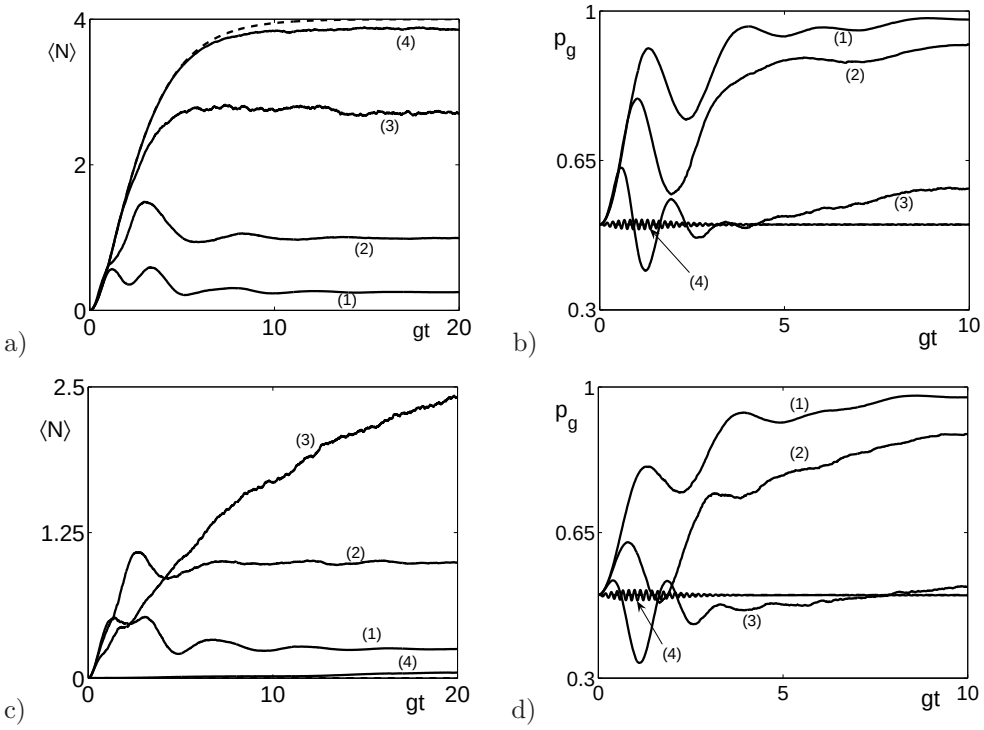

Figure 3.6: Effect of driving parameter $\tilde{\Omega}$ for negligible atomic decay $\tilde{\gamma} = 0$, $\tilde{k} = 1$, atoms prepared in the Bell state $|\Phi^+\rangle$ ((a),(b)) and $|\Phi^-\rangle$ ((c),(d)), for values of $\tilde{\Omega}$: 0.5 (1), 1 (2), 2 (3), 20 (4). The theoretical functions are the dashed lines. We show in (a),(c) the mean photon number $\langle\hat{N}(\tilde{t})\rangle$, and in (b),(d) the atomic probability $p_g(\tilde{t})$. The number of trajectories is $N_{tr} = 500$.

spontaeous emission, we numerically solve, by Monte Carlo Wave Function (MCWF) method [17], the ME (3.7) in the resonant case $\delta = 0$, that we rewrite in the Lindblad form:

$$\dot{\hat{\rho}}_I = -\frac{i}{\hbar}(\hat{\mathcal{H}}_e\hat{\rho}_I - \hat{\rho}_I\hat{\mathcal{H}}_e^\dagger) + \sum_{i=1}^{3}\hat{C}_i\hat{\rho}_I\hat{C}_i^\dagger \tag{3.51}$$

where the non-Hermitian effective Hamiltonian $\hat{\mathcal{H}}_e$ is given by

$$\hat{\mathcal{H}}_e = \frac{\hat{\mathcal{H}}^I}{g} - \frac{i\hbar}{2}\sum_{i=1}^{3}\hat{C}_i^\dagger\hat{C}_i, \tag{3.52}$$

the Hamiltonian $\hat{\mathcal{H}}^I$ is that of Eq. (3.2) for $\delta = 0$, and the collapse operators are $\hat{C}_{1,2} = \sqrt{\tilde{\gamma}}\hat{\sigma}_{1,2}$, $\hat{C}_3 = \sqrt{\tilde{k}}\hat{a}$. We have introduced the scaled time $\tilde{t} = gt$ so that the relevant dimensionless system parameters are:

$$\tilde{\Omega} = \frac{\Omega}{g} \quad \tilde{k} = \frac{k}{g} \quad \tilde{\gamma} = \frac{\gamma}{g}. \tag{3.53}$$

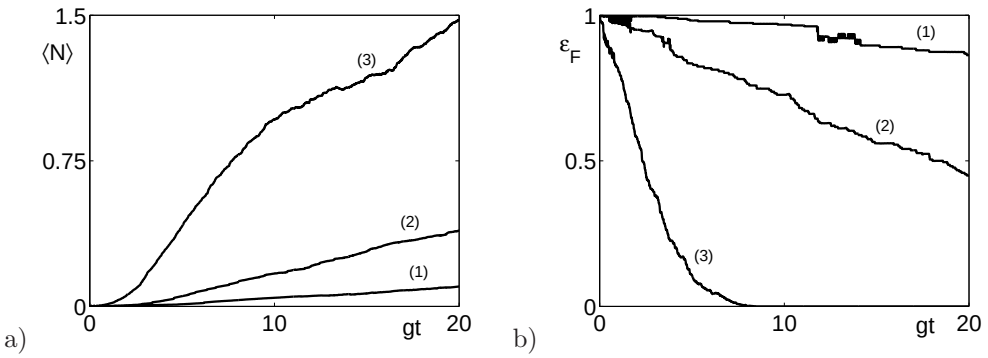

Figure 3.7: Effect of atomic decay $\tilde{\gamma}$ in the strong driving condition $\tilde{\Omega} = 20$, atoms prepared in the Bell state $|\Phi^-\rangle$ and $\tilde{k} = 1$: $\tilde{\gamma} = 0.001(1)$, 0.01 (2), 0.1 (3). (a) Mean photon number $\langle\hat{N}(\tilde{t})\rangle$, (b) Entanglement of formation $\epsilon_F(\tilde{t})$. The number of trajectories is $N_{tr} = 500$.

The system dynamics can be simulated by a suitable number N_{tr} of trajectories, i.e. stochastic evolutions of the whole system wave function $|\psi_j(\tilde{t})\rangle$ $(j = 1, 2, ...N_{tr})$. Therefore, the statistical operator of the whole system can be approximated by averaging over the N_{tr} trajectories, i.e.,

$$\hat{\rho}_I(\tilde{t}) \cong \frac{1}{N_{tr}} \sum_{i=j}^{N_{tr}} |\psi_j(\tilde{t})\rangle\langle\psi_j(\tilde{t})|$$

.

First we consider negligible atomic decay $\tilde{\gamma} = 0$ to confirm the analytical solutions and to evaluate the effect of the driving parameter $\tilde{\Omega}$. For numerical convenience we consider the case $\tilde{k} = 1$ so that the steady state mean photon number assumes small enough values. We consider the atoms prepared in the maximally entangled states $|\Phi^{\pm}\rangle$. We recall that for the state $|\Phi^+\rangle$ the theoretical mean photon number is $\langle\hat{N}(\tilde{t})\rangle = |\alpha(\tilde{t})|^2$, the atomic populations $P_{e,g}(\tilde{t}) = 0.5$, the atomic purity $\mu_a(\tilde{t}) = \frac{1+f_2^2(\tilde{t})}{2}$, and the entanglement of formation $\epsilon_F(t)$ is given by (3.33) where the concurrence $C(t)$ coincides with $f_2(t)$. In Fig. 3.6 we show e.g. the mean photon number and the atomic probability $p_g(t)$. In the strong driving limit, $\tilde{\Omega} = 20$, we find an excellent agreement with the predicted theoretical behavior. We note that we simulated the system dynamics without the RWA approximation so that $p_g(\tilde{t})$ exhibits oscillations due to the driving field. We remark that the entanglement of formation in the case of state $|\Phi^+\rangle$ evolves almost independently of parameter $\tilde{\Omega}$ and becomes negligible after times $gt \approx 2$. In the case of state $|\Phi^-\rangle$ $\epsilon_F(t)$ decays in a similar way for small values of $\tilde{\Omega}$, but it remains close to 1 for large enough values of the driving parameter as predicted in our analysis.

Finally, we consider the effect of the atomic decay. For example, we consider the atoms prepared in the Bell state $|\Phi^-\rangle$ in the strong driving limit and for the cavity field decay rate $\tilde{k} = 1$. In Fig. 3.7 we show the mean photon number and the entanglement of formation.

We see that for $\tilde{\gamma}$ up to 10^{-3} the effect of atomic decays is negligible and the results of our treatment still apply. For larger decay rates the atomic dynamics becomes no more restricted within the decoherence free subspace.

3.3 N-qubit case

In this section we want to generalize the previous model for two qubits and a single cavity mode in contact with a lossy environment. Firstly we recast the problem with a more general formalism for the N atoms Hilbert space, in order to derive a compact set of differential equations. In this general treatment we include the atomic spontaneous emission dissipative channel, since in the ME (3.9) the corresponding Liouvillian superoperator in Eq. (3.8) possess a particular structure that leaves uncoupled the differential equations. Secondly we focus our attention to the topic of decoherence free subspaces (DFS), entering into the details of $N = 3$ and $N = 4$ atoms case.

3.3.1 Analytical solution

In this section we will exploit the Hilbert space of the N atoms to get a general solution of the system ME (3.9). To this purpose we write the effective Hamiltonian (3.3) in the compact form

$$\hat{\mathcal{H}}_{\text{eff}} = \hbar g(\hat{a} + \hat{a}^\dagger)\hat{S}_x \tag{3.54}$$

where we have introduced the collective atomic operator $\hat{S}_x = \frac{1}{2}\sum_{l=1}^{N}\hat{\sigma}_{x,l} = \frac{1}{2}\sum_{l=1}^{N}(\hat{\sigma}_l^\dagger + \hat{\sigma}_l)$. We recall that the eigenstates of the spin operator $\hat{\sigma}_{x,l}$ are the rotated states $|\pm\rangle_l$ with $\hat{\sigma}_{x,l}|\pm\rangle_l = \lambda_l^{\pm}|\pm\rangle_l$ and $\lambda_l^{\pm} = \pm 1$. For the whole atomic subspace we consider the collective basis of 2^N states $\{|i\rangle_N\}$ where any $|i\rangle_N$ is an eigenstate of the operator $\hat{S}_x$. The associated eigenvalue $s_i = (1/2)\sum_{l=1}^{N}\lambda_{l,i}^{\pm}$ is half the difference between the number of $|+\rangle$ and $|-\rangle$ components of state $|i\rangle_N$, regardless of the exchange of any qubit pair, and it can assume $N+1$ values from $-N/2$ to $N/2$ with steps $|\Delta s_i| = 1$. Each eigenvalue s_i has a degeneracy order $n(s_i) = \frac{N!}{(N/2+s_i)!(N/2-s_i)!}$ which is greater than one if $s_i \neq \pm N/2$. Summarizing we have:

$$\hat{S}_x = \frac{1}{2}\sum_{l=1}^{N}\hat{\sigma}_{x,l} \tag{3.55}$$

$$\hat{S}_x|i\rangle_N = s_i|i\rangle_N \tag{3.56}$$

Since atoms are represented in the ME (3.9) only by $\hat{\sigma}_{x,l}$ operators, we introduce a decomposition of the density operator $\hat{\rho}(t)$ on the basis $\{|i\rangle_N\}$. Equation (3.9) is then equivalent to the following set of 2^{2N} uncoupled evolution equations for the field operators $\hat{\rho}_{ij} = {}_N\langle i|\hat{\rho}(t)|j\rangle_N$

$$\dot{\hat{\rho}}_{ij} = -\mathrm{i}g\big[s_i(\hat{a} + \hat{a}^\dagger)\hat{\rho}_{ij} - s_j\hat{\rho}_{ij}(\hat{a} + \hat{a}^\dagger)\big] + \hat{\mathcal{L}}_f\hat{\rho}_{ij} - \frac{\gamma}{2}m_{ij}\hat{\rho}_{ij} \tag{3.57}$$

where $m_{ij} = \frac{1}{2}\sum_{l=1}^{N}\Big[1-\lambda_{l,i}^{\pm}\lambda_{l,j}^{\pm}\Big]$. We remark that the coefficients m_{ij} can assume the values $0, 1, ..., N$, that is the number of single-qubit spin-flips for each atomic coherence ${}_N\langle i|\cdots|j\rangle_N$. This means that the atomic damping affects all the off-diagonal matrix elements of $\hat{\rho}$, leaving the diagonal ones unchanged. In order to obtain a solution for each time evolution equation, we use the characteristic function [73] defined in the phase space associated to the cavity field as $\chi_{ij}(\beta) = \mathrm{Tr}[\hat{D}(\beta)\hat{\rho}_{ij}]$, where $\hat{D}(\beta)$ is the displacement operator. As before we remark that $\chi_{ij}(\beta)$ are not true characteristic functions, since $\hat{\rho}_{ij}$ are not density operators. Nevertheless, they are continuous and square integrable functions and this is enough for our purposes. Each operator equation (3.57) becomes a partial differential equation in phase space

$$\begin{aligned}\dot{\chi}_{ij} = -\mathrm{i}g\Big[s_i\Big(\frac{\partial}{\partial\beta} - \frac{\partial}{\partial\beta^*} - \frac{\beta+\beta^*}{2}\Big) - s_j\Big(\frac{\partial}{\partial\beta} - \frac{\partial}{\partial\beta^*} + \frac{\beta+\beta^*}{2}\Big)\\ - \frac{k}{2}\Big(\beta\frac{\partial}{\partial\beta} + \beta^*\frac{\partial}{\partial\beta^*} + |\beta|^2\Big) - \frac{\gamma}{2}m_{ij}\Big]\chi_{ij}.\end{aligned} \tag{3.58}$$

We choose as initial preparation of the whole system the cavity in the vacuum state $|0\rangle$ and the atoms in a general pure state

$$|\Psi(0)\rangle = |0\rangle \otimes \sum_{i=1}^{2^N} c_{N,i}|i\rangle_N \tag{3.59}$$

with the normalization condition $\sum_{i=1}^{2^N}|c_{N,i}|^2 = 1$. After a change from complex to real variables $\beta = x + \mathrm{i}y$ and the use of the method of characteristics [67], we obtain the solution $\chi_{ij}(x, y, t)$. Hence, back in the original variables, the solution of the ME (3.9) for the whole system density operator can be written in a remarkably compact form as

$$\hat{\rho}(t) = \sum_{i,j=1}^{2^N} c_{N,i}c_{N,j}^*[f(t)]^{(s_i-s_j)^2}\mathrm{e}^{-\frac{\gamma}{2}m_{ij}t}|-2s_i\alpha(t)\rangle\langle-2s_j\alpha(t)| \otimes |i\rangle_N\langle j| \tag{3.60}$$

where the atomic states are correlated with coherent cavity field states of amplitude proportional to

$$\alpha(t) = \mathrm{i}\frac{g}{\kappa}\left(1 - \mathrm{e}^{-\frac{\kappa}{2}t}\right) \tag{3.61}$$

and $f(t)$ is the decoherence function due to the cavity environment coupling. It can be written as $f(t) = f_1(t)\mathrm{e}^{2|\alpha(t)|^2}$, where $\mathrm{e}^{2|\alpha(t)|^2}$ is a coherent state normalization and

$$f_1(t) = e^{-\frac{2g^2}{\kappa}t + \frac{4g^2}{\kappa^2}\left(1-\mathrm{e}^{-\frac{\kappa}{2}t}\right)}. \tag{3.62}$$

We remark that the product $f_1(t)\mathrm{e}^{-\frac{\gamma}{2}t}$ describes the basic one-atom decoherence, that includes either the cavity loss or the atomic spontaneous emission contributions.

The solution we have found comes straightforwardly from that of the one-qubit case, in fact we recover the basic one-atom decoherence function, generalized to the case of $\gamma \neq 0$.

3.3.2 Global system dynamics

In the Hamiltonian limit, $\{\kappa t, \gamma t\} \ll 1$, both decoherence functions $f_1(t)$ and $\mathrm{e}^{-\frac{\gamma}{2}t}$ approach unity, $\alpha(t) \to \tilde{\alpha}(t) \equiv \mathrm{i}\frac{gt}{2}$ and $\hat{\rho}(t) \to |\tilde{\Psi}(t)\rangle\langle\tilde{\Psi}(t)|$ with the pure state

$$|\tilde{\Psi}(t)\rangle = \sum_{i=1}^{2^N} c_{N,i}|-2s_i\tilde{\alpha}(t)\rangle \otimes |i\rangle_N. \tag{3.63}$$

Hence we find the generation of global (N qubits and cavity mode) cat-like states, discussed in [69] and [68], also in connection with the conditioned generation of entangled states.
In the steady state limit $\{\kappa t, \gamma t\} \gg 1$ the density operator $\hat{\rho}(t)$ becomes a statistical mixture of the pure states superimposed in the global cat-like state (3.63) generated in the transient

$$\hat{\rho}^{SS} = \sum_{i=1}^{2^N} |c_{N,i}|^2|-2s_i\alpha^{SS}\rangle\langle-2s_i\alpha^{SS}| \otimes |i\rangle_N\langle i|, \tag{3.64}$$

where $\alpha^{SS} = \mathrm{i}\frac{g}{\kappa}$.
From Eq. (3.60) we can evaluate the time evolution of the whole system purity

$$\mu(t) = Tr[\hat{\rho}^2(t)] = \sum_{i,j=1}^{2^N} |c_{N,i}|^2|c_{N,j}|^2[f(t)]^{2(s_i-s_j)^2}\mathrm{e}^{-\gamma m_{ij}t}. \tag{3.65}$$

3.3.3 Subsystems dynamics

Now we discuss the time evolution of the subsystems. The cavity field dynamics, obtained by tracing over the atomic degrees of freedom, holds as discussed in [69]. Here we recall only the expressions of the reduced density operator

$$\hat{\rho}_f(t) = \sum_{i=1}^{2^N} |c_{N,i}|^2|-2s_i\alpha(t)\rangle\langle-2s_i\alpha(t)|, \tag{3.66}$$

that is a statistical mixture of coherent states, and whose purity is

$$\mu(t) = Tr[\hat{\rho}^2(t)] = \sum_{i,j=1}^{2^N} |c_{N,i}|^2|c_{N,j}|^2[\mathrm{e}^{2|\alpha(t)|^2}]^{2(s_i-s_j)^2}. \tag{3.67}$$

From the density operator $\hat{\rho}_{N,f}(t)$ we can derive the expression of the mean photon number

$$\langle\hat{a}^\dagger\hat{a}\rangle(t) = Tr_f[\hat{\rho}_f(t)\hat{a}^\dagger\hat{a}] = 4|\alpha(t)|^2\sum_{i=1}^{2^N} s_i^2|c_{N,i}|^2. \tag{3.68}$$

In the case of all atoms prepared in the ground state, $c_{N,i} = 1/\sqrt{2^N}$, we obtain

$$\langle\hat{a}^\dagger\hat{a}\rangle(t) = \frac{|\alpha(t)|^2}{2^{N-2}}\sum_{l=0}^{N}\left(l-\frac{N}{2}\right)\binom{N}{l} = N|\alpha(t)|^2 \tag{3.69}$$

which assumes the value $N|\alpha^{SS}|^2 = N\big(g/\kappa\big)^2$ at steady-state. This result shows that each atom gives the same average contribution $|\alpha(t)|^2$ to the cavity field. The result (3.68) corresponds to transforming $g \to g\sqrt{N}$ relative to the one-atom theory of [64].
By tracing the whole system density operator (3.60) over the field variables, we obtain the reduced atomic density operator

$$\hat{\rho}_a(t) = \sum_{i,j=1}^{2^N} c_{N,i} c^*_{N,j} [f_1(t)]^{(s_i - s_j)^2} \mathrm{e}^{-\frac{\gamma}{2} m_{ij} t} |i\rangle_N \langle j|. \tag{3.70}$$

Its purity μ_a has the form of Eq. (3.65), provided that $f(t)$ is replaced by $f_1(t)$. In the steady-state limit the two purities assume the same value $\mu^{SS} = \sum_i^{2^N} |c_{N,i}|^4$ and for atoms all prepared in the excited or ground state it becomes $\frac{1}{2^N}$, that is the value of a maximally mixed state for an N-qubit system.

3.3.4 Decoherence free subspaces and completely symmetric Dicke states

The presence of atomic spontaneous emission has the obvious consequence to destroy all the off-diagonal terms of $\hat{\rho}(t)$, bringing the system to a statistical mixture in the steady state. What we could ascertain in the previous section, is that for $\gamma \simeq 0$ and the only presence of cavity mode dissipation, particular dark states of the system are not affected by decoherence induced from the environment, that span what we call *decoherence free subspaces* (DFS). Here we want to generalize that situation to the case of N atoms.
The first step is to exploit the system dynamical invariance under exchange of any atom pair, considering initial states (Eq. (3.59)) having in the atomic part only symmetric states or symmetrized combinations of states $|i\rangle_N$. In this case the atomic part of $\hat{\rho}(t)$ is confined in the subspace spanned by only $N+1$ (instead of 2^N) states that we denote as $|\frac{N}{2}, s\rangle$, where $-\frac{N}{2} \leq s \leq \frac{N}{2}$ with steps $|\Delta s| = 1$. We notice that these states are analogous to the so-called completely symmetric Dicke (CSD) states [79], with the only difference that here they are written in the rotated basis. All the previous treatment can be adapted correspondingly. In particular, starting from any superposition of CSD states

$$|\Psi(0)\rangle = |0\rangle \otimes \sum_{s=-N/2}^{N/2} b_{N,s} |\frac{N}{2}, s\rangle \tag{3.71}$$

with the normalization condition $\sum_{s=-N/2}^{N/2} |b_{N,s}|^2 = 1$, the general solution (3.60) can be rewritten as

$$\hat{\rho}(t) = \sum_{s,s'=-N/2}^{N/2} b_{N,s} b^*_{N,s'} [f(t)]^{(s-s')^2} |-2s\alpha(t)\rangle\langle -2s'\alpha(t)| \otimes |\frac{N}{2}, s\rangle\langle \frac{N}{2}, s'|. \tag{3.72}$$

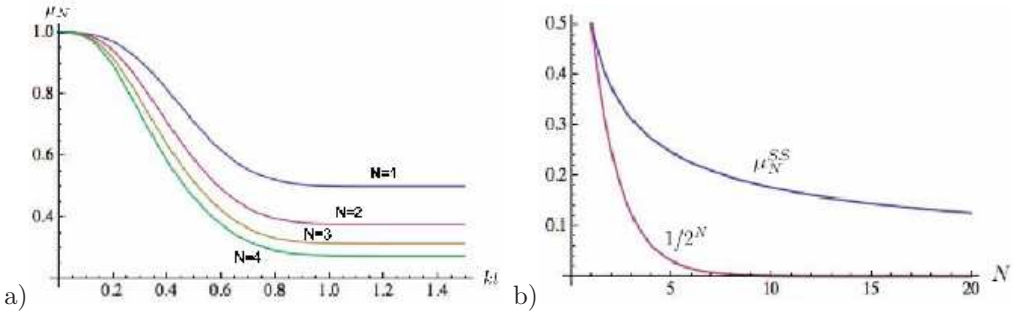

Figure 3.8: a) Time evolution of the purity of the whole system for different values of N and for the fixed dimensionless parameter $g/\kappa = 5$. b) Comparison between the N-qubit purity $\mu_a(t)$ evaluated at steady state and the purity of a maximally mixed state $a/2^N$.

In this case the interaction correlates cavity field coherent states with atomic CSD states. These results include the important acse of all atoms prepared in the ground state, where $b_{N,s} = (1/\sqrt{2^N})n(s)$. In another relevant case, with all atoms prepared in the excited state, the only change in Eq. (3.72) is the replacement $f(t) \to -f(t)$. In such cases the purity (3.65) reduces to

$$\mu(t) = Tr[\hat{\rho}^2(t)] = \frac{1}{2^{2N}} \sum_{s,s'=N/2}^{N/2} [f(t)]^{2(s-s')^2} n(s)n(s') \tag{3.73}$$

whose asymptotic value can be written in a closed form in terms of the Gamma function Γ

$$\mu_N^{SS} = \frac{1}{2^{2N}} \sum_{s,s'=N/2}^{N/2} n^2(s) = \frac{1}{2^{2N}} \sum_{l=0}^{N} \binom{N}{l}^2 = \frac{\Gamma(N+\frac{1}{2})}{\sqrt{\pi}\Gamma(N+1)} \tag{3.74}$$

where $l \equiv s + N/2$ and $\binom{N}{l}$ is the binomial coefficient. In Fig. (3.8) we show the time evolution of the system purity (3.73) fora fixed value of g/κ and different qubit numbers $N = 1, \ldots, 4$, where the steady state values are $\mu_1^{SS} = 1/2, \mu_2^{SS} = 3/8, \mu_3^{SS} = 5/16, \mu_4^{SS} = 35/128$. The greater is the value of N, the faster is the decay of the global coherences. Varying the ration g/κ instead of N, the asymptotic behaviour does not change whereas the decay is faster (slower) for increasing (decreasing) values of g/κ.

We remark that the atomic preparation in one of the CSD states is equivalent to the qubit encoding in the corresponding DFS (see the case $N = 3, 4$ below). In particular, for even values of N, the CSD atomic state with $s = 0$ and the cavity in the vacuum state belongs to a global DFS, where the whole system does not evolve. In fact if the atoms are prepared in any superposition of eigenstates $|i\rangle_N$ corresponding to a degenerate eigenvalue $-\frac{N}{2} \leq s_i \leq \frac{N}{2}$, the state does not evolve and this is equivalent to choose a particular initial atomic Dicke state $|\frac{N}{2}, s\rangle$ Therefore we identify $N-1$ atomic DFSs with dimension $n(s_i) > 1$, where an initial entanglement can be protected.

One of the effect of the presence of DFSs can be put in evidence by the atomic purity

$$\mu_a(t) = \sum_{s,s'=-N/2}^{N/2} |b_{N,s}|^2 |b_{N,s'}|^2 [f_1(t)]^{2(s-s')^2}. \tag{3.75}$$

The decay of the atomic purity ruled by $f_1(t)$ is faster than the global purity decay (3.65), ruled by $f(t)$. However the asymptotic behaviour is the same and we can use the result (3.74) in order to make a comparison with the case of maximally mixed states, whose purity is equal to $1/2^N$. In Fig. (3.8(b)) we see that the atomic state is maximally mixed only for $N = 1$, where actually the atom becomes maximally entangled with the cavity field [64]. For any $N > 1$ the state is never maximally mixed due to the survival of coherences in DFSs. Also we notice that the field purity (3.67)remains slightly larger than the atomic one because the decoherence function $f_1(t)$ is replaced by a non-vanishing exponential function.

3.3.5 The $N = 3$ and $N = 4$ cases

Here we discuss interesting results on both atomic and field subsystems in the case of three and four atoms, neglecting the atomic spontaneous emission $\gamma \simeq 0$. We investigate the expression of the joint probabilities for the atomic level populations and we exploit the existence of DFSs for the protection of the multipartite entanglement. We also show the conditional generation of cavity field cat-like states during the transient and propose a way to monitor their decoherence via joint atomic probability measurements.

$N = 3$ qubits

As an application of the atomic subsystem dynamics we rewrite the atomic density matrix equation (3.70) in the standard basis for the case $N = 3$. Starting, for instance, from the three atoms in the ground state, the diagonal matrix elements provide the following joint probabilities for the atomic level populations where equations (3.76b) and (3.76c) represent one third of the probability to detect, respectively, two atoms in the excited state or in the ground, independently from the atomic ordering, that is to say $P_{eeg} = P_{ege} = P_{gee}$ and $P_{egg} = P_{geg} = P_{gge}$. The three-atom joint probabilities (3.76) are shown in Fig. 3.9. We can see that at steady state the joint probability that three atoms are in the same state is equal to 5/16, that is an atomic correlation (bunching) effect, whereas the joint probability of the other two outcomes is 3/16, showing an antibunching effect. By exploiting the above expressions (3.76) it is possible to monitor the two-atom decoherence function $f_1^4(t)$ measuring the sums $P_{eee}(t) + P_{ggg}(t)$ or $P_{eeg}(t) + P_{egg}(t)$. Remarkably the N-qubit decoherence originates from the one-atom decoherence function [64] which can be monitored by atomic population measurements via the relation $f_1(t) = P_g(t) - P_e(t)$, as well as the N-qubit purity according to Eq. (3.75). In that case the atom and the field

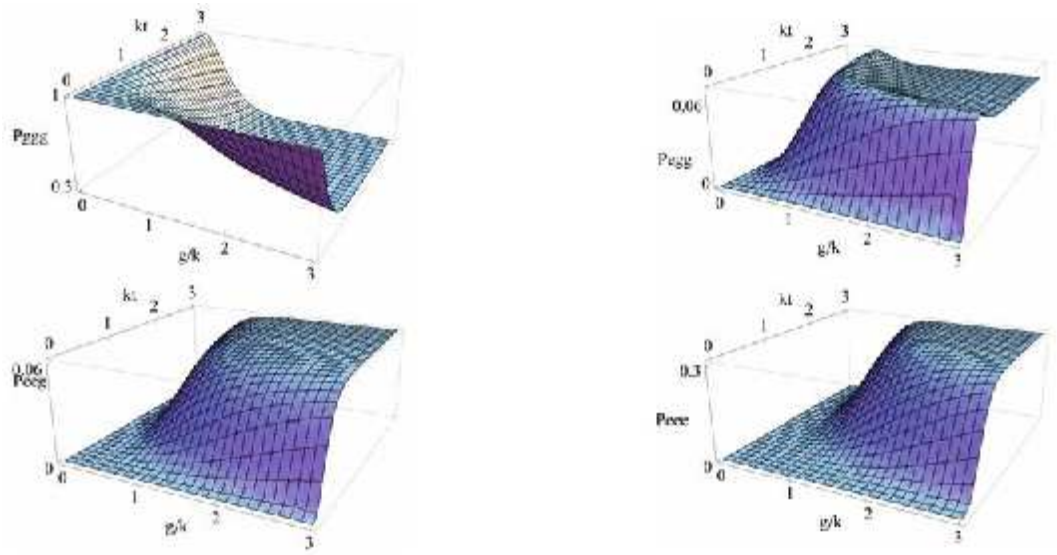

Figure 3.9: Three-atom joint probabilities vs. dimensionless coupling constant g/κ and time κt .

can approach maximally entangled states in the limits $\kappa t \ll 1$ and $(g/\kappa)^2 \gg 1$, and the entanglement (measured by the Von Neumann entropy for one subsystem) is also described by $f_1(t)$.

$$P_{eee}(t) = \frac{1}{32}\left[10 - 15f_1(t) + 6f_1^4(t) - f_1^9(t)\right] \tag{3.76a}$$

$$P_{eeg}(t) = \frac{1}{32}\left[2 - f_1(t) - 2f_1^4(t) + f_1^9(t)\right] \tag{3.76b}$$

$$P_{egg}(t) = \frac{1}{32}\left[2 + f_1(t) - 2f_1^4(t) - f_1^9(t)\right] \tag{3.76c}$$

$$P_{ggg}(t) = \frac{1}{32}\left[10 + 15f_1(t) + 6f_1^4(t) + f_1^9(t)\right] \tag{3.76d}$$

$$\tag{3.76e}$$

Starting from three atoms in the ground state, so that $c_{3,i} = 1/\sqrt{8}$, we obtain in the transient regime ($\kappa t \ll 1$) a pure state that we rewrite in the standard atomic basis

$$\begin{aligned}|\tilde{\Psi}\rangle_3 = \frac{1}{\sqrt{8}}\Big[&(|-3\tilde{\alpha}\rangle - 3|-\tilde{\alpha}\rangle + 3|\tilde{\alpha}\rangle - |3\tilde{\alpha}\rangle) \otimes |eee\rangle \\ &+ (|-3\tilde{\alpha}\rangle + 3|-\tilde{\alpha}\rangle + 3|\tilde{\alpha}\rangle + |3\tilde{\alpha}\rangle) \otimes |ggg\rangle \\ &+ (|-3\tilde{\alpha}\rangle - |-\tilde{\alpha}\rangle - |\tilde{\alpha}\rangle + |3\tilde{\alpha}\rangle) \otimes (|eeg\rangle + |ege\rangle + |gee\rangle) \\ &+ (|-3\tilde{\alpha}\rangle + |-\tilde{\alpha}\rangle - |\tilde{\alpha}\rangle - |3\tilde{\alpha}\rangle) \otimes (|egg\rangle + |geg\rangle + |gge\rangle)\Big]\end{aligned} \tag{3.77}$$

where for brevity we have defined $\tilde{\alpha} \equiv \tilde{\alpha}(t)$. We notice a superposition of mesoscopic cat-like states of the cavity field correlated with atomic states with the same number of ground (or

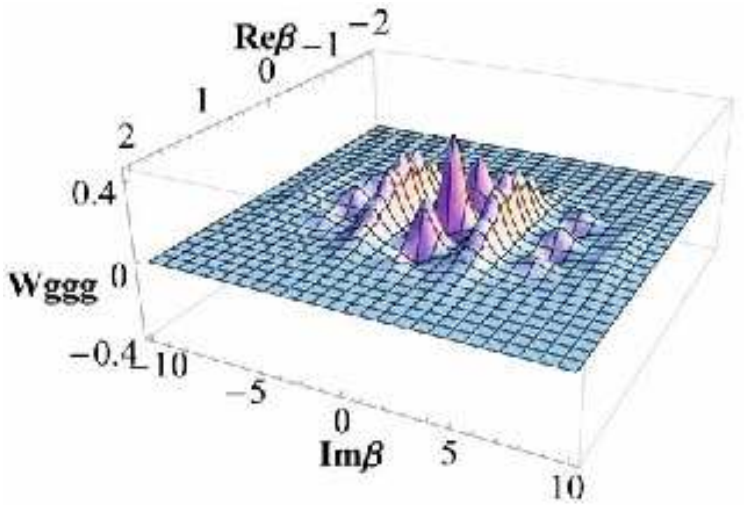

Figure 3.10: Wigner function W_{ggg} of the cavity field state conditioned to the detection of the three atoms in the ground state, for parameters values $\kappa t = 0.05$ and $g/\kappa = 110$.

excited) atoms, which are two fully separable and two entangled 3-qubit states (a W and an inverted-W state) [24]. An interesting consequence of Eq. (3.77) is that a simultaneous detection of the three atoms in any state prepares the cavity field in the corresponding cat-like state. In Fig. 3.10 we show the Wigner function that describes in phase space the cat-like state generated for atomic detections in the ground state.

Now we recall some concepts and tools in order to analyze the multipartite entanglement properties of some atomic states encoded in DFSs. The 3-tangle measure introduced in [26] evaluates the amount of entanglement shared by all the three qubits through the quantity $\tau_{123} = C_{12}^2 + C_{13}^2 - C_{1(23)}^2$, where C_{ij} is the concurrence of the qubit pair (i, j). A generalization to the case of N qubits (with N even) was given in [28] by the N-tangle measure defined as $\tau_N = |\langle\psi|\tilde{\psi}\rangle|^2$ with $|\tilde{\psi}\rangle = \hat{\sigma}_y^{\otimes_N}|\psi^*\rangle$, where $|\psi\rangle$ is the generic N-qubit state, $|\psi^*\rangle$ its complex conjugate and $\hat{\sigma}_y$ one of the Pauli matrices. Another useful tool is the residual bipartite entanglement measure (see [24]) which evaluates the robustness of entanglement against the loss of information; this measure is provided, for instance, by the average squared concurrence $\overline{C^2}$ calculated for any two residual qubits when the other $N-2$ are traced out. The permutational qubits' symmetry allows the existence of atomic DFSs capable of avoiding the loss of coherence due to the coupling to the environment. In the case $N = 3$, there exist four distinct atomic DFSs, as we report in Table 3.1. As an example we choose the balanced combinations $|\Phi(0)\rangle_a^{(s_i)} = (1/\sqrt{3})(|\pm\pm\mp\rangle + |\pm\mp\pm\rangle + |\mp\pm\pm\rangle)$, with $s_i = \pm 1/2$, as two possible initial conditions. These states have no full tripartite entanglement ($\tau_{123} = 0$) according to the 3-tangle measure. However each qubit pair retains the maximal residual bipartite entanglement $\overline{C^2} = 4/9$. These kind of states show a multipartite entanglement characteristic of W-like states.

Table 3.1: Atomic DFSs for $N = 3$ qubits.

$\mathbf{s_i}$	$\mathbf{n(s_i)}$	$\mathbf{\vert i\rangle_3}$
3/2	1	$\{\vert +++\rangle\}$
1/2	3	$\{\vert ++-\rangle,\vert +-+\rangle,\vert -++\rangle\}$
-1/2	3	$\{\vert --+\rangle,\vert -+-\rangle,\vert +--\rangle\}$
-3/2	1	$\{\vert ---\rangle\}$

$N = 4$ **qubits**

We have already mentioned that a remarkable consequence of the general solution of Eq. (3.72) is the existence of a global DFS for any *even* value of the number N of atoms, when the eigenvalue s_i can assume the value zero. In this case there is no time evolution for the initial states of Eq. (3.71) containing only the corresponding $n(0) = N!/[(N/2)!]^2$ atomic eigenstates $|i\rangle_N$. Let us consider for example the case of $N = 4$ atoms. The DFS is spanned by the tensor product of the cavity vacuum state and $n(0) = 6$ states $|i\rangle_4$ with the same number of $|+\rangle$ and $|-\rangle$ components (see Table 3.2). It preserves any initial global state within this subspace, protecting any entangled atomic preparation for quantum information purposes. Another interesting feature of the case with even N follows from the presence in Eq. (3.72) of terms with the cavity field in the vacuum state. Namely, if the optical cavity field is accessible to measurements, the absence of a response by an on/off detector generates a pure N-qubit state, that can be a multipartite entangled state. Starting e.g. from the four atoms prepared in the ground state, the density operator of (3.72) contains a time-independent part $(\sqrt{6}/4)(|0\rangle \otimes |\Psi\rangle_a)$, where $|\Psi\rangle_a = (1/\sqrt{6})(|++--\rangle + |+-+-\rangle + |+--+\rangle + |-++-\rangle + |-+-+\rangle + |--++\rangle)$. Hence a null measurement of the optical cavity field generates the pure 4-qubit state $|\Psi\rangle_a$ whose entanglement properties are discussed in the following.

The four qubits case presents five decoherence-free CSD states $|2, s\rangle$, including two separable states $|2, \pm 2\rangle$, and the multipartite entangled states $|2, \pm 1\rangle$ and $|2, 0\rangle$. The relevance for applications in quantum information processing is that the state $|2, 0\rangle$ turns out to be maximally entangled according to the 4-tangle measure ($\tau_4 = 1$), whereas the states $|2, \pm 1\rangle$ have no four-partite entanglement ($\tau_4 = 0$), but each of them exhibits an equal maximal reduced bipartite entanglement, $\overline{C^2} = 1/4$ (W-like states), by tracing over any qubit pair. We remark that all CSD states of the type $|N/2, \tilde{s}\rangle$ with $\tilde{s} = \pm(N-2)/2$ have entanglement properties similar to that of states $|W_N\rangle$ introduced in [24]. By tracing the atomic density operators $|N/2, \tilde{s}\rangle\langle N/2, \tilde{s}|$ over any $N-2$ parties we always obtain the reduced density

Table 3.2: Atomic DFSs for $N = 4$ qubits.

$\mathbf{s_i}$	$\mathbf{n(s_i)}$	$\mathbf{|i\rangle_4}$
2	1	$\{\|++++\rangle\}$
1	4	$\{\|+++-\rangle,\|++-+\rangle,\|+-++\rangle,\|-+++\rangle\}$
0	6	$\{\|++--\rangle,\|+-+-\rangle,\|+--+\rangle,\|-++-\rangle,\|-+-+\rangle,\|--++\rangle\}$
-1	4	$\{\|---+\rangle,\|--+-\rangle,\|-+--\rangle,\|+---\rangle\}$
-2	1	$\{\|----\rangle\}$

operators for the bipartite system

$$\rho_{\pm} = \frac{1}{N}\left(2|\Phi^-\rangle\langle\Phi^-| + (N-2)|\pm\pm\rangle\langle\pm\pm|\right). \tag{3.78}$$

Hence for the average squared concurrence we simply obtain the value $\overline{C^2} = (2/N)^2$.
We further notice that we can rewrite the states $|2,\pm1\rangle$ and $|2,\pm0\rangle$ as

$$\begin{aligned} |2,\pm1\rangle &= \frac{1}{\sqrt{2}}(|\pm\pm\rangle_{12}|\Phi^-\rangle_{34} + |\Phi^-\rangle_{12}|\pm\pm\rangle_{34}) \\ |2,0\rangle &= \frac{1}{\sqrt{6}}\Big(|\Phi^-\rangle_{12}|\Phi^-\rangle_{34} + |\Phi^-\rangle_{13}|\Phi^-\rangle_{24} + \\ &\quad + |\Phi^-\rangle_{14}|\Phi^-\rangle_{23}\Big) \end{aligned} \tag{3.79}$$

thus generalizing the results derived in [68] where we showed that the two-atom maximally entangled Bell state $|\Phi^-\rangle_{ij} = \frac{1}{\sqrt{2}}(|+-\rangle_{ij} + |-+\rangle_{ij})$ and the two separable states $|\pm\pm\rangle$ do not evolve in time.
Another interesting application is to encode the four qubits in some states of a special basis called Bell gem [80], which is a generalization of the well known Bell basis $|\Phi^{\pm}\rangle = (1/\sqrt{2})(|gg\rangle \pm |ee\rangle)$ and $|\Psi^{\pm}\rangle = (1/\sqrt{2})(|ge\rangle \pm |eg\rangle)$. It is composed by maximally entangled states, according to the 4-tangle measure ($\tau_4 = 1$), which can be obtained by simple quantum logic circuits starting from four unentangled qubits in the computational basis. Let us consider the cavity field prepared in the vacuum state $|0\rangle$ and the four qubits in one of the last three elements of the Bell gem $(1/\sqrt{2})(|\Phi^+\Psi^+\rangle - |\Psi^+\Phi^+\rangle)$, $(1/\sqrt{2})(|\Psi^-\Phi^-\rangle \pm |\Phi^-\Psi^-\rangle)$. The whole system does not evolve in time because these three initial atomic states belong to the DFS corresponding to the eigenvalue $s_i = 0$, thus maintaining the maximum multipartite entanglement in the atomic subsystem.

CHAPTER 4

Beyond the RWA: the ultrastrong coupling regime

The framework of CQED, both in the microwave and in the optical regime, is a natural field for the applicability of the RWA and the validity of the JC model. Here the kind of coupling between a two-level atom and a cavity field mode is the electric dipole coupling, which can reach values in the range $\frac{g}{\omega} \simeq 10^{-6} - 10^{-7}$ in the SC coupling regime. In this way the anti-resonant terms in the interaction Hamiltonian are negligible. By using the perturbative theory argument of the Dyson series of the evolution operator, it is easy to see that the counter rotating terms are associated to the small ratio $\frac{g}{\omega}$, so that they do not contribute to the dynamics of the system.

On the other hand, when, for instance, one considers a matter-radiation interaction like system in circuit QED, the coupling between a two-level "artificial" atom and a single-mode of a transmission line resonator is of inductive or capacitive nature [8, 81]. In this situation the innovations in technology are enhancing and increasing the coupling, reaching such high values that the RWA is no longer applicable ($\frac{g}{\omega} \geq 1$).

What happens in this case is the main topic of this chapter, where our goal is the study of the dynamics of a qubit interacting with a bosonic mode in the so-called USC and DSC regime [82, 83, 84], analyzing the interesting effects of the anti-resonant terms which were neglected before. In particular we will present the interaction model and the analytical solution, under a specific condition, for the density operator describing the system dynamics in the presence of a dissipative environment (Sec. 4.1). Then we focus on the unitary case, where a more a general initial condition is considered, in order to understand the main features of the DSC regime (Sec. 4.2), which are better emphasized for large qubit-oscillator

detuning. We will describe the effect of the detuning parameter, to the limit of resonance conditions, using numerical simulations. Moreover we will explain the passage from a JC to a DSC regime, varying the coupling parameter. Finally, in Sec. 4.3, we will study the effect of dissipation on the dynamics, describing the stationary state and the influence of the detuning parameter.

4.1 The model and the analytical solution

We are considering a system composed by one qubit coupled to a single bosonic field mode, described by the Hamiltonian

$$\hat{H} = \hbar\omega\hat{a}^\dagger\hat{a} + \frac{\hbar}{2}\omega_0\hat{\sigma}_z + \hbar g(\hat{\sigma} + \hat{\sigma}^+)(\hat{a} + \hat{a}^\dagger) \tag{4.1}$$

where ω is the mode frequency, ω_0 is the qubit transition frequency and g is the coupling constant between qubit and field mode. As regards the bosonic mode, $\hat{a}$ and $\hat{a}^\dagger$ are the annihilation and creation operators, while for the qubit $\hat{\sigma}$, $\hat{\sigma}^\dagger$ and $\hat{\sigma}_z$ are the Pauli operators related to ground and excited states $|g\rangle$ and $|e\rangle$.
In order to provide a realistic description of the dynamics of this system, we can think e.g. to a superconducting qubit coupled to a resonator mode [85] and include a thermal bath of harmonic oscillators at zero temperature acting on the mode. The time evolution of the whole system can be described by the following Master Equation (ME):

$$\dot{\hat{\rho}} = -\frac{\mathrm{i}}{\hbar}[\hat{H}, \hat{\rho}] + \hat{\mathcal{L}}_f[\hat{\rho}] \tag{4.2}$$

where $\hat{\mathcal{L}}_f[\hat{\rho}]$ is the standard Liouville superoperator:

$$\hat{\mathcal{L}}_f[\hat{\rho}] = \frac{\kappa}{2}(2\hat{a}\hat{\rho}\hat{a}^\dagger - \hat{a}^\dagger\hat{a}\hat{\rho} - \hat{\rho}\hat{a}^\dagger\hat{a}) \tag{4.3}$$

with the resonator decay rate κ.
We will show in the following that the model described by the ME (4.2) is analytically solvable under the condition $\omega_0 t \ll 1$, whereas numerical results are necessary for a full understanding of a long-times dynamics.

In order to find the analytical solution of Eq. (4.2) we move into the interaction picture by means of the unitary transformation $\hat{U}(t) = \exp\{-\mathrm{i}\omega_0\left(\frac{\hat{\sigma}_z}{2} + \hat{a}^\dagger\hat{a}\right)t\}$. The structure of Eq. (4.2) holds for the the density operator $\hat{\rho}_I = \hat{U}\hat{\rho}\hat{U}^\dagger$ with the interaction Hamiltonian

$$\begin{aligned}\hat{\mathcal{H}}_I &= \hbar\Delta\hat{a}^\dagger\hat{a} + \hbar g(\mathrm{e}^{2\mathrm{i}\omega_0 t}\hat{\sigma}^+\hat{a}^\dagger + \mathrm{e}^{-2\mathrm{i}\omega_0 t}\hat{\sigma}\hat{a} + \hat{\sigma}^+\hat{a} + \hat{\sigma}\hat{a}^\dagger) = \\ &= \hbar\Delta\hat{a}_t^\dagger\hat{a}_t + \hbar g(\mathrm{e}^{\mathrm{i}\omega_0 t}\hat{\sigma}^+ + \mathrm{e}^{-\mathrm{i}\omega_0 t}\hat{\sigma})(\hat{a}_t + \hat{a}_t^\dagger)\end{aligned} \tag{4.4}$$

where we have introduced the detuning parameter $\Delta = \omega - \omega_0$, with $0 \leq \omega_0 \leq \omega$, and $\hat{a}_t \equiv \mathrm{e}^{-\mathrm{i}\omega_0 t}\hat{a}$. Now we expand the density operator $\hat{\rho}_I(t)$ onto the qubit rotated basis $|\pm\rangle = \frac{|g\rangle \pm |e\rangle}{\sqrt{2}}$ introducing the operators, acting on the resonator mode subsystem, $\hat{\rho}_{ij}(t) = \langle i|\hat{\rho}_I(t)|j\rangle$ with

$(ij) = \{++, --, +-, -+\}$. In this way we obtain the following set of coupled differential equations

$$\begin{aligned}\dot{\hat{\rho}}_{++} =& -\mathrm{i}\Delta[\hat{a}_t^\dagger \hat{a}_t, \hat{\rho}_{++}] - \mathrm{i}g\cos(\omega_0 t)[\hat{a}_t + \hat{a}_t^\dagger, \hat{\rho}_{++}] \\ & - g\sin(\omega_0 t)[(\hat{a}_t + \hat{a}_t^\dagger)\hat{\rho}_{-+} - \hat{\rho}_{+-}(\hat{a}_t + \hat{a}_t^\dagger)] + \hat{\mathcal{L}}\hat{\rho}_{++}\end{aligned} \tag{4.5a}$$

$$\begin{aligned}\dot{\hat{\rho}}_{--} =& -\mathrm{i}\Delta[\hat{a}_t^\dagger \hat{a}_t, \hat{\rho}_{--}] + \mathrm{i}g\cos(\omega_0 t)[\hat{a}_t + \hat{a}_t^\dagger, \hat{\rho}_{--}] \\ & + g\sin(\omega_0 t)[(\hat{a}_t + \hat{a}_t^\dagger)\hat{\rho}_{+-} - \hat{\rho}_{-+}(\hat{a}_t + \hat{a}_t^\dagger)] + \hat{\mathcal{L}}\hat{\rho}_{--}\end{aligned} \tag{4.5b}$$

$$\begin{aligned}\dot{\hat{\rho}}_{+-} =& -\mathrm{i}\Delta[\hat{a}_t^\dagger \hat{a}_t, \hat{\rho}_{+-}] - \mathrm{i}g\cos(\omega_0 t)\{\hat{a}_t + \hat{a}_t^\dagger, \hat{\rho}_{+-}\} \\ & - g\sin(\omega_0 t)[(\hat{a}_t + \hat{a}_t^\dagger)\hat{\rho}_{--} + \hat{\rho}_{++}(\hat{a}_t + \hat{a}_t^\dagger)] + \hat{\mathcal{L}}\hat{\rho}_{+-}\end{aligned} \tag{4.5c}$$

$$\begin{aligned}\dot{\hat{\rho}}_{-+} =& -\mathrm{i}\Delta[\hat{a}_t^\dagger \hat{a}_t, \hat{\rho}_{-+}] + \mathrm{i}g\cos(\omega_0 t)\{\hat{a}_t + \hat{a}_t^\dagger, \hat{\rho}_{-+}\} \\ & + g\sin(\omega_0 t)[(\hat{a}_t + \hat{a}_t^\dagger)\hat{\rho}_{++} + \hat{\rho}_{--}(\hat{a}_t + \hat{a}_t^\dagger)] + \hat{\mathcal{L}}\hat{\rho}_{-+}\end{aligned} \tag{4.5d}$$

where brackets [,] and braces { , } denote the standard commutator and anti-commutator symbols. In order to solve these equations we move into the phase space using the continuous and square-integrable functions $\chi_{ij}(\alpha, t) \equiv \mathrm{Tr}[\hat{\rho}_{ij}(t)\hat{D}(\alpha)]$, where $\hat{D}(\alpha) = \mathrm{e}^{\alpha\hat{a}^\dagger - \alpha^*\hat{a}}$ is the displacement operator. We thus get a set of coupled partial differential equations, that does not present an exact solution.

The presence of cavity mode dissipation limits the interest for the study of the system dynamics up to suitable times. Therefore, we can impose the condition $\omega_0 t \ll 1$, to uncouple Eqs. (4.5), since $\cos(\omega_0 t) \simeq 1$ and $\sin(\omega_0 t) \simeq 0$, so that the analytical treatment is possible by generalizing previous results [64] found under resonance condition $\Delta = 0$ (see Chapter 3).

Here we present the analytical solution for the system prepared in the initial state

$$\hat{\rho}_I(0) = |g\rangle\langle g| \otimes |0\rangle\langle 0|,$$

that in the phase space is given by the following functions $\chi_{ij}(\alpha, t)$:

$$\chi_{\pm\pm}(\alpha, t) = \frac{1}{2}\exp\Big\{ -\frac{|\alpha|^2}{2} \mp \beta(t)\alpha^* \pm \beta^*(t)\alpha \Big\} \tag{4.6a}$$

$$\chi_{\pm\mp}(\alpha, t) = \frac{1}{2}F(t)\exp\Big\{ -\frac{|\alpha|^2}{2} \mp \beta(t)\alpha^* \mp \beta^*(t)\alpha \Big\}. \tag{4.6b}$$

The corresponding operators $\hat{\rho}_{ij}(t)$ take the form:

$$\hat{\rho}_{\pm\pm}(t) = \frac{1}{2}|\pm\beta(t)\rangle\langle\pm\beta(t)| \tag{4.7a}$$

$$\hat{\rho}_{\pm\mp}(t) = \frac{1}{2}\frac{F(t)}{\mathrm{e}^{-2|\beta(t)|^2}}|\pm\beta(t)\rangle\langle\mp\beta(t)| \tag{4.7b}$$

where the field coherent states amplitude $\beta(t)$ and the decoherence function $F(t)$ are defined as

$$\beta(t) \equiv \frac{\mathrm{i}g}{z}\Big(\mathrm{e}^{-zt} - 1\Big) \tag{4.8a}$$

$$F(t) \equiv \mathrm{e}^{-\frac{2g^2}{|z|^2}\left[\kappa t + \frac{2}{g}\Im\mathrm{m}(z^*\beta(t))\right]} \tag{4.8b}$$

with the complex variable $z = \frac{k}{2} + \mathrm{i}\Delta$. The density operator $\hat{\rho}_I(t)$ can be expressed also in the original qubit basis $\{|g\rangle, |e\rangle\}$:

$$\begin{aligned}\hat{\rho}_I(t) = \frac{1}{4}\Big\{ &\Big[|\beta(t)\rangle\langle\beta(t)| + |-\beta(t)\rangle\langle-\beta(t)| + \frac{F(t)}{\mathrm{e}^{-2|\beta(t)|^2}}\Big(|\beta(t)\rangle\langle-\beta(t)| + \text{h.c.}\Big)\Big] \otimes |g\rangle\langle g| + \\ &+\Big[|\beta(t)\rangle\langle\beta(t)| - |-\beta(t)\rangle\langle-\beta(t)| - \frac{F(t)}{\mathrm{e}^{-2|\beta(t)|^2}}\Big(|\beta(t)\rangle\langle-\beta(t)| - \text{h.c.}\Big)\Big] \otimes |g\rangle\langle e| + \\ &+\Big[|\beta(t)\rangle\langle\beta(t)| - |-\beta(t)\rangle\langle-\beta(t)| + \frac{F(t)}{\mathrm{e}^{-2|\beta(t)|^2}}\Big(|\beta(t)\rangle\langle-\beta(t)| - \text{h.c.}\Big)\Big] \otimes |e\rangle\langle g| + \\ &+\Big[|\beta(t)\rangle\langle\beta(t)| + |-\beta(t)\rangle\langle-\beta(t)| - \frac{F(t)}{\mathrm{e}^{-2|\beta(t)|^2}}\Big(|\beta(t)\rangle\langle-\beta(t)| + \text{h.c.}\Big)\Big] \otimes |e\rangle\langle e|\Big\}\end{aligned} \tag{4.9}$$

Remembering that

$$\langle n|\beta\rangle\langle\beta|n\rangle = \langle n|-\beta\rangle\langle-\beta|n\rangle = \mathrm{e}^{-|\beta|^2}\frac{|\beta|^{2n}}{n!} \tag{4.10a}$$

$$\langle n|\beta\rangle\langle-\beta|n\rangle = \langle n|-\beta\rangle\langle\beta|n\rangle = (-1)^n\mathrm{e}^{-|\beta|^2}\frac{|\beta|^{2n}}{n!} \tag{4.10b}$$

it is straightforward to derive the probabilities for the whole system states $|Qn\rangle$:

$$P_{Q,n}(t) = \frac{1}{2}\mathrm{e}^{-|\beta(t)|^2}\frac{|\beta(t)|^{2n}}{n!}\Big[1 \pm (-1)^n F(t)\mathrm{e}^{2|\beta(t)|^2}\Big] \tag{4.11}$$

where the sign + (or −) holds for the qubit state $Q = g$ (or e).
As regards the qubit and bosonic mode subsystems we derive the expressions for the qubit levels populations $P_Q(t)$ and the photon number distribution $P_n(t)$:

$$P_Q(t) = \frac{1}{2}\left[1 \pm F(t)\right] \tag{4.12}$$

$$P_n(t) = \mathrm{e}^{-|\beta(t)|^2}\frac{|\beta(t)|^{2n}}{n!} \tag{4.13}$$

where $P_n(t)$ is a Poissonian distribution with a mean value $|\beta(t)|^2 = \langle N(t)\rangle$, that corresponds to the resonator mean photon number. Moreover we notice that the photon statistics is given by $P_n(t) = P_{g,n}(t) + P_{e,n}(t)$, that is the partial trace over the qubit degree of freedom $Tr_Q[\hat{\rho}_I|n\rangle\langle n|]$.

4.1.1 Generic initial state (part one)

Now we focus our attention on a generic initial preparation of the system in the pure state

$$|\Psi(0)\rangle_I = (a_+|+\rangle + a_-|-\rangle) \otimes |l\rangle \tag{4.14}$$

with the normalization condition for the qubit's coefficients $|a_+|^2 + |a_-|^2 = 1$, and $|l\rangle$ a generic Fock state for the bosonic mode. In order to obtain an analytical solution for the ME (4.2) , we follow the same procedure in (4.5) and we solve the equations in the phase

space. The solutions for the functions $\chi_{ij}(\alpha,t)$, through the method of characteristics, are given by

$$\chi_{\pm\pm}(\alpha,t) = |a_\pm|^2 L_l(\eta|\alpha|^2)\exp\Big\{-\frac{|\alpha|^2}{2} \mp \beta(t)\alpha^* \pm \beta^*(t)\alpha\Big\} \tag{4.15a}$$

$$\chi_{\pm\mp}(\alpha,t) = a_\pm a_\mp^* F(t) L_l(\eta|\alpha \mp 2\beta^*(t)\mathrm{e}^{z^* t}|^2)\exp\Big\{-\frac{|\alpha|^2}{2} \mp \beta(t)\alpha^* \mp \beta^*(t)\alpha\Big\}. \tag{4.15b}$$

with $\eta \equiv \mathrm{e}^{-\kappa t}$, whereas the coherent field amplitude $\beta(t)$ and the decoherence function $F(t)$ are the same as in (4.8). The Laguerre polynomials $L_l(\cdot)$ come from the initial condition in the phase space $\chi_{ij}(\alpha,0) = a_i a_j^* \langle l|\hat{D}(\alpha)|l\rangle = a_i a_j^* \mathrm{e}^{-\frac{1}{2}|\alpha|^2} L_l(|\alpha|^2)$. The general solution $\hat{\rho}_I(t)$ for $l \neq 0$ is not known at the time of writing this thesis[1], nevertheless here we provide the correct analytical solution for two specific initial states of the qubit and, in the next section, a more general result for the unitary case. Moreover we remark that when $l = 0$, $L_0(x) = 1$ for every argument x, generalizing the previous solution to every initial pure state for the qubit and zero photons in the resonator.

Suppose the system is prepared at $t = 0$ in the state $|\Psi(0)\rangle = |+\rangle \otimes |l\rangle$ or $|\Psi(0)\rangle = |-\rangle \otimes |l\rangle$. Among the equations (4.15), only the functions $\chi_{\pm\pm}(\alpha,t)$ evolve in time, while the others are null at any time t. Such a characteristic function corresponds to a well defined and unique density operator $\hat{\rho}_{\pm\pm}(t)$. The intuition is to use a known formula [87] for the evolution of a generic Fock state under only the lossy channel $\dot{\hat{\rho}} = \hat{\mathcal{L}}_f[\hat{\rho}]$, described by the Liouvillian superoperator for the bosonic mode. The exact solution for the initial field state $\hat{\rho}_{\pm\pm}(0) = |l\rangle\langle l|$ is a linear map

$$\xi[\hat{\rho}_{\pm\pm}(0)] = \sum_{m=0}^{l} c_{m,l}(\eta)|m\rangle\langle m| \tag{4.16}$$

where the coefficients are:

$$c_{m,l}(\eta) = \binom{l}{m}(1-\eta)^{l-m}\eta^m. \tag{4.17}$$

When the complete ME (4.2) is considered, the evolved field state is

$$\hat{\rho}_{\pm\pm}(t) = \hat{D}(\pm\beta(t))\xi[\hat{\rho}_{\pm\pm}(0)]\hat{D}^\dagger(\pm\beta(t)) \tag{4.18}$$

with $\beta(t)$ defined in (4.8), and the evolved state of the whole system is

$$\hat{\rho}_I(t) = \hat{D}(\pm\beta(t))\xi[\hat{\rho}_{\pm\pm}(0)]\hat{D}^\dagger(\pm\beta(t)) \otimes |\pm\rangle\langle\pm|. \tag{4.19}$$

It is clear from this solution that the probabilities for the states $|g,n\rangle$ and $|e,n\rangle$ are equal and can be expressed in the form

$$P_{g,n} = P_{e,n} = \frac{1}{2}\mathrm{e}^{-|\beta(t)|^2} A_n(t) \tag{4.20}$$

[1] We are not still able to find the time evolution for the coherences $\hat{\rho}_{\pm\mp}(t)$ of the density operator when the initial photon number $l \neq 0$, but for the diagonal terms the problem is already solved.

where the coefficients $A_n(t)$ are

$$\sum_{m=0}^{l} c_{m,l}(\eta)|\beta(t)|^{2|n-m|}\Big[\frac{m!}{n!}\Big(L_m^{n-m}(|\beta(t)|^2)\Big)^2\theta(n-m)+\frac{n!}{m!}\Big(L_n^{m-n}(|\beta(t)|^2)\Big)^2\theta(m-n-1)\Big] \tag{4.21}$$

and $\theta(x)$ is the step function that assumes the values $\theta(x) = 1$ if $x \geq 0$ and $\theta(x) = 0$ if $x < 0$. This formula has been derived through the relations

$$\langle n|\hat{D}(\beta)|m\rangle = \sqrt{\frac{n!}{m!}}\mathrm{e}^{-\frac{1}{2}|\beta|^2}(-\beta)^{m-n}L_n^{m-n}(|\beta|^2) \qquad \text{for } n \leq m \tag{4.22a}$$

$$\langle n|\hat{D}(\beta)|m\rangle = \sqrt{\frac{m!}{n!}}\mathrm{e}^{-\frac{1}{2}|\beta|^2}(-\beta)^{n-m}L_m^{n-m}(|\beta|^2) \qquad \text{for } n \geq m \tag{4.22b}$$

for the generalized Laguerre polynomials $L_r^s(x)$, defined as

$$L_r^s(x) = \binom{r+s}{r}\sum_{i=0}^{r}(-1)^i\frac{\binom{r}{i}}{\binom{i+s}{i}}\frac{x^i}{i!}. \tag{4.23}$$

The mean photon number for the bosonic mode $\langle N(t)\rangle = Tr[\hat{\rho}_I(t)\hat{a}^\dagger\hat{a}]$, referring to Eq. (4.19), is

$$\langle N(t)\rangle = |\beta(t)|^2 + l\eta \tag{4.24}$$

which corresponds to the result found in (4.12) with the addition of a decay of the initial photon number l.

4.2 Unitary dynamics

The unitary limit, corresponding to the choice $\kappa = 0$, allows to better understand the dynamics of the qubit-oscillator system in the DSC regime. We begin analyzing the nature of the interaction part of the Hamiltonian (4.1), composed by two resonant ($\hat{\sigma}^\dagger\hat{a}$ and $\hat{\sigma}\hat{a}^\dagger$) and two anti-resonant terms ($\hat{\sigma}^\dagger\hat{a}^\dagger$ and $\hat{\sigma}\hat{a}$), and we notice that the Hilbert space of the system states is thus splitted into two orthogonal and unconnected subspaces, called *parity chains*

$$|g,0\rangle \leftrightarrow |e,1\rangle \leftrightarrow |g,2\rangle \leftrightarrow |e,3\rangle \leftrightarrow \ldots \leftrightarrow |g,2N\rangle \leftrightarrow |e,2N+1\rangle \tag{4.25a}$$

$$|e,0\rangle \leftrightarrow |g,1\rangle \leftrightarrow |e,2\rangle \leftrightarrow |g,3\rangle \leftrightarrow \ldots \leftrightarrow |e,2N\rangle \leftrightarrow |g,2N+1\rangle \tag{4.25b}$$

where $N = 0, 1, 2, \ldots$ is an integer number.
Defining a parity operator

$$\hat{\Pi} \equiv -\hat{\sigma}_z(-1)^{\hat{a}^\dagger\hat{a}} = \mathrm{e}^{\mathrm{i}\pi\hat{N}_\mathrm{e}} \tag{4.26}$$

the states of the first parity chain (4.25a) are eigenstates of $\hat{\Pi}$ with eigenvalue $p = 1$, while those of the second chain (4.25b) have parity $p = -1$. The operator $\hat{N}_\mathrm{e} = |e\rangle\langle e| + \hat{a}^\dagger\hat{a}$ is the number of total excitations of the system. In the JC regime, that is in the domain of applicability of the RWA, $\hat{N}_e$ is a constant of motion since $[\hat{N}_e, \hat{\mathcal{H}}_\mathrm{res}] = 0$, where $\hat{\mathcal{H}}_\mathrm{res} \propto$

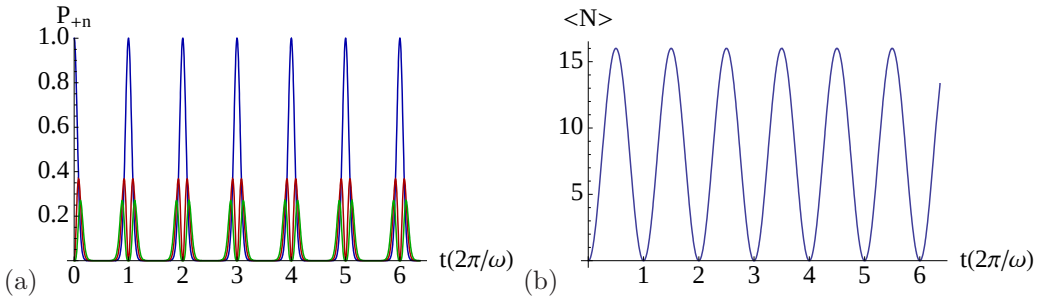

Figure 4.1: (a) $P_{+n}(t)$ for the first states $n = 0, 1, 2$ (blue, red, green) and (b) $\langle N(t)\rangle$. The values of the parameteres are $\frac{\Delta}{\omega} \simeq 1$, $\frac{g}{\omega} = 2$ and initial state $|g, 0\rangle$.

$\hat{\sigma}^\dagger \hat{a} + \hat{\sigma}\hat{a}^\dagger$. In the general case of a USC regime, a constant of motion is the parity operator $\hat{\Pi}$ since $[\hat{\Pi}, \hat{\mathcal{H}}] = 0$. Thus there are two independent Hamiltonians, corresponding to the two eigenvalues $p = \pm 1$ of the parity operator, that describe the unitary dynamics of the system in terms of independent parity chains. The parity $p = 1$, for instance, is related to the states that have an even number of total excitations, while $p = -1$ for those states with an odd number of total excitations.

Let us consider the case of the system prepared at $t = 0$ in the state $|g, 0\rangle$. In the unitary limit, the system is at any time in the pure state

$$|\Psi(t)\rangle = \frac{1}{\sqrt{2}} \left[|\beta(t)\rangle \otimes |+\rangle + |-\beta(t)\rangle \otimes |-\rangle\right] \tag{4.27}$$

that is a typical Schrödinger cat-like state. The probabilities that the system is in a state of one of the two chains $P_{pn}(t)$ are

$$P_{pn}(t) = \frac{|\beta(t)|^{2n}}{n!} P_{Q,0}. \tag{4.28}$$

since the decoherence function becomes $F(t) = \mathrm{e}^{-2|\beta(t)|^2}$ so that the first probabilities $P_{g,0}(t) = \mathrm{e}^{-|\beta(t)|^2}$ and $P_{e,0}(t) = 0$. Hence starting from $|g, 0\rangle$ the evolved state vector remains in the subspace corresponding to parity chain $p = 1$. As far as the mean photon number is concerned, the coherent state amplitude is

$$\beta(t) = \frac{g}{\Delta} \left(\mathrm{e}^{-\mathrm{i}\Delta t} - 1\right)$$

and

$$\langle N(t)\rangle = \left[\frac{2g}{\Delta} \sin\left(\frac{\Delta}{2} t\right)\right]^2.$$

In Figs. 4.1(a,b) we show the time evolution of $P_{+n}(t)$ for the first three states of the even parity chain and $\langle N(t)\rangle$ in the large detuning regime $\frac{\Delta}{\omega} \simeq 1$ and with a coupling constant $\frac{g}{\omega} = 2$, in units of dimensionless times $\frac{\omega t}{2\pi} t$. The oscillations of $\langle N(t)\rangle$ occur at half the frequency of $P_{+n}(t)$ and the maximum value of photons in the resonator is $|\beta|^2_{\max} = \frac{4g^2}{\omega^2} = 16$. In Fig. 4.2 we illustrate, at different dimensionless time intervals, the behaviour of the

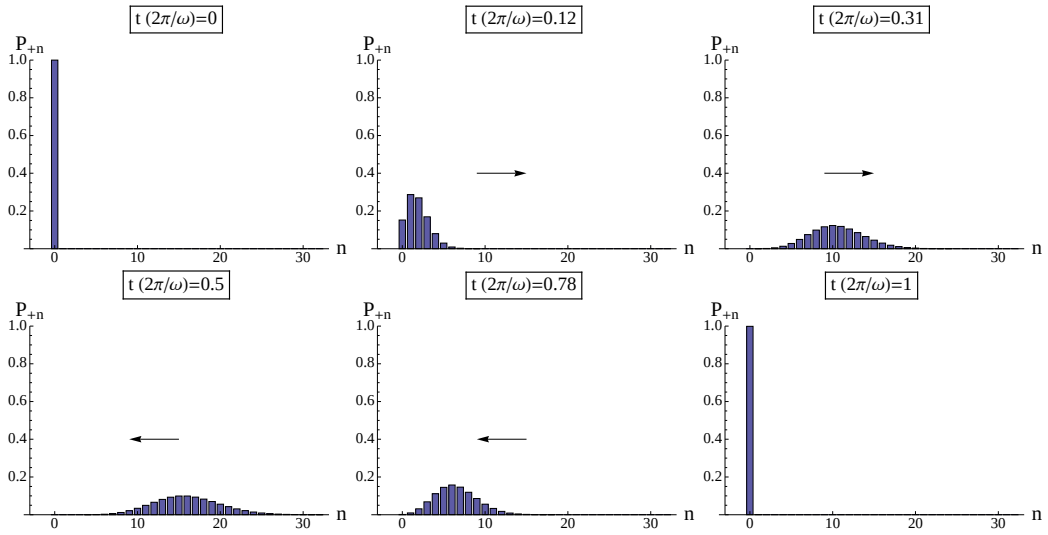

Figure 4.2: Time shots of the propagation of $P_{+n}(t)$ during the first oscillation $0 \leq \frac{\omega t}{2\pi} \leq 1$. The photon number wavepacket reaches the maximum "distance" from $n = 0$ at $\langle N \rangle_{\max} = 16$, since $\frac{g}{\omega} = 2$.

probabilities for every involved state of the parity chain. It is shown that, since $P_{-n}(t) = 0$ at all times, the photon statistics $P_n(t) = P_{+n}(t)$ is a Poissonian distribution with a time-dependent mean value equal to the mean photon number, representing a propagating photon number wavepacket. The value of the coupling constant g is responsible for the maximum mean photon number and, consequently, for the number of involved states in the parity chain.

4.2.1 Generic initial state (part two)

Referring to the results in the phase space (4.15), for a generic initial state (4.14), the analytical solutions for $\hat{\rho}_{ij}(t)$ corresponding to $\chi_{ij}(\alpha, t)$ are:

$$\hat{\rho}_{\pm\pm}(t) = |a_{\pm}|^2 \hat{D}(\pm\beta(t))|l\rangle\langle l|\hat{D}^{\dagger}(\pm\beta(t)) \tag{4.29a}$$

$$\hat{\rho}_{\pm\mp}(t) = a_{\pm}a_{\mp}^{*} \hat{D}(\pm\beta(t))|l\rangle\langle l|\hat{D}^{\dagger}(\mp\beta(t)). \tag{4.29b}$$

Equivalentely the evolved state of the system is a pure entangled state

$$|\Psi(t)\rangle = a_{+}\hat{D}(\beta(t))|l\rangle \otimes |+\rangle + a_{-}\hat{D}(-\beta(t))|l\rangle \otimes |-\rangle \tag{4.30}$$

which can be written on the standard basis $\{|g\rangle, |e\rangle\}$ as

$$|\Psi(t)\rangle = \Big[a_{+}\hat{D}(\beta(t)) + a_{-}\hat{D}(-\beta(t))\Big]|l\rangle \otimes |g\rangle + \Big[a_{+}\hat{D}(\beta(t)) - a_{-}\hat{D}(-\beta(t))\Big]|l\rangle \otimes |e\rangle. \tag{4.31}$$

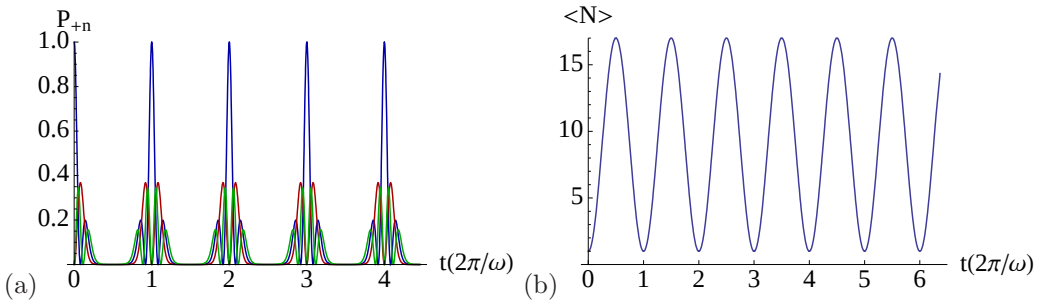

Figure 4.3: (a) $P_{+n}(t)$ for the first states $n = 0, 1, 2$ (blue, red, green) and (b) $\langle N(t)\rangle$. The values of the parameteres are $\frac{\Delta}{\omega} \simeq 1$, $\frac{g}{\omega} = 2$ and initial state $|g, 1\rangle$.

By using the relations (4.22) we obtain the expressions for the probabilities of the system states $|Q, n\rangle$:

$$P_{Q,n}(t) = \frac{1}{2}\Big\{ \mathrm{e}^{-|\beta(t)|^2} |\beta(t)|^{2|l-n|} \Big[(|a_+|^2 + |a_-|^2) \pm (-1)^{|l-n|} (a_+ a_-^* + a_+^* a_-) \Big] \times \\ \times \Big[\theta(l-n-1) \frac{n!}{l!} \Big(L_n^{l-n}(|\beta(t)|^2) \Big)^2 + \theta(n-l) \frac{l!}{n!} \Big(L_l^{n-l}(|\beta(t)|^2) \Big)^2 \Big] \Big\} \tag{4.32}$$

where the sign + (or −) corresponds to the qubit state $Q = g$ (or $Q = e$). The mean photon number for the bosonic mode $\langle N(t)\rangle = Tr[\hat{\rho}_I(t)\hat{a}^\dagger \hat{a}]$, referring to Eq. (4.30), is

$$\langle N(t)\rangle = |\beta(t)|^2 + l \tag{4.33}$$

that is, simply, a translation of the usual oscillations of the mean photon number according to the initial photon number l.

Starting from any pure state of the system, the time evolution of $P_{pn}(t)$ takes place independently in each parity chain [86]. We illustrate here, as an example, the time evolution of the probabilities of the parity chains states and the resonator mean photon number for two different initial pure states.

The first case (see Fig. 4.3) is that of the system initially prepared in $|g, 1\rangle$, that is, according to our notation in (4.14), $a_+ = a_- = \frac{1}{\sqrt{2}}$ and $l = 1$. This state has parity $p = -1$, since the number of total excitations is $N_e = 1$, and for this reason only the parity chain to which it belongs will be excited during the time evolution. In fact $P_{+n}(t) = 0$ at any time t, because it corresponds to the states $|g, n\rangle$ with n even and $|e, n\rangle$ with n odd. Since we use the same values of the parameters in (4.1) as in the previous case, we expect a similar behavior for the evolution of the system. In fact, the mean photon number oscillates at the same frequency as in the case of $|g, 0\rangle$, with the same amplitude, but with the addition of one photon more (cfr. Fig. 4.1(b)). The probability to be in the initial state $|g, 1\rangle$ has a main oscillation at the dimensionless frequency $\frac{1}{\omega t}$, but it also present a sort of "diffraction" pattern with two side peaks. This happens since from the initial state start two photon number wavepackets, one to the right and the other to the left. This last one is "reflected" by the lower limit

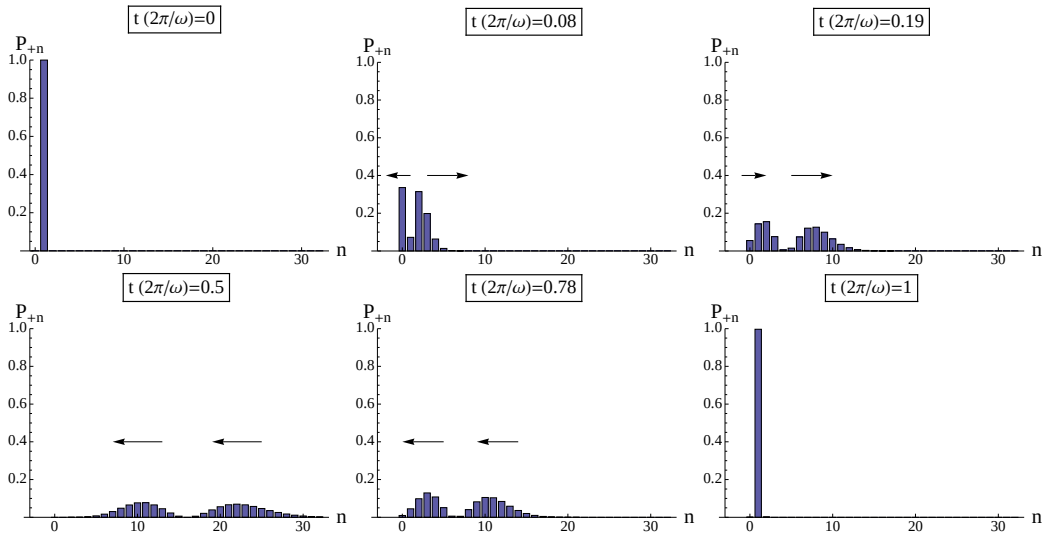

Figure 4.4: Time shots of the propagation of $P_{+n}(t)$ during the first oscillation $0 \leq \frac{\omega t}{2\pi} \leq 1$. The photon number wavepacket reaches the maximum "distance" from $n = 0$ at $\langle N \rangle_{\max} = 16$, since $\frac{g}{\omega} = 2$.

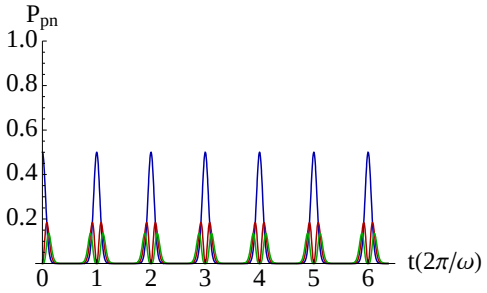

Figure 4.5: $P_{pn}(t)$ for the first states $n = 0, 1, 2$ (blue, red, green) of the two parity chains. The values of the parameteres are $\frac{\Delta}{\omega} \simeq 1$, $\frac{g}{\omega} = 2$ and initial state $|+\rangle|0\rangle$.

state $|e, 0\rangle$ of the parity chain ($p = -1$) and then propagates to the right (see Fig. 4.4). As the phenomenon is inherently coherent, there is interference between the two propagating packets of states, with the appearence of secondary peaks.

Now we wonder what happens whether the system is prepared in a superposition state like, for instance, $\frac{1}{\sqrt{2}}(|g, 0\rangle + |e, 0\rangle) = |+\rangle \otimes |0\rangle$, with $a_+ = 1$, $a_- = 0$ and $l = 0$. We have already pointed out that the two parity chains states undergo the same dynamics, but they are unconnected at the same time. Since the initial probability to be in $|g, 0\rangle$ or in $|e, 0\rangle$ is equal to 0.5, the probabilities $P_{pn}(t)$ will oscillate independentely in the two chains with this maximum value. In fact in this case Eq. (4.32), or equivalentely Eq. (4.20) in the unitary

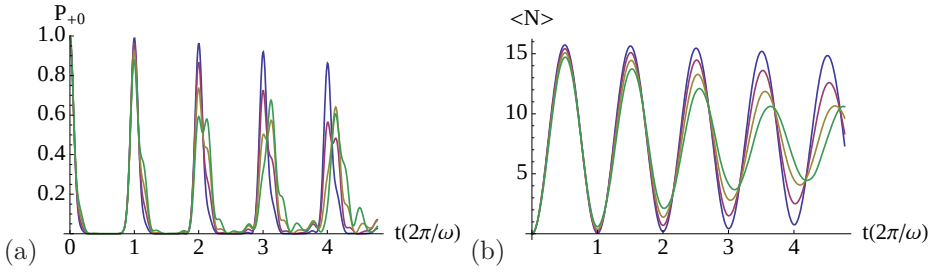

Figure 4.6: (a) $P_{+0}(t)$ and (b) $\langle N\rangle(t)$ for different values of the detuning parameter: $\frac{\Delta}{\omega} = 0.75$ (blue), 0.5 (red), 0.25 (yellow), 1 (green). The initial state is $|g,0\rangle$ and the coupling parameter is $\frac{g}{\omega} = 2$.

regime with $\eta = 1$, reduces to

$$P_{p,n}(t) = \frac{1}{2}\mathrm{e}^{-|\beta(t)|^2}\frac{|\beta(t)|^{2n}}{n!} \tag{4.34}$$

which has the same structure of Eq. (4.11), but here the dynamics in the two parity chains is the same for each value of n. In Fig. 4.5 we show the time evolution of the first three states probabilities in the two parity chains, choosing the coupling parameter $\frac{g}{\omega} = 2$ and the detuning parameter $\frac{\Delta}{\omega} = \simeq 1$.

4.2.2 From large detuning to resonance

We have seen up to now that an analytical solution of the ME (4.2) can be obtained only under the condition $\omega_0 t \ll 1$, but we are also interested in studying the behavior of the dynamics for longer times, i.e. for any values of the detuning parameter. To this purpose we numerically solve the ME in the interaction picture by the Monte Carlo wave function (MCWF) method [17]. We are referring always to the unitary case ($\kappa = 0$) since the effect of approaching a resonance condition is more evident, as we will discuss later for the dissipative case.

When we are out of the condition for solving analytically the ME, we can notice that the four differential equations of the system (4.5) couple and the qubit transition frequency ω_0 begins to affect the dynamics. As we can see by numerical simulations in Fig. 4.6, the presence of ω_0 finite or, equivalently, $0 < \frac{\Delta}{\omega} < 1$, introduces a perturbation of the regular oscillations of $P_{pn}(t)$ and $\langle N\rangle(t)$. As regards the populations of the parity chains, the shape is modified as another frequency is introduced in the dynamics with the result of decreasing the peak values of the probability revivals. We have plotted in Fig. 4.6(a) only the first element of the chain with parity $p = 1$ for simplicity, but we can state that all the other states behave in the same manner. As far as the mean photon number is concerned, it undergoes a reduction of the amplitude of oscillations and a small shift in the peak values. The most important result is that the independence in the dynamics of the two parity chain

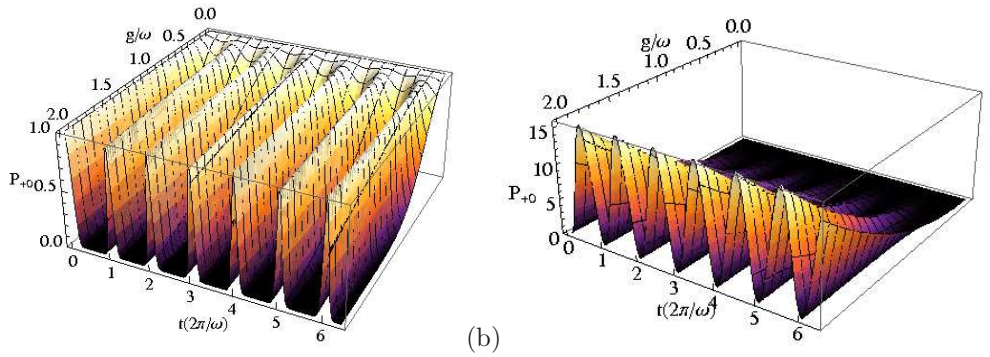

Figure 4.7: (a) $P_{+0}(t)$ and (b) $\langle N\rangle(t)$ for different values of the coupling parameter $0 \leq \frac{g}{\omega} \leq 2$, with initial state $|g,0\rangle$ and detuning parameter $\frac{\Delta}{\omega} = 1$.

is maintained with the presence of $\omega_0 \neq 0$. Thus, in the case we are examining, the chain of states with parity $p = -1$ remains unexcited.

4.2.3 Recovering the JC dynamics

The intuitive picture of the parity chains we have now in mind can be also helpful in describing the crossing of different coupling regimes: DSC → USC → SC. We have seen that when the coupling constant $\frac{g}{\omega}$ is increased, the mean photon number, and consequentely the photon number wavepacket, reaches higher values involving dynamically more states of the parity chains. What happens when we lower the couling parameter until values in the domain of appplicability of the RWA? Trivially we recover the well known results of the JC dynamics. We have shown up to now results for the system evolution from the initial state $|g,0\rangle$, demonstrating that it is no longer a ground state in the DSC regime. This happens since a higher coupling constant provides enough energy to excite states of the parity chains through the anti-resonant terms of the Hamiltonian. When we go into the regime of the JC model these terms do not play any more role, $|g,0\rangle$ becomes the ground state of the system and only the couples of states $\{|g,2N+1\rangle, |e,2N\rangle\}$, belonging to a 2x2-dimensional Hilbert space, are involved in the dynamics. Consequentely the mean photon number oscillates between a minimum of $2N$ and a maximum of $2N+1$ with the resonance condition $\Delta = 0$. In the far detuning regime $\frac{\Delta}{\omega}$ we expect a dispersive dynamics, with no exchange of energy between the qubit and the quantized field mode, leaving the states unchanged.

Here we provide a wider view about the passage through the different coupling regimes showing, in particular, the time evolution of $P_{+0}(t)$ and of $\langle N\rangle(t)$ also as a function of the coupling constant in the range $0 \leq \frac{g}{\omega} \leq 2$ (see Fig. 4.7). Indeed, if the system is prepared in the pure state $|g,0\rangle$, in the far detuning regime $\frac{\Delta}{\omega} \simeq 1$, we can see that as $\frac{g}{\omega}$ approaches small values $|g,0\rangle$ shows the features of the JC dynamics for which it is a ground state. The plot puts in evidence the smooth passage to the DSC regime, where $|g,0\rangle$ is no longer the

ground state, but its dynamics provides oscillations in the mean photon number.

4.3 The role of dissipation

The main role of a dissipative environment is obviously that of inducing decoherence in the dynamics of a quantum system. In this section we show the results obtained when the dissipative decay rate for the resonator mode is not negligible ($\kappa \neq 0$). At the beginning of the chapter we have presented the analytical solution under the assumption $\omega_0 t \ll 1$ and for the initial condition $|g,0\rangle$. Considering the rearrangement of the states of the system in terms of parity chains, described in the unitary limit, we notice that the dissipation connects the two chains. In fact the jump operator $\sqrt{\kappa}\hat{a}$ in the Liouvillean superoperator $\hat{\mathcal{L}}_f$ annihilates a photon of the bosonic field mode, leaving untouched the qubit state. For instance the state $|e,6\rangle$ belonging to the parity chain with $p=-1$, can decay through the dissipative channel into the state $|e,5\rangle$, which is in the parity chain with $p=1$. In turn this last one can be transformed into the state $|e,4\rangle$, back into the first chain, and so on. This process puts in communication the two parity chains and the dynamics can be analytically described through the results obtained in the first section.
We will discuss also interesting numerical results obtained outside the validity of the analytical solution, showing the dynamics of the system for the whole range of values of the detuning parameter at long times.

4.3.1 Analytical results

Here we focus on the case $g/\omega = 2$ and in the regime of very large detuning $\Delta/\omega \simeq 1$. In Fig. 4.8 we show different time shots of the statistics $P_{pn}(t)$ in the two parity chains. We notice that, starting from $|g,0\rangle$ and with a decay rate $\kappa/\omega = 0.01$, the two chains are connected via the dissipative channel and the effect is more evident as time increases, breaking the rule of independent time evolution of parity chains typical of the unitary regime. In fact in this case the product $F(t)\mathrm{e}^{2|\beta(t)|^2} < 1$ for $t > 0$, where $F(t)$ is the decoherence function (4.8), and the probabilities $P_{-n}(t) \neq 0$, in Eq. (4.28), since $P_{e,0}(t)$ is no longer null. We notice that the states of the second parity chain with $p=-1$ begin to be excited and their probabilities grow, while those of the first parity chain with $p=1$ decrease[2]. This happens beacuse the value of the decay rate κ is quite low, but after about the fifth peak the dynamics in the two chain states is the same for each value of the photon number n, as shown in Fig. 4.9. The peak values of the oscillations of $P_{p0}(t)$ occur at times $t_j = \frac{2\pi j}{\omega}$ with $j = 0, 1, 2....$

We show for completeness also the behaviour under dissipation of the probabilities and mean photon number, in the case of the system initially prepared in the state $\frac{1}{\sqrt{2}}(|g,1\rangle + |e,1\rangle)$. The parity chain states probabilities, which are equal, are given by Eq. (4.20) and the mean

[2]The profile of the time evolution of the first three bars, representing the probabilities of the first three elements of the two parity chains, correspond to the plot in Fig. 4.9, until the time $t = \frac{8\pi}{\omega}$.

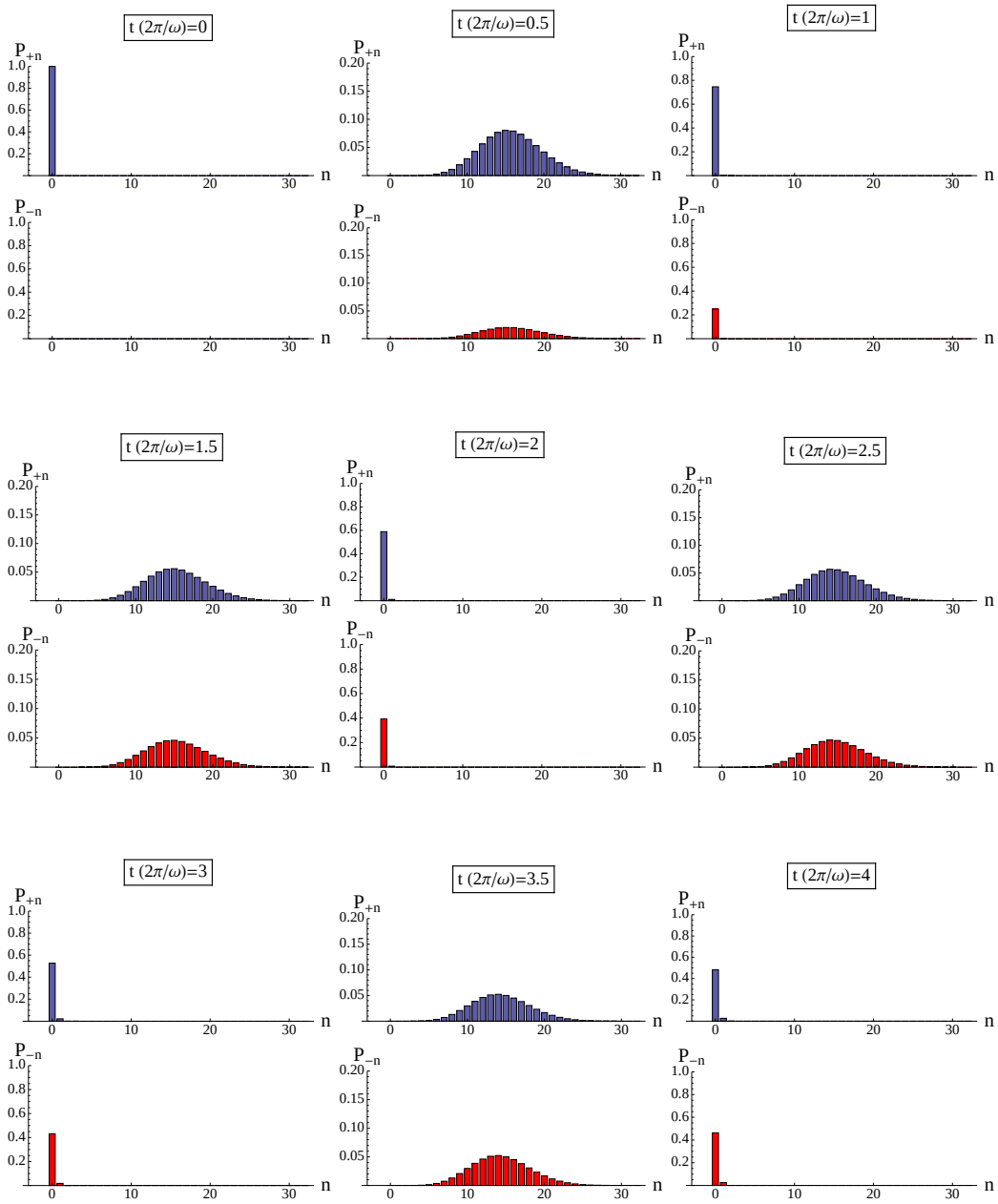

Figure 4.8: Time shots of the propagation of parity chains probabilities $P_{pn}(t)$. At times $t_j = \frac{2\pi j}{\omega}$ occur peaks in the $P_{p0}(t)$, while at $\frac{t_j}{2}$ occur the maxima of $\langle N(t)\rangle$. The choice of parameters is $\frac{g}{\omega} = 2$, $\frac{\Delta}{\omega} = 1$ and initial state $|g, 0\rangle$.

photon number by Eq. (4.24). Also in this case we point out a decrease in the peak values of oscillations, which occur always at dimensionless times t_j for $P_{p1}(t)$ and at $t_j/2$ for $\langle N(t)\rangle$. Increasing the dissipative decay rate until, for instance, the value $\frac{\kappa}{\omega} = 0.2$, always in the large detuning limit $\frac{\Delta}{\omega}$, the system reaches a stationary state, in the range of dimensionless

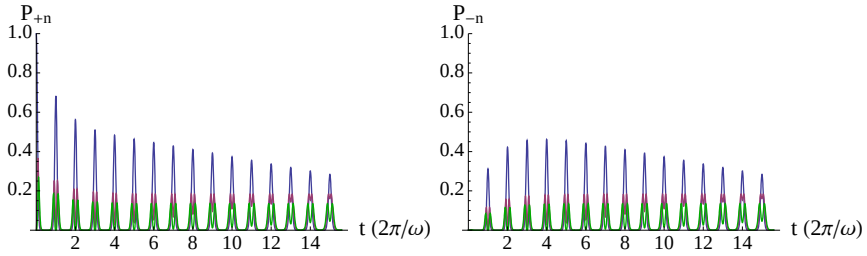

Figure 4.9: Time evolution of (a) P_{+n} and (b) P_{-n} for $n = 0$ (blue), 1 (red), 2 (green) in the two parity chains, with parameters $g/\omega = 2$, $\Delta/\omega \simeq 1$ and $\kappa/\omega = 0.01$.

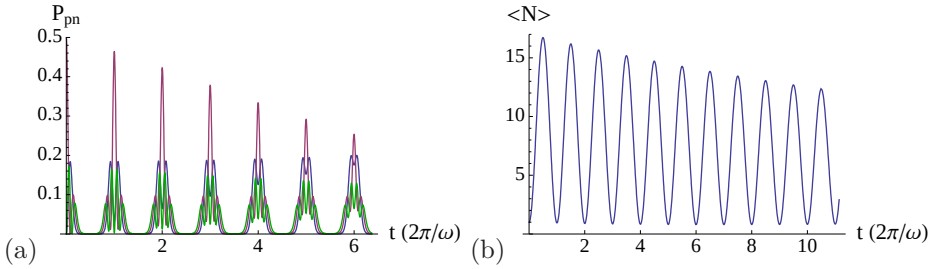

Figure 4.10: Time evolution of (a) P_{pn} and (b) $\langle N \rangle$ for $n = 0$ (blue), 1 (red), 2 (green), with parameters $g/\omega = 2$, $\Delta/\omega \simeq 1$ and $\kappa/\omega = 0.01$.

times of interest (say $t_j \leq 10$), which has the form

$$\hat{\rho}_S = \frac{1}{2}\Big[|\beta_S\rangle\langle\beta_S| \otimes |+\rangle\langle+| + |-\beta_S\rangle\langle-\beta_S| \otimes |-\rangle\langle-|\Big] \tag{4.35}$$

where $\beta_S = -\frac{ig}{z}$ is the steady amplitude of the field coherent state. The structure of the steady state is noteworthy, since it is a statistical mixture of two parts, one that associates $|\beta_S\rangle$ to the qubit state $|+\rangle$ and the other connects $|-\beta_S\rangle$ to $|-\rangle$. This means that the system relaxes upon two degenerate eigenstates $|\pm, \pm\beta_S\rangle$ of the interaction Hamiltonian Eq. (4.4) with $\Delta/\omega \simeq 1$ corresponding to the same energy mean value $\hbar\Delta|\beta_S|^2 + \hbar g(\beta_S + \beta_S^*)$. We remark that $P_{p0}(t)$ vanishes at long times, while the other probabilities reach a non-zero constant value, so that the steady state Poissonian photon statistics $P_n(t) = P_{+n}(t) + P_{-n}(t)$ has a mean value $\langle N \rangle_S = |\beta_S|^2 = \frac{4g^2}{|z|^2}$, which depends only on the coupling constant g and the decay rate κ.

If we consider a more general initial state (4.14), but with $l = 0$ initial photons in the resonator mode, the steady state assumes the same form of Eq. (4.35), but with the different weights $|a_\pm|^2$ for the two parts related to $|\pm\rangle\langle\pm|$. One of the two parts of stationary state (4.35) is reached when the system is prepared in a state like $|\pm\rangle \otimes |l\rangle$, with a generic intial number of photons l. In fact the linear map (4.19), at long times, approaches one of the two stationary parts $|\pm\beta_S\rangle \otimes |\pm\rangle$, with the mean photon number $\langle N \rangle_S$, independent of the initial number of photons l (see Eq. (4.24)). In Fig. 4.11 we show how the first elements of

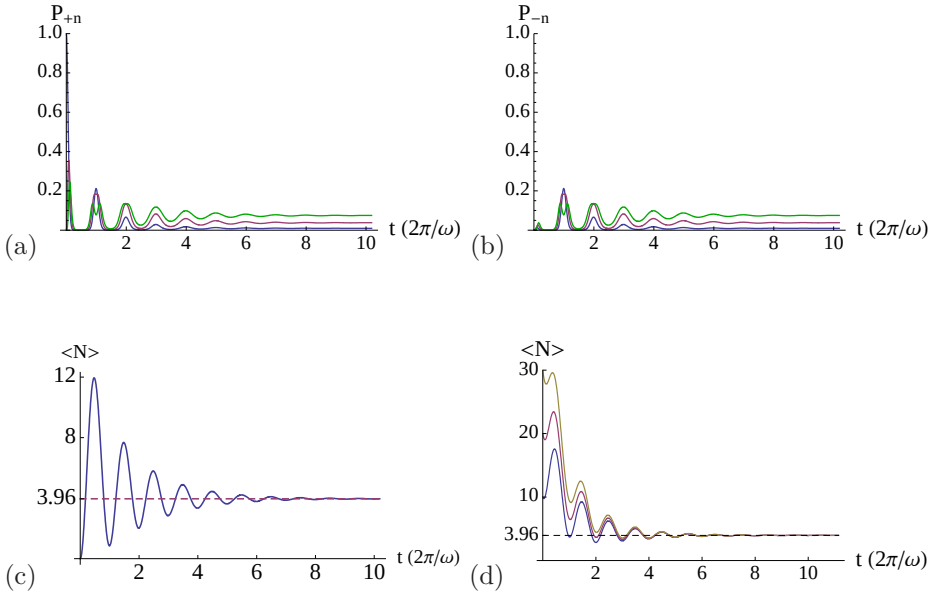

Figure 4.11: Steady state approach of $P_{+n}(t)$ (a) and $P_{-n}(t)$ (b) for $n = 0, 1, 2$, and of (c) $\langle N(t)\rangle$, with $g/\omega = 2$, $\Delta/\omega \simeq 1$ and $\kappa/\omega = 0.2$, for the initial state $|g, 0\rangle$. (d) Mean photon number $\langle N(t)\rangle$, with the same parameters as in (a) and (b), for different initial states $|+\rangle|l\rangle$ ($l = 10, 20, 30$). The steady state value is in all cases $|\beta_S|^2 = 3.96$.

the two parity chains $P_{pn}(t)$ ($n = 0, 1, 2$) and the mean photon number $\langle N(t)\rangle$, for different initial states, approach the steady state for the relatively large value of decay rate $\kappa/\omega = 0.2$.

4.3.2 Numerical simulations beyond the analytical regime

We have seen up to now that an analytical solution of the ME (4.2) can be obtained only under the condition $\omega_0 t \ll 1$, but we are also interested in studying the behavior of the dynamics for longer times, i.e. for any values of the detuning parameter. To this purpose we numerically solve the ME in the interaction picture by the Monte Carlo wave function (MCWF) method [17].

In Fig. 4.12(a, b, c) we show the effect of the detuning parameter on system dynamics for a low decay rate $\kappa/\omega = 0.01$. The behavior of parity chains probabilities $P_{pn}(t)$ is quite similar to that already explained before in the unitary case. Indeed it is heavily affected when the detuning parameter Δ/ω is reduced. As an example in Fig. 4.12(a) we show that $P_{+0}(t)$ is progressively spoiled and the shape of oscillations lose the symmetry of the case $\Delta/\omega \simeq 1$ (see Fig. 4.9(a)). The same occurs also for $P_{-0}(t)$ in Fig.4.12(b) after an initial growth. Despite the distortions in the shape of $P_{pn}(t)$, we see in Fig. 4.12(c) that the mean photon number $\langle N(t)\rangle$ exhibits regular oscillations. The effect of decreasing the detuning parameter, towards a resonance condition $\frac{\Delta}{\omega} = 0$, is to reduce the amplitude of oscillations

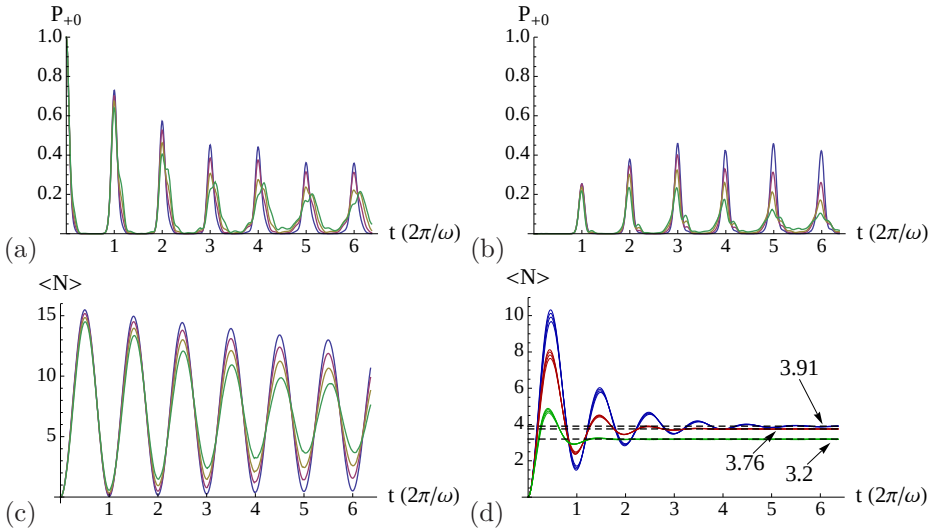

Figure 4.12: Effect of the detuning parameter in the range $0 \leq \frac{\Delta}{\omega} \leq 1$, with, in particular, $\frac{\Delta}{\omega} = 0.75,\ 0.5,\ 0.25,\ 0$. (a) $P_{+0}(t)$, (b) $P_{-0}(t)$ and (c) $\langle N(t)\rangle$. In all cases $\frac{g}{\omega} = 2$ and $\frac{\kappa}{\omega} = 0.01$. (d) Mean photon number for $\frac{\kappa}{\omega} = 0.3,\ 0.5,\ 1$ and, for each one, the four curves, corresponding to the same values of $\frac{\Delta}{\omega}$ as before, reaches the steady state value $|\beta_S|^2$ as in the case of $\frac{\Delta}{\omega} \simeq 1$.

and to induce a small shift in correspondence of the peak times t_j. Now we consider in Fig. 4.12(d) the mean photon number behavior for larger values of the decay rate. We observe that, for each value of κ/ω, the asymptotic value of $\langle N(t)\rangle$ is in good agreement, within numerical precision, with the analytical value $|\beta_S|^2$ in the large detuning regime of $\Delta/\omega \simeq 1$. In addition we notice that, after the first oscillation, the effect of decreasing detuning parameter becomes almost negligible. This means that for high values of the decay rate κ, the dynamics of the system in the DSC regime is almost independent of the detuning parameter, putting in evidence that the main features of this new and interesting regime are caught at large detuning conditions.

Conclusions

In this PhD work we have studied and explored three leading topics in the field of Quantum Optics, applied to interesting and promising "hardwares" like cavity and circuit QED. The central thread is the JC model, which was introduced firstly in the framework of CQED for atom-cavity mode interactions, and it owes its large popularity to the RWA, typical of these systems. Another common feature is the analysis of open dynamics, where a dissipative environment acts as a source of decoherence for the quantum system, allowing a more realistic description to be applied in real experiments. Moreover, we provided a quantitative analysis on the entanglement dynamics, with a particular attention to multipartite entanglement properties and its behavior under dissipation.

More in detail, we described a model for the mapping of a tripartite state and its quantum correlations, from an entangled three-mode radiation to three separated qubits placed in separated cavities. The Hamiltonian dynamics is basically described by the TC model when the three subsytems interact together and, then, by a triple JC model between atoms and the corresponding cavity modes when the external radiation coupling is turned off. We analyzed different situations which include the effect of changing the cavity mirror transmittance and that of multi-mode fibers coupling, the case of a continuous variables initial state and that of mapping mixed states of radiation. In this last case we observed ESD and ESB effects during and after the transfer of the state. We analyzed also the consequences of adding a dissipative environment to the dynamics of the system, observing and quantifying the detrimental effects on the entanglement transfer protocol, comparing also different reference initial states.

As widely explained in the introduction, there exist many extensions of the JC model that apply, for instance, to externally driven systems in CQED. We analyzed the dynamics of a system composed by N qubits interacting with a single cavity mode, strongly driven by a classical field, in the presence of dissipation both for the two-level atoms and the cavity mode. The unitary dynamics is ruled by an effective Hamiltonian that includes simultaneously rotating and counter rotating terms. This becomes important when the system undergoes an open dynamics, since the effective Hamiltonian interaction induces a

protection against decoherence for particular subspaces of the qubits Hilbert space. If the atoms are prepared in one of these states, the dynamics is blind with respect to the external environment action.

Finally we studied the dynamics of an interacting system of which the RWA is no more applicable. There are, at the present time, several experimental clues that such a quantum system can be realized in the framework of circuit QED with superconducting qubits, where the coupling could reach high values. Thus it becomes important to find a solid description both under an analytical and a numerical point of view. We studied the dynamics of these kind of systems, introducing the concept of parity chains, a rearrangement of the system Hilbert space that shows symmetry properties, due to the presence of counter resonant terms. We introduced the unitary model, underlying the fact that the dynamics occurs independently in the two chains, showing a characteristic behavior of collapses and revivals in the populations of the states of the system. As usual, we introduced a dissipative reservoir to the model and we showed how it connects the two parity chains inducing the same kind of dynamics. We could provide anlytical results for different initial states of the system, but still we do not have a general solution of the problem. Nevertheless we provided a quite general treatment of the open dynamics of a quantum system in the ultrastrong and in the deep strong coupling regime.

Future works

Several and interesting issues emerge from the research work we have presented here. Above all, the problem of the non-applicability of the RWA is still open and it provides many theoretical and experimental new challenges.
The first step is to generalize the analytical results shown in Chapter 4 to any initial state of the resonator field mode, Fock states and coherent states, allowing a better characterization of the open dynamics and the stationary state of the system. Secondly, we want to study the dynamics in the presence of a dissipative channel for the qubit, such as the spotaneous emission of the excited energy level.
Another main topic we want to face is the open dynamics of two qubits interacting with a single bosonic mode in the DSC regime, studying, in particular, the entanglement properties. As regards the unitary evolution it is already known that the Hilbert space splits again into two parity chains. We want to analyze the dynamics of entanglement of the two qubits, whether it is possible to generate entanglement starting from a separable state through a DSC dynamics, manipulating the coupling parameters, the qubit and the mode frequencies. The subject is quite new and very challenging and it requires a solid theoretical structure upon which lean on, but the final response must come, as usual, by the experiments.

List of publications

1. *Entanglement transfer in a multipartite cavity QED open system* M. Bina, F. Casagrande, M. G. Genoni, A. Lulli and M. G. A. Paris, *Int. J. Quant. Inf. (special issue on "Advances in foundations of Quantum Mechanics and Quantum Informatio" (2010))*, accepted.

2. *Tripartite quantum state mapping and discontinuous entanglement transfer in a cavity QED open system* M. Bina, F. Casagrande, M. G. Genoni, A. Lulli and M. G. A. Paris, *Phys. Scr. T* **140**, 014015 (2010).

3. *Dynamical description of state mapping and discontinuous entanglement transfer for tripartite systems* M. Bina, F. Casagrande, M. G. Genoni, A. Lulli and M. G. A. Paris, Eur. Phys. Lett. **90**, 30010 (2010).

4. *Decoherence in the solvable dynamics of N strongly driven atoms coupled to a cavity mode* M. Bina, F. Casagrande and A. Lulli, *Opt. and Spectr.* **108**, 356 (2010).

5. *Decoherence-free multipartite atomic entanglement in a cavity QED system* M. Bina, F. Casagrande and A. Lulli, *Int. J. Quant. Inf.* **7**, 229 (2009).

6. *Solvable Dynamics of N Driven Two-Level Atoms Coupled to a Dissipative Cavity Mode* M. Bina, F. Casagrande and A. Lulli, *Laser Physics* **19**, 362 (2009).

7. *Exact results on decoherence and entanglement in a system of N driven atoms and a dissipative cavity mode*, M. Bina, F. Casagrande, A. Lulli, *Eur. Phys. J. D* **49**, 257 (2008).

8. *Monitoring atom-atom entanglement and decoherence in a solvable tripartite open system in cavity QED* , M. Bina, F. Casagrande, A. Lulli and E. Solano, *Phys. Rev. A* **77**, 033839 (2008).

List of conferences

1. "Quantum 2010: V Workshop ad memoriam of Carlo Novero. Advances in Foundations of Quantum Mechanics and Quantum Information with atoms and photons", Turin (Italy) INRIM, 24-28/05/2010.
   Title of the talk: *Entanglement transfer in a multipartite cavity QED open system.*

2. "Central European Workshop on Quantum Optics 2009", Turku (Finland), 23-27/05/2009.
   Title of the talk: *Tripartite entanglement transfer from radiation modes to trapped atoms in dissipative environments.*

3. "XII International Conference on Quantum Optics and Quantum Information", Vilnius (Lithuania), 20-23/09/2008.
   Title of the talk: *Decoherence-free states in the solvable dynamics of N strongly driven atoms coupled to a dissipative cavity mode.*

4. International Summer School"QUROPE 09", Cortona (Arezzo, Italy), 3-16/05/2009.
   Title of the poster: *Analytical results for a cavity QED system of N driven atoms and one dissipative field mode: decoherence and entanglement.*

5. "Quantum Entanglement and Decoherence: 3rd International Conference on Quantum Information (ICQI)", Boston (MA, USA), 13-16/07/2008.
   Title of the poster: *Analytical results for a cavity QED system of N driven atoms and one dissipative field mode: decoherence and entanglement.*

6. "Quantum 2008: IV Workshop ad memoriam of Carlo Novero. Advances in Foundations of Quantum Mechanics and Quantum Information with atoms and photons", Turin (Italy) INRIM, 19-23/05/2008.
   Title of the poster: *Analytical results for a cavity QED system of N driven atoms and one dissipative field mode: decoherence and entanglement.*

BIBLIOGRAPHY

[1] E. T. Jaynes and F. W. Cummings, *Proc. IEEE* **51**, (1963) 89.

[2] S. Haroche and J. M. Raimond, *Exploring the Quantum* (Oxford University Press, 2006).

[3] D. Meschede, H. Walther and G. Müller, *Phys. Rev.Lett.* **54**, (1985) 551.

[4] K. An, J. J. Childs, R. R. Dasari and M. S. Feld, *Phys. Rev. Lett.* **73** (1994) 3375; W. Choi, J.-H. Lee, K. An, C. Fang-Yen, R. R. Dasari and M. S. Feld, *Phys. Rev. Lett.* **96**, (2006) 093603.

[5] J. M. Raimond, M. Brune and S. Haroche, *Rev. Mod. Phys.* **73**, (2001) 565.

[6] H. Walther, B. T. H. Varcoe, B.-G. Englert and T. Becker, *Reports on Progress in Physics* **69**, (2006) 1325.

[7] H. Mabuchi and A.C. Doherty, *Science* **298**, (2002) 1372.

[8] A. Wallraff *et al.*, *Nature* **431**, (2004) 162.

[9] D. Leibfried, R. Blatt, C. Monroe and D. Wineland, *Rev. Mod. Phys.* **75**, (2003) 281.

[10] E.K. Irish *et al.*, *Phys. Rev. B* **72**, (2005) 195410; E.K. Irish, *Phys. Rev. Lett.* **99**, (2007) 173601; M. Amniat-Talab, S. Guérin and H.R. Jauslin, *J. Math. Phys.* **46**, (2005) 042311.

[11] M. A. Nielsen and I. L. Chuang, *Quantum Computation and Quantum Information* (Cambridge University Press, Cambridge, 2000).

[12] C. H. Bennett *et al.*, *Phys. Rev. Lett.* **70**, (1993) 1895.

[13] N. Gisin *et al.*, *Rev. Mod. Phys.* **74**, (2002) 1458.

[14] G. M. D'Ariano, P. Lo Presti and M. G. A. Paris, *Phys. Rev. Lett.* **87**, (2001) 270404.

[15] O. Gühne and G. Toth, *Phys. Rep.* **474**, (2009) 1.

[16] E. Joos *et al.*, *Decoherence and the Appearance of a Classical World in Quantum Theory* (Springer, Berlin, 1996); H.-B. Breuer and F. Petruccione, *The theory of open quantum systems* (Oxford University Press, Oxford 2002).

[17] J. Dalibard, Y. Castin and K. Mølmer, *Phys. Rev. Lett.* **68**, (1992) 580.

[18] A. Peres, *Phys. Rev. Lett.* **77**, (1996) 1413.

[19] M. Horodecki, P. Horodecki and R. Horodecki, *Phys. Lett. A* **223**, (1996) 1.

[20] K. Zyczkowski, P. Horodecki, A. Sanpera and M. Lewenstein, *Phys. Rev. A* **58**, (1998) 883.

[21] C.H. Bennett, D.P. Di Vincenzo, J.A. Smolin, and W.K. Wootters, *Phys. Rev. A* **54**, (1996) 3824.

[22] S. Hill and W.K. Wootters, *Phys. Rev. Lett.* **78**, (1997) 5022.

[23] D. M. Greenberger, M. A. Horne, A. Zeilinger, "Going beyond Bells theorem", in: M. Kafatos (Ed.), "Bells Theorem, Quantum Theory, and Conceptions of the Universe", Kluwer, Dordrecht, (1989), pp. 6972.

[24] W. Dür, G. Vidal and J. I. Cirac, *Phys. Rev. A* **62**, (2000) 062314.

[25] A. Acín and *et al.*, *Phys. Rev. Lett.* **85**, (2000) 1560.

[26] V. Coffman, J. Kundu and W. K. Wootters, *Phys. Rev. A* **61**, (2000) 052306.

[27] C. Sabin and G. Garcia-Alcaine, *Eur. Phys. J. D* **48**, (2008) 435.

[28] A. Wong and N. Christensen, *Phys. Rev. A* **63**, (2001) 044301.

[29] M. Horodecki, P. Horodecki and R. Horodecki, *Phys. Rev. Lett.* **80**, (1998) 5239.

[30] M. Paternostro, W. Son and M. S. Kim, *Phys. Rev. Lett.* **92**, (2004) 197901.

[31] W. Son *et al.*, *J. Mod. Opt.* **49**, (2002) 1739; M. Paternostro *et al.*, *Phys. Rev. A* **70**, (2004) 022320; J. Zou *et al.*, *Phys. Rev. A* **73**, (2006) 042319; F. Casagrande, A. Lulli and M. G. A. Paris, *Phys. Rev A* **75**, (2007) 032336; A. Serafini *et al.*, *Phys. Rev. A* **73**, (2006) 022312; M. Paternostro, G. Adesso and S. Campbell, *Phys. Rev. A* **80**, (2009) 062318.

[32] F. Casagrande, A. Lulli and M. G. A. Paris, *Eur. Phys. J. ST* **160**, (2008) 71.

[33] M. Paternostro *et al.*, *Phys. Rev. B* **69**, (2004) 214502.

[34] J. Hald *et al.*, *J. Mod. Opt.* **47**, (2000) 2599; B. Julsgaard *et al.*, *Nature* **432**, (2004) 482.

[35] J. Lee *et al.*, *Phys. Rev. Lett.* **96**, (2006) 080501.

[36] F. Casagrande, A. Lulli and M. G. A. Paris, *Phys. Rev. A* **79**, (2009) 022307.

[37] J. Zhang *et al.*, *Phys. Rev. A* **66**, (2002) 032318; J. Jing *et al.*, *Phys. Rev. Lett.* **90**, (2003) 167903; T. Aoki *et al.*, *Phys. Rev. Lett.* **91**, (2003) 080404.

[38] M. Bondani *et al.*, *Opt. Lett.* **29**, (2004) 180; A. Ferraro *et al.*, *J. Opt. Soc. Am. B* **21**, (2004) 1241; A. Allevi *et al.*, *Las. Phys.* **16**, (2006) 1451.

[39] A. Allevi *et al.*, *Phys. Rev. A* **78**, (2008) 063801.

[40] A. Furusawa *et al.*, *Science* **282**, (1998) 706.

[41] A. S. Bradley *et al.*, *Phys. Rev. A* **72**, (2005) 053805; O. Pfister *et al.*, *Phys. Rev. A* **70**, (2004) 020302(R).

[42] A. S. Villar *et al.*, *Phys. Rev. Lett.* **97**, (2006) 140504.

[43] S. B. Papp *et al.*, *Science* **324**, (2009) 764.

[44] A. E. B. Nielsen *et al.*, arXiv:1002.0127.

[45] P. Lougovski, E. Solano and H. Walther, *Phys. Rev. A* **71**, (2005) 013811.

[46] M. Bina *et al.*, *Eur. Phys. Lett.* **90**, (2010) 30010.

[47] S. Nussmann *et al.*, *Nat. Phys.* **1**, (2005) 122; K. M. Fortier *et al.*, *Phys. Rev. Lett.* **98**, (2007) 233601; J. Ye, H. J. Kimble and H. Satori, *Science* **320**, (2008) 1734.

[48] A. B. Mundt *et al.*, *Phys. Rev. Lett.* **89**, (2002) 103001; M. Keller *et al.*, *Nature* **431**, (2004) 1075.

[49] K. Zyczkovski *et al.*, *Phys. Rev. A* **65**, (2001) 012101; C. Simon and J. Kempe, *Phys. Rev. A* **65**, (2002) 052327; P. J. Dodd and J. J. Halliwell, *Phys. Rev. A* **69**, (2004) 052105; T. Yu and J. H. Eberly, *Phys. Rev. Lett.* **93**, (2004) 140404; C. E. López *et al.*, *Phys. Rev. Lett.* **101**, (20089) 080503.

[50] M. P. Almeida *et al.*, *Science* **316**, (2007) 579; J. Laurat *et al.*, *Phys. Rev. Lett.* **99**, (2007) 180504; A. Salles *et al.*, *Phys. Rev. A* **78**, (2008) 022322.

[51] J. I. Cirac *et al.*, *Phys. Rev. Lett.* **78**, (1996) 3221; A. D. Boozer *et al.*, *Phys. Rev. Lett.* **98**, (2007) 193601.

[52] A. Serafini *et al.*, *Phys. Rev. A* **73**, (2006) 022312.

[53] T. Pellizzari, *Phys. Rev. Lett.* **79**, (1997) 5242; A. Serafini, S. Mancini and S. Bose, *Phys. Rev. Lett.* **96**, (2006) 010503.

[54] N. Linden, S. Popescu and W. K. Wootters, *Phys. Rev. Lett.* **89**, (2002) 207901.

[55] A. Acín *et al.*, *Phys. Rev. Lett.* **87**, (2001) 040401.

[56] O. Gühne and M. Seevinck, *New J. Phys.* **12**, (2010) 053002.

[57] G. Vidal and R. F. Werner, *Phys. Rev. A* **65**, (2002) 032314.

[58] M. Tavis and F. W. Cummings, *Phys. Rev.* **188**, (1969) 692.

[59] A. O. Pittenger and M. H. Rubin, *Opt. Commun.* **179**, (2000) 447.

[60] B. Kraus, *PhD thesis available on line as MPQ282.*

[61] M. Ge, L.-F. Zhu and L. Qiu, *Commun. Theor. Phys.* **49**, (2008) 1443.

[62] J. Zhang, C. Xie and K. Peng, *Phys. Rev. A* **66**, (2002) 032318; J. Jing *et al.*, *Phys. Rev. Lett.* **90**, (2003) 167903; T. Aoki *et al.*, *Phys. Rev. Lett.* **91**, (2003) 080404; A. Allevi *et al.*, *Phys. Rev. A* **78**, (2008) 063801.

[63] S. Tamaryan, T-C. Wei and D. Park, *Phys. Rev. A* **80**, (2009) 052315.

[64] P. Lougovski, F. Casagrande, A. Lulli, and E. Solano, *Phys. Rev. A* **76**, (2007) 033802.

[65] L.M. Duan and G.C. Guo, *Phys. Rev. Lett.* **79**, (1997) 1953; P. Zanardi and M. Rasetti, *Phys. Rev. Lett.* **79**, (1997) 3306; D.A. Lidar and K.B. Whaley, in: *Irreversible Quantum Dynamics*, F. Benatti and R. Floreanini, editors (Springer, Berlin, 2003), 83.

[66] D.L. Moehring et al., J. Opt. Soc. Am. B **24**, 300 (2007); P. Zoller et al., *Eur. Phys. J. D* **36**, (2005) 203.

[67] S.M. Barnett and P.M. Radmore, *Methods in Theoretical Quantum Optics* (Clarendon Press, Oxford 1997).

[68] M. Bina, F. Casagrande, A. Lulli and E. Solano, *Phys. Rev. A* **77**, (2008) 033839.

[69] M. Bina, F. Casagrande and A. Lulli, *Eur. Phys. J. D* **49**, (2008) 257; M. Bina, F. Casagrande and A. Lulli, *Opt. and Spectr.* **108**, (2010) 356.

[70] M. Bina, F. Casagrande and A. Lulli, *Laser Physics* **19**, (2009) 362; M. Bina, F. Casagrande and A. Lulli, *Int. J. Quant. Inf.* **7**, Supplement (2009) 229.

[71] E. Solano, G.S. Agarwal and H. Walther, *Phys. Rev. Lett.* **90**, (2003) 027903.

[72] P. Lougovski, E. Solano and H. Walther, *Phys. Rev. A* **71**, (2005) 013811.

[73] K.E. Cahill and R.J. Glauber, *Phys. Rev.* **177**, (1969) 1882.

[74] P. Lougovski, F. Casagrande, A. Lulli, B.-G. Englert, E. Solano and H. Walther, *Phys. Rev. A* **69**, (2004) 023812.

[75] R.S. Minns, M.R. Kutteruf, H. Zaidi, L. Ko, and R.R. Jones, Phys. Rev. Lett. **97**, 040504 (2006).

[76] F. Casagrande and A. Lulli, *Eur. Phys. J. D* **46**, (2008) 165.

[77] M.S. Kim, J. Lee, D. Ahn, and P.L. Knight, *Phys. Rev. A* **65**, (2002) 040101(R).

[78] A. Ferraro, S. Olivares and M.G.A. Paris. *Gaussian States in Quantum Information* (Napoli, Series on Physics and Astrophysics, 2005).

[79] L. Mandel, E. Wolf, *Optical coherence and quantum optics* (Cambridge University Press, Cambridge, 1995)

[80] G. Jaeger, *Quantum Information* (Springer, New York, 2007).

[81] A. A. Abdumalikov *et al.*, *Phys. Rev. B* **78**, 180502(R) (2008).

[82] M. Devoret, S. Girvin and R. Schoelkopf, *Ann. Phys.* **16**, 767 (2007).

[83] P. Nataf and C. Ciuti *et al.*, *Phys. Rev. Lett.* **104**, 023601 (2010).

[84] T. Niemczyk *et al.*, *Nat. Phys.* **6**, 772 (2010).

[85] A. Blais *et al.*, *Phys. Rev. A* **69**, 062320 (2004); Y. Nakamura, Yu.A. Pashkin and J.S. Tsai, *Nature* **398**, (1999) 786.

[86] J. Casanova *et al.*, arXiv:1008.1240v1.

[87] G. M. D'Ariano, *Phys. Lett. A* **187**, 231 (1994).

Acknowledgements

Firstly I would like to thank my supervisor Prof. Federico Casagrande, who has always been present in every day of my doctorate course and in every moment of need. I have learned a lot from him, even with many nice discussions outside the physics orbit, and I owe him the possibility to have travelled so much and to have held my first university lessons.

A special thank is for Dr. Alfredo Lulli, who has given me a great technical support with an admirable "stay-behind" strategy and who has taught me so many things.

I would like to thank my co-tutor Matteo G. A. Paris for our collaboration and several fruitful discussions.

Another special aknowledgement is for Prof. Enrique Solano, who motivated me a lot in the study of a really exciting new field in physics and for his kindness and patience during my stay in Bilbao. Together with his group of young researchers, he has been able to make me spend a really glad period in the Basque Country.

A due and deep thank is for my parents and my family, which has recently enlarged with a promising small human being, for their support and their simple presence.

Last but not least, I must thank all my friends composing a very long list, that I don't want to unwrap for the fear of forgetting some of them. Anyway, a special thought is for Francesca, who has been able to really strengthen and ecouraging me and for always being there, even when I wasn't, for make me taste the real world of theatre, and for her great voice. Thanks to Marco for his patience in working with me and for the most funny friendship in evenings and conferences. A special gratitude is for Vera, who has been always close to me with her

wisdom and her advices and to whom I wish the best for her life. Thanks to old and new friends in university, thanks to my band and all the friends supporting us, and thanks to old and new friends of my hometown.